Technology Development for Iron and Cobalt Fischer-Tropsch Catalysts

Quarterly Report

July 1, 2000 to September 30, 2000

Burtron H. Davis

Enrique Iglesia (UC/B Subcontract)

DE-FC26-98FT40308

University of Kentucky Research Foundation

201 Kinkead Hall

Lexington, KY 40506

University of California-Berkeley (Subcontract)

Laboratory for the Science and Application of Catalysis

Department of Chemical Engineering

University of California at Berkeley

Berkeley, CA 94720

Disclaimer

This report was prepared as an account of work sponsored by an agency of the United States Government. Neither the United States Government nor any agency thereof, nor any of their employees, makes any warranty, express or implied, or assumes any legal liability or responsibility for the accuracy, completeness, or usefulness of any information, apparatus, product, or process disclosed, or represents that its use would not infringe privately owned rights. Reference herein to any specific commercial product, process, or service by trade name, trademark, manufacturer, or otherwise does not necessarily constitute or imply its endorsement, recommendation or favoring by the United States Government or any agency thereof. The views and opinions of authors expressed herein do not necessarily state or reflect those of the United States Government or any agency thereof.

Abstract

CAER

The use of alkali promoters has been widely practiced. However, data to compare various promoters is limited for the iron-based catalysts and much of the available data were obtained at low pressure or under a variety of reaction conditions. The importance of the alkali promoter in determining catalytic activity, stability and selectivity merits a comparison of the promoters under suitable reaction conditions. The present study utilizes medium pressure synthesis conditions to compare the alkali promoters under the same reaction conditions and over a wide range of conversion levels.

Iron-based Fischer-Tropsch (FT) catalysts undergo a series of phase transformations during activation and use. Activation with carbon monoxide or syngas typically results in the conversion of Fe_2O_3 to Fe_3O_4 and ultimately to one or more carbides. During FT synthesis, iron carbides can be oxidized to Fe_3O_4 if the H_2O/H_2 or CO_2/CO ratios are high enough. There has been considerable debate about the active phase of the FT synthesis. Some studies have indicated an active oxide species while most have supported a carbide species. Mössbauer spectroscopy has proven to be an effective technique for the analysis of iron-based FT catalysts. *In situ* Mössbauer studies have been reported; however, these studies have been performed at low pressure and low conversions. Studies performed at industrially relevant conditions have generally involved removing the catalyst from the reactor followed by passivation which, if not performed properly, will oxidize the catalyst. Herein are reported the Mössbauer results obtained on an unpromoted precipitated iron catalyst that was activated and reacted in a slurry phase, continuous stirred tank reactor at high conversion and under industrially relevant conditions.

Strict measures were observed to prevent oxidation of the catalyst samples. The Fe-Si, Fe-K, Fe-Si-K catalysts were all studied using the same methods.

We have studied and are continuing to study the impact on reducibility of cobalt by the use of different supports and by the incorporation of different promoters and additives to supported cobalt catalysts. Although the use of different supports and promoters is well documented, what is less well understood are the reasons for the differences in deactivation rates of these catalysts. Only by rigorous characterization can the properties of the catalysts brought about by differences in preparation, support, and degree and type of promoter be linked to the resulting catalytic properties under reaction. We therefore have spent considerable attention on the characterization of not only the fresh catalysts, but also the spent catalysts sampled after many days on stream in the continuously stirred tank reactor. With this approach, it is our goal to understand what properties are required for high initial activity and, just as importantly, for the maintaining of high stability, and how to achieve them in the catalyst preparation and activation steps. Interestingly, while addition of promoters can markedly improve the reducibility of cobalt FTS catalysts, leading to more available catalytic sites for reaction, these catalysts often display significantly high rates of deactivation. This raises many questions, which should be able to be addressed through careful characterization. To address these questions, we are employing several characterization techniques, including temperature programmed reduction (TPR), hydrogen chemisorption, X-ray diffraction (XRD), transmission electron microscopy (TEM), and in the near future, diffuse reflectance infrared Fourier transform spectroscopy (DRIFTS) and X-ray absorption spectroscopy methods (XAS) such as extended X-ray absorption fine structure (EXAFS) and X-ray absorption near edge structure (XANES).

Currently, the CAER is utilizing the Prototype Integrated Process Unit (PIPU) system for scale-up research of the Fischer-Tropsch Synthesis (FTS).

The PIPU is a pilot plant system built in the early 1980s for studying a multitude of synthetic fuel/chemical processes. In the mid 1990s, a direct coal liquefaction reactor within the PIPU plant was reconfigured as a SBCR for FTS studies. The reactor was originally designed to operate with coarse catalyst pellets (>500 μm). Consequently, the reactor system did not contain a wax separation system sufficient for smaller catalyst particles that are typically used in FTS. Therefore, a slurry accumulator and a batch wax filtration system were installed.

UC/B

Treatment temperatures play a major role in determining the surface area of Fe-Zn oxides. H_2O removal is critical in preparing high surface area Fe-Zn precursors. Decreasing the surface tension of liquids during drying processes and increasing the space velocity of dry air in subsequent treatment processes can significantly increase the surface area of catalyst precursors. Each impregnation slightly decreases the surface area of Fe-Zn precursors. However, the previous impregnation history on Fe-Zn precursors does not appear to influence the ultimate surface area of promoted Fe-Zn oxides at a given treatment temperature. High surface area Fe-Zn-K4-Cu2 oxide (Zn/Fe=0.1, K/Fe=0.04, Cu/Fe=0.02) reduces at slightly higher temperatures in H_2 but reduces and carburizes at lower temperatures (~30 K) in CO than on Fe-Zn-K2-Cu1 oxide (Zn/Fe=0.1, K/Fe=0.02, Cu/Fe=0.01), suggesting its slightly higher surface K/Cu ratio than on Fe-Zn-K2-Cu1 oxide. CO chemisorption on Fe-Zn-K-Cu oxides after FTS reaction showed that the amount of CO adsorbed is proportional to the surface area of each sample. Zn, Cu and K promoter lead to higher surface area Fe carbides, which provide a higher density of binding sites for adsorption and also for FTS reactions. Fixed bed reactor studies with high surface area Fe-Zn-Cu-K samples showed that

an increase in surface area led to proportionally higher FTS rates with negligible changes in the product selectivity. This effect is attributed to an improvement in dispersion of the active Fe_xC structure upon increase in surface area. Similarly, the addition of Ru to Fe-Zn-K also increases FTS rates by improving the availability of active sites on the catalyst surface. Tests conducted with increased surface hydrogen coverage on Fe-based catalysts showed an increase in the paraffin content and a decrease in the product molecular weight at conditions normally utilized for Co-based catalysts. Similarly, when a Co/SiO_2 catalyst is operated at higher CO surface coverages and at conditions utilized for Fe-based catalysts, an increase in the olefin content and lower CH_4 selectivity were observed. The primary difference between FTS reactions on Fe and Co catalysts appear to be due to the lack of secondary olefin readsorption reactions in the case of the former, which could explain the observed differences in product selectivity. Studies with a Co/SiO_2 catalyst at different reaction pressures showed the existence of the autocatalytic water effect even at lower pressures (i.e., 5 atm).

Table of Contents

Executive Summary

CAER

A study to determine the importance of alkali promoters (K, Li, Cs, Rb) on an iron catalyst (100Fe:4.5Si) in determining the catalytic activity, selectivity and stability was begun this quarter. The study utilizes medium pressure synthesis conditions to compare the alkali promoters under the same reaction conditions and over a wide range of conversions. The ranking of the alkali promoters for the activity of the Fe catalyst depended on the CO conversion level. At a CO conversion of approximately 20%, the activity of the K and Li promoted catalysts are approximately the same with the Li promoted catalyst being slightly more active. At a CO conversion level of 40%, the K promoted catalyst is much more active. As the CO conversion increases to 60%, the four metals have a similar impact on activity. The selectivity of the products by carbon number is essentially the same for the four promoters studied. The activity for the water-gas-shift reaction depended on the alkali promoter. These data suggest that the Li promoter may produce an Fe catalyst that more closely resembles cobalt in producing less WGS than the "normal" iron catalyst.

A study was begun this quarter to characterize the iron phase changes during FTS using individually relevant conditions. An unpromoted iron catalyst and Fe-Si, Fe-K and Fe-Si-K catalysts were studied in the CSTR's using the same methods. To date, only the Mössbauer results for the unpromoted catalyst are available. Catalyst samples were withdrawn immediately after activation and at 23h, 168h and 453 hr. The Mössbauer results show that parallel to an activity decline, the amount of iron present as χ-Fe_5C_2 declines, until after 453 hrs of FTS, the only phase detected was Fe_3O_4. The data suggests that a steady-state surface carbide phase/Fe_2O_3 core phase is not formed for the unpromoted iron catalyst. Work is continuing with the single

and doubly promoted catalysts to define the role of each promoter in determining the composition of the working catalysts.

The results obtained this quarter for the on-going study of the impact on the reducibility of cobalt by the use of different supports and by the incorporation of different promoters and additives to the supported Co catalysts are reported.

The activity of cobalt catalysts is generally ascribed to the active sites located on the surface of cobalt metal clusters formed after reduction of the oxidic species formed after calcination. However, the reducibility of cobalt catalysts is strongly influenced by the nature of the support and the degree of promotion by additives, which is the focus of this work. In general, a tradeoff exists as one increases the reduction temperature to activate the cobalt catalyst. Although more sites are reduced, cobalt clusters sinter at higher reduction temperatures. Therefore, TPR and hydrogen chemisorption studies should be conducted prior to catalytic testing, in order to determine the appropriate temperature for catalyst activation. In general, the number of active sites available after reduction varies with support, promoter type, and degree of promotion. The reason for deactivation of promoted FTS catalysts is a subject requiring further study. TPR studies suggest that there is a difference in the degree of interaction of the promoter with the cobalt after reaction testing for each promoter. However, further experiments, using such techniques as EXAFS, are necessary to determine the extent of these morphological changes. Not only will EXAFS allow the determination of cluster size, but the local structure surrounding Co, including the promoter interaction, may be quantified for the fresh and spent catalysts.

The addition of Pt or Ru to the support had a similar effect on each of the fresh supported catalysts. All the reduction peak positions shifted markedly to lower temperatures, due to

spillover of H_2 from the reduced promoter to reduce Co oxide species. Of particular importance, peaks attributed to the metal support interaction for Co species on TiO_2 and Al_2O_3 are reduced at much lower temperatures, freeing up the availability of metal sites for reaction. For the case of Re, the reduction of Re occurs at higher temperatures than Pt or Ru. Although the low temperature peaks are not significantly affected, Re still plays a valuable role in reducing the reduction temperature of species for which there is a significant metal-support interaction.

TPR analysis of spent promoted 15%Co/Al_2O_3 catalysts revealed that while observed peaks for Ru and Re promoted catalysts remained shifted to low temperatures, the peaks had shifted substantially to higher temperatures in the case of the Pt catalyst. This suggests that the Co and Pt interaction is rapidly lost under reaction, and may be the reason for the higher observed deactivation rate.

The following discussion describes the work done to enhance the CAER's SBCR system. A 5.08 cm diameter by 2 m tubular reactor had been modified to operate in a Fischer-Tropsch SBCR mode. The previous work had focused primarily on catalyst separation from the wax products. Problems with maintaining a constant catalyst inventory within the reactor have been addressed and design modifications are underway. Heat load/loss calculations have been performed to evaluate the need for cooling with high space velocities.

UC/B

In this reporting period, we have started the preparation of a new series of high surface area catalysts based on K- and Cu-promoted Fe-Zn oxides under different treatment protocols. Various factors that influence the surface area of the catalysts have been examined in order to guide the preparation of high surface area catalysts. Using alcohol instead of water to wash the Fe-Zn precipitates increased their surface area markedly (215 vs 148 m^2/g) because low surface

tension alcohols within intraparticle pores in precipitates inhibit pore mouth pinching during drying. Treatment temperatures play a critical role in determining the ultimate surface area of catalysts. It appears that a suitable treatment temperature is ~300 ºC; these temperatures allow the decomposition of Fe hydroxide while preventing loss of surface area of the resulting Fe oxides due to sintering. Since water evolves during hydroxide decomposition and it can cause catalyst sintering, a high space velocity flow of air is required for treating the catalysts (>2000 h^{-1}). Each impregnation slightly decreased the surface area of Fe-Zn precursors (~10-20%). However, the previous impregnation history on Fe-Zn precursors (impregnation promoters on Fe-Zn hydroxide or on oxide precursors) does not appear to influence the ultimate surface area of promoted Fe-Zn oxides at given treatment temperatures.

The structure, reduction and carburization behavior, and catalytic properties of Fischer-Tropsch synthesis (FTS) on these high surface area catalysts were studied using temperature-programmed reduction and carburization in H_2 and CO. The results showed that alcohol-washed Fe-Zn oxides consist of highly dispersed Fe_2O_3 crystallites, which grow larger as the treatment temperatures increase. High surface area Fe-Zn-K4-Cu2 oxides (Zn/Fe=0.1, K/Fe=0.04, Cu/Fe=0.02) reduce at slightly higher temperatures in H_2, but they reduces and carburizes at lower temperatures (~30 K) in CO than on Fe-Zn-K2-Cu1 oxides (Zn/Fe=0.1, K/Fe=0.02, Cu/Fe=0.01). It appears that the surface K/Cu ratio is slightly higher on Fe-Zn-K4-Cu2 oxides.

CO chemisorption was performed on Fe-Zn-K-Cu oxides after FTS reaction at 250 ºC for 1 h in order to examine the effect of promoters on the adsorption behaviors of Fe oxides. The results show higher amounts of desorbed H_2, CO and CO_2 on Fe-K-Cu oxides (20-50 mmol/g-atom Fe) than on Fe-Zn (5-20 mmol/g-atom Fe), but lower amounts than on Fe-Zn-K-Cu oxides (30-80 mmol/g-atom Fe). This reflects a role of each promoter (Zn, Cu, and K) in leading to the

formation of are responsible for higher surface area Fe carbides, which provide a higher density of binding sites for adsorption and also for FTS. The amount of CO chemisorbed on the catalysts is proportional to the surface area of each samples. The presence of K and Cu significantly increases the reduction and carburization rates of Fe oxides, leading to higher surface area Fe carbides, which provide more sites for CO chemisorption and for FTS reactions.

Fischer-Tropsch synthesis reactions were carried out with a high surface area Fe-Zn-K4-Cu2 catalyst prepared during this reporting period. When compared to the FTS reaction data obtained on the low surface area Fe-Zn-Cu-K samples (Zn/Fe=0.1, K/M=0.02, Cu/M=0.01) studied previously, the high surface area sample exhibited higher CO conversions (38% and 16% respectively at 220^{o}C and a CO space velocity of 5 NL/hr.g-Fe) and CO rates (4.2 and 2 mol/hr.g-at.Fe respectively at 220^{o}C and ~18% CO conversion). The increase in surface area however did not result in significant changes in product selectivities at any of the reaction conditions used. The CO_2 selectivity in both cases were identical, while the CH_4 selectivity was slightly higher on the high surface area sample (2.6% and 1.8% respectively at 220^{o}C, and ~18% CO conversion); and these are likely to be due to a higher surface K/Fe ratio in the high surface area sample.

FTS reactions were also carried out on the high surface area Fe-Zn-Cu-K catalyst at conditions normally used in Co-based FTS reactions (200^{o}C, 20 atm and H_2/CO=2). The H_2/CO ratio was increased on the Fe-Zn-Cu-K sample in order to match the CH_4 selectivity obtained on the Co/SiO_2 catalyst. At this condition (H_2/CO=20), space velocity runs conducted on the Fe-Zn-Cu-K sample showed much lower C_{5+} selectivity (68% compared to 85% for the Co/SiO_2 catalyst). CO_2 selectivities were smaller at higher H_2/CO ratios (6% and 14% respectively at ~16% CO conversion), and independent of CO conversion indicating that secondary water gas

shift reactions do not occur at these high H_2 partial pressures on Fe-Zn-Cu-K. The higher hydrogen surface coverage also leads to a higher termination of chains at lower carbon numbers and hence to a decrease in the product molecular weight. The Fe catalyst also had a higher paraffin content at the higher H_2/CO ratio (*1*-C_6H_{12}/*1*-C_6H_{14} ratio being 0.35 compared to 2.0 at H_2/CO=2, and independent of CO conversion).

Studies on Ru-promotion on a Fe-Zn-K catalyst showed an increase in CO rates and hydrocarbon productivities with an increase in Ru content in the 0-1 at.% range. The primary effect of Ru appears to be in improving dispersion of the Fe_xC structure and hence an increase in the number of available sites for the FTS reaction.

FTS reactions were also carried out with a 21.9 % Co/SiO_2 catalyst at conditions normally used in Fe-based FTS reactions (220°C, 31.6 atm and H_2/CO=2). The H_2/CO ratio was decreased on the Co/SiO_2 sample (to 1.0) in order to approach the CH_4 selectivity obtained on the Fe-Zn-Cu-K catalyst. At these conditions (H_2/CO=1), space velocity runs conducted on the Co/SiO_2 sample showed higher CH_4 selectivities than that of the Fe-Zn-Cu-K catalyst (6% and 2.6% at ~20% CO conversion). The higher CO surface coverage also led to the inhibition of secondary hydrogenation reactions of α-olefins (as shown by the *1*-C_6H_{12}/*1*-C_6H_{14} ratio being unchanged with space time). At this high temperature, secondary chain growth by readsorption of α-olefins is also non-existent as indicated by a fairly linear Flory plot.

During the current reporting period, experiments were also conducted to test the effect of reaction pressure on the performance of a 21.9% Co/SiO_2 catalyst. FTS reactions at 5 atm showed the existence of the water effect even at these conditions. These tests were in preparation for our *in situ* FTIR spectroscopic experiments, which will be conducted to study the autocatalytic water effect on Co catalysts in an infrared reaction cell capable of pressures up to 5 atm.

Task 1. Iron Catalyst Preparation

The objective of this task is to produce robust intermediate- and high-α catalysts.

See Task 2.

Task 2. Catalyst Testing

The objective of this task is to obtain catalyst performance on the catalysts prepared in Task 1.

A. Fischer-Tropsch Synthesis. Comparison of alkali Metals as Promoters

Introduction

The use of alkali promoters has been widely practiced. However, data to compare various promoters is limited for the iron-based catalysts and much of the available data were obtained at low pressure or under a variety of reaction conditions. The importance of the alkali promoter in determining catalytic activity, stability and selectivity merits a comparison of the promoters under suitable reaction conditions. The present study utilizes medium pressure synthesis conditions to compare the alkali promoters under the same reaction conditions and over a wide range of conversion levels.

Experimental

A precipitated iron-silica catalyst base (100Fe:4.6Si atomic ratio) was prepared by continuous precipitation. The calculated quantity of aqueous alkali metal nitrate was added to the dried base material to provide an alkali metal:iron atomic ratio of 100:1.44. As described previously, a 1-L stirred autoclave was used to effect catalyst activation using CO and they subsequent synthesis at 270°C, 1.2 MPa (175 psig), H_2:CO = 0.7, and various space velocities as described previously (same as above). During the course of the run, the conditions were returned

to 3.1 NL/hr/g. Fe, the base flow rate, to obtain data to establish the catalyst deactivation rate and to correct each measured conversion to that of the fresh catalyst.

Results and Discussion

The conversion of CO as a function of the reciprocal of the space velocity shows that the ranking of the alkali metals as a promoter for the activity of an iron catalyst will depend upon the CO conversion level (Figure 1). At low (CO conversion about 20%) the activity of the K and Li promoted catalysts are about the same with the Li promoted catalyst being slightly more active. These two alkali metals are about 2.8 and 2.9 times more active than for Cs and Rb, respectively. However, at 40% CO conversion, potassium is much more active than the other metals with the time required, relative to K, to attain 40% conversion being K:Li:Cs:Rb = 1:2.76:3.24:3.14. As the CO conversion increases to 60% the four metals begin to have a similar impact on activity with K:Li:Cs:Rb = 1:2.15:2.06:1.98. Thus, K is equal to or superior to the other three alkali metals over the entire CO conversion range.

For the selectivity of products by carbon number (alpha value), the four promoters are essentially the same. Thus, while the total activity varies, the distribution of products by carbon number is essentially the same.

The activity for the water-gas-shift (WGS) reaction depends upon the alkali promoter (figure 2). The lower WGS activity will result in a higher partial pressure of water in the exit gas and this is clearly shown in figure 2. The water partial pressure is the highest for the entire range of CO conversions for the catalyst containing the Li promoter. At lower CO conversion levels, K produces the next least effective catalyst for the WGS reaction. Over the lower CO conversion range, Rb and Cs promoters produce a catalyst that is more active than the other two alkali metals; at higher conversion levels the catalysts containing K, Cs and Rb have about the same

water partial pressure. This indicates that using the Li promoter may produce an iron catalyst that more closely resembles cobalt in producing less WGS than the "normal" iron catalyst.

The alkene fraction in the C_2-C_4 olefins also are consistent with Li being different from the other alkali promoters. As the K content of a catalyst is increased, the alkene fraction of the C_2-C_4 products increase and the increase is greatest for the C_2 products. This is the case for the products obtained in the present study. At the lower CO conversion levels, alkenes account for about 85% or more of the C_3-C_4 carbon number products for all four promoters, and there is little difference in the slow decrease in the olefin fraction as the CO conversion increases. However, ethene accounts for only about 55% of the C_2 products with the Li promoter whereas it accounts for 75-80% of the C_2 products with the other three promoters.

References

1. The Fischer-Tropsch and related synthesis, H. H. Storch, N. Golumbic, R. B. Anderson, John Wiley & Son, Inc, New York, 1951, P227

2. R. J. O'Brien, L. Xu, R. - Spicer and B. H. Davis, Energy & Fuels, 10, 921-926 (1996))

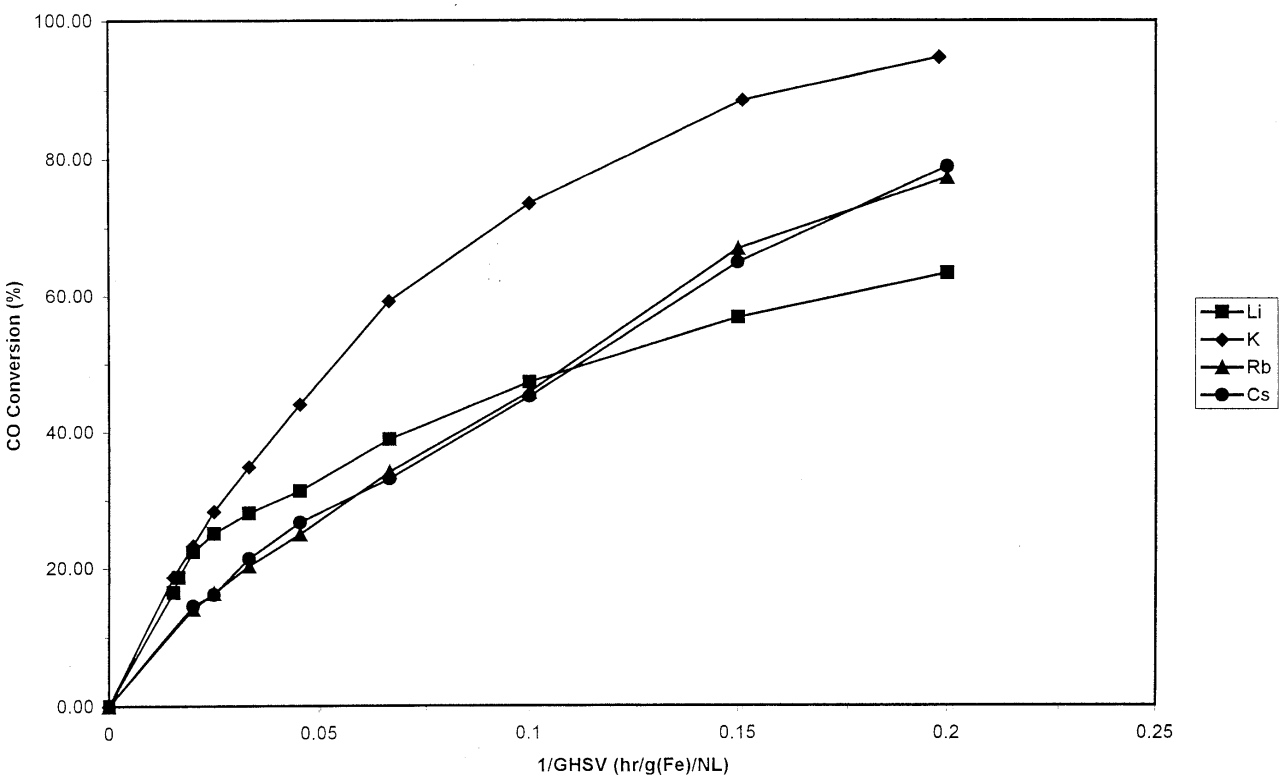

Figure 1. CO conversion corrected as a function of space time, 1.44Li, 1.44K, 1.44Rb, 1.44Cs.

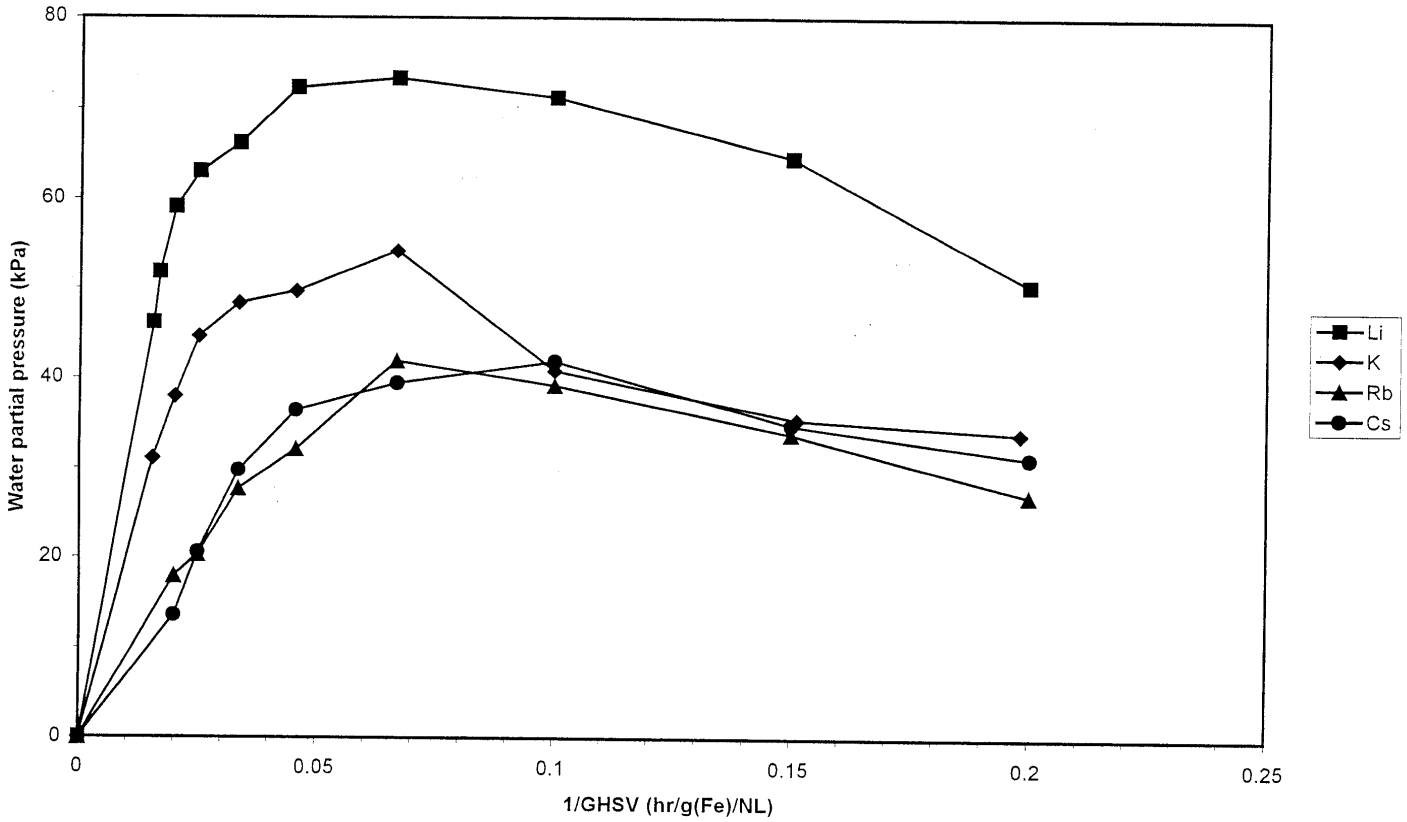

Figure 2. Water partial pressure as a function of space time, 1.44Li, 1.44K, 1.44Rb, 1.44Cs.

Task 3. Catalyst Characterization

The objective of this task is to obtain characterization data of the prepared catalysts using routine and selected techniques.

A. Characterization of Iron Phase Change During Fischer-Tropsch Synthesis Reaction

Introduction

Iron-based Fischer-Tropsch (FT) catalysts undergo a series of phase transformations during activation and use (1). Activation with carbon monoxide or syngas typically results in the conversion of Fe_2O_3 to Fe_3O_4 and ultimately to one or more carbides (2). During FT synthesis, iron carbides can be oxidized to Fe_3O_4 if the H_2O/H_2 or CO_2/CO ratios are high enough (1). There has been considerable debate about the active phase of the FT synthesis. Some studies have indicated an active oxide species (3) while most have supported a carbide species (2,4). Mössbauer spectroscopy has proven to be an effective technique for the analysis of iron-based FT catalysts. *In situ* Mössbauer studies have been reported (5,6); however, these studies have been performed at low pressure and low conversions. Studies performed at industrially relevant conditions have generally involved removing the catalyst from the reactor followed by passivation (7) which, if not performed properly, will oxidize the catalyst (4). Herein are reported the Mössbauer results obtained on an unpromoted precipitated iron catalyst that was activated and reacted in a slurry phase, continuous stirred tank reactor at high conversion and under industrially relevant conditions. Strict measures were observed to prevent oxidation of the catalyst samples. The Fe-Si, Fe-K, Fe-Si-K catalysts were all studied using the same methods.

Experimental

Catalysts were prepared by a previously described procedure (2). A slurry of 64.4 g of catalyst (32.2 g Fe) and 290 g of Ethylflo 164 decene trimer was charged into a one liter

autoclave operated as a continuous stirred tank reactor. The catalyst was activated with carbon monoxide (2 L h^{-1} g·Fe^{-1}, STP) at 270^{O}C and 1.3 MPa for 24 hours. Following activation, syngas flow was initiated (3.1 L h^{-1} g·Fe^{-1}, STP) and the temperature and pressure were maintained. Catalyst slurry samples (5-10 g) were removed from the reactor under an argon atmosphere via a dipleg immediately after activation and at various times during FT synthesis. Light wax was extracted from the cooled slurry samples under an argon atmosphere with deoxygenated tetrahydrofuran. Catalyst samples were loaded into sealed plexiglass holders for analysis by Mössbauer spectroscopy. The spectra were collected by a conventional constant acceleration spectrometer using a 30 mCi ^{57}Co in rhodium matrix.

Results

Syngas conversion versus time on stream for unpromoted iron catalyst is shown in Figure 1. Syngas conversion after 24 hours of FT synthesis was above 84%. Catalyst activity declined steadily throughout the run with an average rate of deactivation of 0.16 % h^{-1} (absolute syngas conversion).

Catalyst samples for Mössbauer spectroscopy were withdrawn immediately after activation and at 23 h, 168 h and 453 h of FT synthesis. The distribution of iron in the catalyst after activation with carbon monoxide was 94 % χ-Fe_5C_2 and 6 % Fe_3O_4. Exposure to syngas initiated oxidation of the χ-Fe_5C_2 to Fe_3O_4. After 23 hours of FT synthesis, 83 % of the iron was present as χ-Fe_5C_2 and the balance was Fe_3O_4. The amount of iron present as χ-Fe_5C_2 had decreased to 18 % after 168 hours of FT synthesis. The only detectable phase after 453 hours of FT synthesis was Fe_3O_4.

The deactivation rates of Fe-Si, Fe-K, and Fe-K-Si have been determined and the catalyst samples have been withdrawn from the reactor right after activation and at different conversion

levels. The Mössbauer spectra of the catalysts are going to be recorded to identify the phase changes.

The Fischer-Tropsch synthesis activity of unpromoted, potassium promoted (100Fe/0.71K), silica promoted (100Fe/4.6Si) and double promoted (100Fe/4.6Si/0.71K) catalysts were plotted in Figure 2. It can been seen from Figure 2 that Fe and Fe-K catalysts have essentially the same activity during the initial induction period (within 50hrs time on stream) which is higher than Fe-Si and Fe-Si-K catalysts. But the activity of both Fe and Fe-K catalyst decrease steadily with time on stream. For Fe-Si and Fe-Si-K catalysts, they both undergoes an induction period, the activity first goes up until it reaches the maximum and then decrease slowly. After 94 hours of synthesis, the CO conversion of Fe-Si catalyst was 76.1% while the Fe-Si-K catalyst reaches its maximum conversion of 84.04% at 163 hrs time on stream. The average deactivation rate for the catalysts are Fe-K(48%/week), Fe(41%/week), Fe-Si(39%/week) and Fe-Si-K(33%).

Discussion

Based on data generated from several catalysts, a model of the working FT catalyst was developed. In this model, the initial catalyst was essentially comprised of a mixture of iron carbides. As the reaction progressed, the carbide fraction decreased to attain a value of about 30-40%. During this phase change, the conversion did not decrease appreciably. To account for the nearly constant activity while the phase changed a model was proposed. This model had the assumption that the core of each particle was oxidized to form Fe_3O_4 and an out layer remained a carbide form; thus, the surface of the catalyst remained essentially the carbide form while the ratio of oxide/carbide increased as the core consisting of Fe_3O_4 expanded to approach a “steady state at carbide/oxide ratio.

The results with the unpromoted catalyst do not agree with this model. Instead, it appears that the catalyst particle converts from the carbide to the oxide form in parallel with the decline in conversion. Thus, it appears that a steady-state surface carbide phase/core Fe_3O_4 phase is not formed for the unpromoted iron catalyst. One explanation to account for this is that the rate of carbide oxidation is dependent upon the particle size for the unpromoted catalyst. Work underway with single and doubly promoted catalysts should allow us to define the role of each promoter in determining the composition of the working catalysts.

References

1. Dry, M. E. In Catalysis-Science and Technology; Anderson, J. R., Boudart, M. Eds.; Springer-Verlag: New York, 1981; Vol. 1, pp 196-198.
2. O'Brien, R. J., Xu, L., Spicer, R. L., Davis, B. H., Energy & Fuels, 10, 921 (1996).
3. Reymond, J. P., Mériaudeau, P., Teichner, S. J., J. Catal., 75, 39 (1982).
4. Shroff, M. D., Kalakkad, D. S., Coulter, K. E., Köhler, S. D., Harrington, M. S., Jackson, N. B., Sault, A. G., Datye, A., J. Catal., 156, 185 (1995).
5. Berry, F. J., Smith, M. R., J. Chem. Soc. Faraday Trans., 85, 467 (1989).
6. Raupp, G. B., Delgass, W. N., J. Catal., 58, 361, (1979).
7. Huang, C. S., Ganguly, B., Huffman, G. P., Huggins, F. E., Davis, B. H., Fuel Sci. Technol. Int., 11, 1289 (1993).

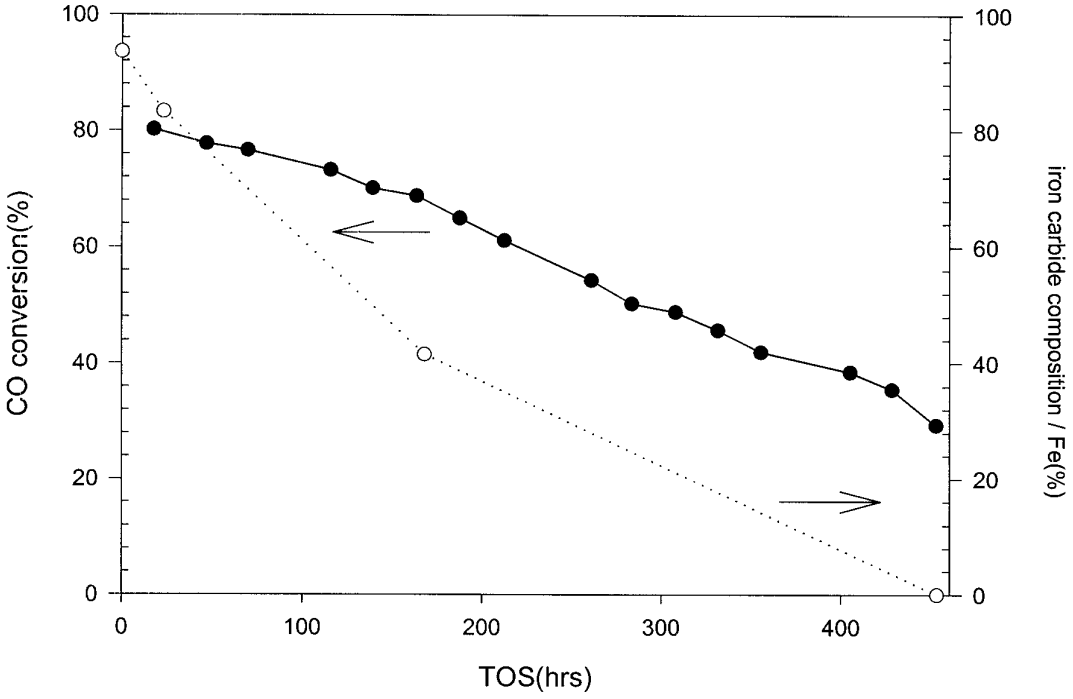

Figure 1. Catalytic activity and iron carbide percentage versus reaction time.

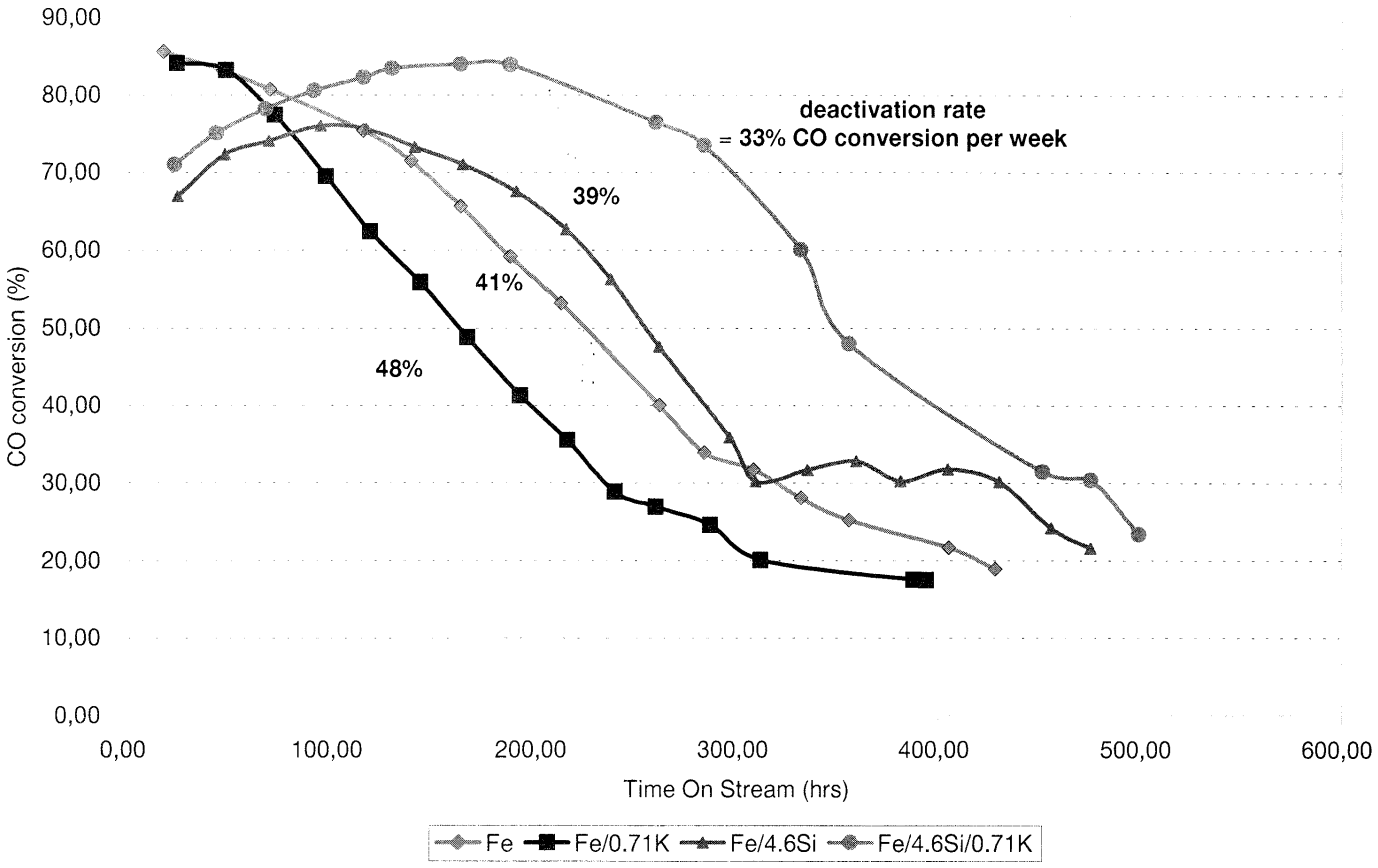

Figure 2. CO conversion as a function of time-on-stream.

B. Characterization of promoted Cobalt FTS Catalysts

Introduction

We have studied and are continuing to study the impact on reducibility of cobalt by the use of different supports and by the incorporation of different promoters and additives to supported cobalt catalysts. Although the use of different supports and promoters is well documented, what is less well understood are the reasons for the differences in deactivation rates of these catalysts. Only by rigorous characterization can the properties of the catalysts brought about by differences in preparation, support, and degree and type of promoter be linked to the resulting catalytic properties under reaction. We therefore have spent considerable attention on the characterization of not only the fresh catalysts, but also the spent catalysts sampled after many days on stream in the continuously stirred tank reactor. With this approach, it is our goal to understand what properties are required for high initial activity and, just as importantly, for the maintaining of high stability, and how to achieve them in the catalyst preparation and activation steps. Interestingly, while addition of promoters can markedly improve the reducibility of cobalt FTS catalysts, leading to more available catalytic sites for reaction, these catalysts often display significantly high rates of deactivation. This raises many questions, which should be able to be addressed through careful characterization. For example, is the reducibility of the metal sites changing under reaction conditions and if so, what are the reasons? Is the cobalt and/or promoter cluster size changing under reaction or is there loss in the degree of interaction between the two? Are we forming mobile metal carbonyl species by the addition of CO that leads to loss of metallic sites and changes in the morphology of the clusters with time onstream? To address these questions, we are employing several characterization techniques, including temperature programmed reduction (TPR), hydrogen chemisorption, X-ray diffraction (XRD), transmission

electron microscopy (TEM), and in the near future, diffuse reflectance infrared Fourier transform spectroscopy (DRIFTS) and X-ray absorption spectroscopy methods (XAS) such as extended X-ray absorption fine structure (EXAFS) and X-ray absorption near edge structure (XANES).

Experimental

BET Surface Area Measurements

BET measurements for all catalysts were conducted to determine the loss of BET surface area with loading. These experiments were conducted using a Micromeritics Tri-Star system. Prior to testing, samples were slowly ramped to 160°C and evacuated for 4hrs to approximately 50mTorr.

Hydrogen Chemisorption by the Temperature Programmed Desorption (TPD) Method

Hydrogen chemisorption was measured using a Zeton Altamira AMI-200 unit which incorporates a thermal conductivity detector (TCD). Catalysts were activated using pure hydrogen at the desired reduction temperature (usually 300 or 350°C) for 10hrs and cooled under flowing hydrogen to 100°C. The sample was held at that temperature under flowing argon to remove physisorbed and weakly bound species, prior to increasing the temperature slowly to the activation temperature. At that temperature, the catalyst was held under flowing argon to desorb remaining chemisorbed hydrogen until the TCD signal returned to the baseline. The TPD spectra was integrated and the amount of desorbed hydrogen determined by comparing to the areas of calibrated hydrogen pulses. Table 2 shows the resulting dispersion based on total weight of metal in the sample for a number of cobalt FTS catalysts.

X-ray Diffraction

Diffraction patterns were recorded using a Rigaku X-ray diffractometer utilizing CuK_{Alpha} radiation. Because quantitative information was desired on particle size, we scanned the

oxidized samples for the peak corresponding to the (311) planes of Co_3O_4, which appears at a 2θ value of approximately 37. Scans were taken using a step size of 0.010°. Because of the level of noise for small cobalt clusters, each point was scanned for 10 seconds to improve resolution. Two different software packages were used to fit the results, Jade and Winfit. Peak position and size values for both software packages are included in Table 2.

Transmission Electron Microscopy

Transmission electron microscopy (TEM) imaging was conducted using a JEOL2000FX, which incorporates a 200keV LaB_6 gun. Samples were first reduced in hydrogen at 350°C for 10hrs in a 2:1 Ar:H_2 mixture (as performed prior to catalytic activity testing) and passivated using 1%O_2 in helium passivation gas. Next, they were passed through a 75 micron sieve, and suspended in isopropyl alchohol, prior to loading onto the Lacey carbon on Cu grid, and subsequent drying. Imaging was conducted at various magnifications including 50, 100, 250 and 400K. Negatives and prints were developed, and clusters counted with size to obtain a distribution, where possible. Figures 1 a and b show a TEM micrograph and resulting particle size distribution for a fresh 0.5% Re promoted 15%Co/Al_2O_3 catalyst, while Figures 2 a and b display results for a spent 0.2% Re promoted 15%Co/Al_2O_3 catalyst sampled after reaching a steady state conversion in the CSTR.

Temperature Programmed Reduction

Temperature programmed reduction (TPR) profiles of fresh and spent catalysts were also recorded using the Zeton Altamira AMI-200 unit. Calcined fresh samples were first purged in flowing inert gas to remove traces of water. Spent catalysts were either removed from the reactor via a dip tube during the run, or sampled after completion of a run. In each case, the catalyst sampled reflected the steady state condition of the run. The wax was first extracted using

xylenes in a Soxhlet apparatus and the catalyst collected in a 33mm×80mm extraction thimble. The catalyst was dried in an oven at 110°C and then reoxidized under flowing dry air after ramping to 250°C before TPR was conducted. TPR was performed using a 10%H_2/Ar mixture and referenced to Ar. Resulting profiles were normalized to the height of the main peak so that shifts in the peak positions could be ascertained.

Results and Discussion

BET Surface Area Measurements

Table 1 displays the BET surface area results. The 15%Co catalysts loaded onto Condea Vista B Al_2O_3 had an average BET surface area of 157 m^2/g. The Davisil SiO_2 supported catalysts had higher BET surface areas, with the 15% loaded catalysts on Davisil 644 SiO_2 support averaging 208 m^2/g and the 15% loaded catalysts on Davisil 952 SiO2 support averaging 229 m^2/g. The 20% loaded catalysts on Davisil 952 SiO_2 support modified by ZrO_2 had a lower average BET area of 197 m^2/g. Not surprisingly, the series of catalysts supported on Davisil 952 (ZYQ028 through ZYQ032) exhibited decreasing surface areas with increasing Co loading. Each 5% increase in loading yielded drops in BET surface area in the order 260, 234, 226, 190, and 170 m^2/g, respectively. The 15% Co catalysts prepared on Shell 980F had an average BET surface area of 103 m^2/g, while the one prepared on Shell 980G was much lower at 52.3 m^2/g. The 15% cobalt catalyst on Dagussa P25 TiO_2 had the lowest BET surface area of 41.8 m^2/g.

H_2 Chemisorption, XRD and TEM

Dispersion calculations were based on the assumption that the H:Co stoichiometric ratio was 1:1. In general, particle size estimates from H_2 chemisorption measurements are based on the assumption that the metal clusters are completely reduced. One determines the total number of atoms from knowledge of the weight % of loading of the metal and the surface atoms from the

desorption of hydrogen. By assuming a particular geometry (e.g., a spherical or cubic structure), one is able to deduce the average cluster size. However, in our case, the assumption of complete reduction may or may not be valid, depending on the support used and type and degree of promotion. TPR results provide a general indicator for the extent of reduction. In the case where metal oxide clusters remain on the surface during chemisorption (incomplete reduction), the cluster size determination will overestimate the cluster size. This may be particularly important for unpromoted catalysts supported on TiO_2 and Al_2O_3, where significant metal-support effects occur. For these samples, a considerable fraction of clusters is reduced at very high temperatures in the TPR profiles. For example, assuming complete reduction for 15%Co/Al_2O_3 leads to a value of 64 nm for the average cluster size. XRD clearly reveals, however, that the cluster is no different in size from the promoted catalysts, however, which are accurately predicted by H_2 chemisorption measurements. Despite the problem with cluster size approximation, the calculated dispersion based on hydrogen uptake should provide an accurate indicator of the number of surface atoms available for reaction, and these can be used appropriately for determining turnover numbers in catalytic testing.

Reaction testing in CSTRs has been conducted primarily on promoted 15%Co/Al_2O_3 catalysts (ZYQ036, 039, 040, and 041). These catalysts displayed the highest uptakes of H_2, significantly higher than that of the unpromoted catalyst (ZYQ000). Assuming complete reduction of the Co in the case of the promoted catalysts, the clusters for fresh catalysts were determined to be approximately 12 nm, 14 nm, 12 nm, and 11 nm for 0.5%Pt-15%Co/Al_2O_3, 0.2%Re-15%Co/Al_2O_3, 0.5%Re-15%Co/Al_2O_3, and 1%Re-15%Co/Al_2O_3 catalysts, respectively. These values are in reasonably good agreement with the values determined by XRD and TEM. For the 0.5%Re-15%Co/Al_2O_3 catalyst, the metal clusters were found to be primarily

approximately 10 nm. For the case of XRD, to convert to the metallic particle size, the multiplier 0.75 should be used. Therefore, it appears that the XRD fitting software Jade fits the results more closely to the actual value, while Winfit apparently underestimates the cluster size.

Characterization of the spent samples was also attempted, and values are reported in parentheses. Further testing is currently being conducted to verify the validity of the results. For example, in hydrogen chemisorption, clusters must be cleaned sufficiently of wax before accurate TPD measurements are obtained. Due to time constraints, in XRD, we only scanned the range where the Co_3O_4 (311) peak occurred at a 2θ of 37. However, further tests are necessary to determine if any other species are present. For example, cobalt rhenium oxide may form after reoxidation for the case of the Re promoted catalysts. Interestingly, a new peak formed at 2θ = 38.5 for spent catalysts, and often dominated in intensity over the peak positioned at 2θ = 37. We are currently investigating the nature of this new peak, which did not appear in the case of the fresh catalysts.

Temperature Programmed Reduction

Figure 3 shows the TPR profiles for the unpromoted cobalt catalysts. For the two SiO_2 supported catalysts, two peaks emerged, attributed to the reduction of Co_3O_4 to CoO, which decomposes at higher reduction temperatures to metallic Co. As shown in the figure, the addition of surface ZrO_2 to silica did not significantly change the reducibility. In addition to the two peaks observed for the Co/SiO_2 catalysts, the TiO_2 and Al_2O_3 supported cobalt catalysts displayed broad peaks at higher temperatures, due to the metal support interaction, which increases with decreasing cluster size. For the Co/Al_2O_3 catalyst, an additional low temperature peak is observed, which we assign to the reduction of cobalt nitrate species. Calcining the

catalyst at higher temperatures removed this low temperature (200°C) peak.. Therefore, the decomposition of Co precursors was concluded to be more difficult on Al_2O_3 support.

Figure 4 shows a TPR comparison of noble metal promoted catalysts prepared using a variety of supports. The addition of Pt or Ru to the support had a similar effect on each of the supported catalysts. All the peaks shifted markedly to lower temperatures, presumably due to spillover of H_2 from the reduced promoter to reduce Co oxide species. Of particular importance, peaks attributed to the metal support interaction for Co species on TiO_2 and Al_2O_3 are reduced at much lower temperatures, freeing up the availability of metal atoms for reaction. For the case of Re, the reduction of Re occurs at higher temperatures than Pt or Ru. This is clearly shown in Figure 4. Although the low temperature peaks are not significantly affected, Re still plays a valuable role in reducing the reduction temperature of species for which there is a significant metal-support interaction.

Figures 5 through 12 show the effect of increasing promoter or additive loadings on the reduction temperature for different supported cobalt catalysts. Figure 5 reports the addition of Ru to the 15%Co/SiO_2 catalysts. With the addition of 0.2% Ru, the greatest shift was found to be that of the low temperature peak which we ascribed to the reduction of Co_3O_4 to CoO. The position of the higher temperature peak assigned to further reduction of CoO to metallic increased slightly. However, further increases in promoter shifted both peaks to lower temperatures. Interestingly, further addition of Ru beyond 1% loading led to only marginal further decrease in temperature.

For the Pt series, the same atomic ratios were used as with Ru, so higher weight percentages of Pt were used. Increasing the Pt loading, in general, led to expected decreases in the reduction temperature, and lower temperatures were achieved on a molar basis with Pt

relative to Ru. One exception to the trend was the 0.97% loaded catalyst. Catalysts will be tested in the future by ICP to verify weight percentages.

Figure 7 demonstrates the impact of modifying the surface of SiO_2 with ZrO_2 and incorporating noble metal promoters. As with the SiO_2 catalysts, a large shift was observed for the low temperature peak when Ru or Pt was added, while only a modest shift to lower reduction temperatures was observed for the higher temperature peak. Interestingly, the Re promoted catalyst behaved much differently, where both peaks shifted slightly to higher temperatures. This suggests that reduction of Re occurs at much higher temperatures than the Pt or Ru catalysts.

Examination of Figure 8 reveals an interesting result when the K concentration is increased for the 15%Co/SiO_2 support. Addition of a small amount (0.5%K) to the catalyst resulted in a remarkable shift to lower temperatures for both peaks (160°C for the low temperature peak and 60°C for the high temperature peak). However, further increases in the K content shifted both peaks back up to higher temperatures, beyond the peak positions of the unpromoted reference catalyst.

Figures 9 through 12 focus on promoting Al_2O_3 support. Unlike the SiO_2 supported cobalt catalysts, there is a strong interaction of the cobalt with the support for a large fraction of the cobalt clusters. Again, evidence for this effect is demonstrated by the broad peak at high temperatures in the TPR profile for the unpromoted catalyst. Therefore, the potential for achieving gains in activity by promoting the support are high.

Figures 9 and 10 show profiles for Re promoted 15%Co/Al_2O_3 catalysts. The difference between the two series of catalysts is in the preparation. The series in Figure 9 references catalysts ZYQ039, 040 and 041, which were prepared by loading the Co three times by successive incipient wetness impregnation steps, where the catalyst was dried between each step.

Only one calcination was used after the last step. Figure 10 references catalysts ZYQ051, 052, and 052. These catalysts were prepared in a similar manner, except that the each of the catalysts was calcined after each sequential impregnation and drying step, for a total of three times. Comparing Figure 10 to Figure 9 reveals that no benefit to reducibility was achieved by calcining the catalyst sequentially.

Figure 9 shows that with each increase in loading of Re promoter, the low temperature peak did not change. Again, we ascribe this to the higher reduction temperature of Re in comparison with the Ru and Pt promoters. Interestingly, however, the high temperature peak shifts markedly with each increase in the Re loading. Therefore, we conclude that after reduction temperature of Re is reached, then spillover of H_2 occurs to lower the reduction temperature of Co oxide species for which there is a significant interaction with the support.

As described earlier, both Pt and Ru promoters behave in a similar manner and shift both reduction peaks to lower temperatures for 15%Co/Al_2O_3. Figure 11 demonstrates that by increasing the loading of Ru, both reduction peaks shift to lower temperatures, with the effect being more pronounced for the low temperature peak. Remarkably, when a loading of 0.5% Ru is achieved, the broad high temperature peak ascribed to the interaction of the support with the metal has shifted by approximately 100°C. Unfortunately, further increases in loading, and in fact doubling the loading, shows only a marginal improvement in reducibility. Two additional catalysts were prepared incorporating La and Zr to the catalysts. However, no change in the low temperature peak was observed.

Metal-support effects were also seen for the 10%Co/TiO_2 catalysts. Therefore, the potential benefits for increasing available metal atoms for reaction by promoting the catalyst were high. A number of different promoted catalysts were tested by TPR, and results are

depicted in Figure 13. While addition of B to the catalyst had adverse effects on reducibility, the noble metals had an enhancing effect. In a similar manner with Al_2O_3, both Pt and Ru shifted all peaks in the TPR profiles to lower temperatures, while Re only benefitted the high temperature peaks.

Although promoted catalysts displayed a higher initial activity as expected, due to increased availability of metal atoms for reaction, the deactivation rates differed greatly. In an effort to further understand the differences in deactivation patterns of promoted supported Co catalysts, we have begun to characterize the spent samples, either removed during the run by a dip tube or after the run. In each case, the catalyst was removed after a steady state conversion was achieved. Again, catalysts was sampled, the wax was removed first by extraction with xylenes in a Soxhlet apparatus, and the catalyst was oxidized in flowing dry air at 250°C.

We wished to determine if significant differences in reducibility occurred by comparing TPR profiles for the spent catalysts in reference to the fresh catalyst. We hypothesized that one route to deactivation might be if the promoter-cobalt interaction was decreased due to segregation, agglomeration, or removal by the leaching out of one or both metals as a mobile species (e.g., a metal-carbonyl). If the reducibility changed, then the TPR for the spent would become more like the TPR profile of the unpromoted catalyst. Therefore, in Figures 15 through 18, we have displayed TPR spectra of the fresh, spent, and unpromoted catalysts such that qualitative comparisons could be ascertained.

Before examining the TPR profiles of the promoted catalysts, it is instructive to first review the TPR profiles of the fresh and spent unpromoted catalysts (see Figure 14). Interestingly, both peaks shift to higher reduction temperatures, and the high temperature peak for the spent catalyst is significantly sharpened. This raises questions as to the reducibility of the

Co with changes in the cluster size. XRD results indicate a decrease in cluster size for the unpromoted catalyst. One might conclude that a smaller cluster would lead to an increase in the interaction between the support and the cobalt and a shift to higher reduction temperatures in the TPR spectra.

Although Pt promotion gave the largest shifts in reduction temperature for the fresh catalysts, in comparison with other promoted catalysts such as Re and Ru, a 0.53% promoted 14.3%Co catalyst displayed a very high rate of deactivation under FTS reaction. Comparison of the TPR for the spent catalyst in reference to the fresh catalyst showed a strong shift to higher reduction temperatures. There is a strong possibility, therefore, that the metal-promoter surface interface decreases under reaction conditions. Future EXAFS investigations may reveal these changes, as EXAFS is one of the most powerful techniques available for determining local structure surrounding the atom of interest. The TPR spectra for the spent catalyst looks much more like the spectra of the unpromoted catalyst than that of the fresh.

Interesting the comparisons for Re and Ru display a much different result. For these catalysts, the reduction peaks appear near or below the peaks observed for the fresh catalysts, indicating that the metal-promoter interaction remains intact under reaction. Interestingly, these catalysts displayed lower rates of deactivation in comparison with the Pt. The peaks of the Re catalysts also were found to be sharper for the case of the spent catalysts. Again, future EXAFS, XRD, and H_2 chemisorption experiments may reveal the reason for the sharpening.

Conclusions

The activity of cobalt catalysts is generally ascribed to the active sites located on the surface of cobalt metal clusters formed after reduction of the oxidic species formed after calcination. However, the reducibility of cobalt catalysts is strongly influenced by the nature of

the support and the degree of promotion by additives, which is the focus of this work. In general, a tradeoff exists as one increases the reduction temperature to activate the cobalt catalyst. Although more sites are reduced, cobalt clusters sinter at higher reduction temperatures. Therefore, TPR and hydrogen chemisorption studies should be conducted prior to catalytic testing, in order to determine the appropriate temperature for catalyst activation. In general, the number of active sites available after reduction varies with support, promoter type, and degree of promotion. The reason for deactivation of promoted FTS catalysts is a subject requiring further study. TPR studies suggest that there is a difference in the degree of interaction of the promoter with the cobalt after reaction testing for each promoter. However, further experiments, using such techniques as EXAFS, are necessary to determine the extent of these morphological changes. Not only will EXAFS allow the determination of cluster size, but the local structure surrounding Co, including the promoter interaction, may be quantified for the fresh and spent catalysts.

The addition of Pt or Ru to the support had a similar effect on each of the fresh supported catalysts. All the reduction peak positions shifted markedly to lower temperatures, due to spillover of H_2 from the reduced promoter to reduce Co oxide species. Of particular importance, peaks attributed to the metal support interaction for Co species on TiO_2 and Al_2O_3 are reduced at much lower temperatures, freeing up the availability of metal sites for reaction. For the case of Re, the reduction of Re occurs at higher temperatures than Pt or Ru. Although the low temperature peaks are not significantly affected, Re still plays a valuable role in reducing the reduction temperature of species for which there is a significant metal-support interaction.

TPR analysis of spent promoted 15%Co/Al_2O_3 catalysts revealed that while observed peaks for Ru and Re promoted catalysts remained shifted to low temperatures, the peaks had

shifted substantially to higher temperatures in the case of the Pt catalyst. This suggests that the Co and Pt interaction is rapidly lost under reaction, and may be the reason for the higher observed deactivation rate.

Table 1

Catalyst Characteristics

Sample ID	Sample Composition	Calcination	BET SA (m_2/g)	+/-	Avg. Pore (nm)	Additional Comments
ZYQ000	15%Co/Al_2O_3	400ºC, flow, 1X	157.7	0.2	4.2	IWI (3X); Condea Vista B, 100-200 mesh
ZYQ001	15%Co/SiO_2	400ºC, no flow, 1X	217.1	0.7	7.7	IWI (3X); Davisil 644 SiO_2
ZYQ002	0.2%Ru-15%Co/SiO_2	400ºC, no flow, 1X	222.0	0.6	7.7	IWI (3X); Davisil 644 SiO_2
ZYQ003	0.5%Ru-15%Co/SiO_2	400ºC, no flow, 1X	233.6	0.5	7.4	IWI (3X); Davisil 644 SiO_2
ZYQ004	1.0%Ru-15%Co/SiO_2	400ºC, no flow, 1X	205.6	0.6	7.6	IWI (3X); Davisil 644 SiO_2
ZYQ005	2.0%Ru-15%Co/SiO_2	400ºC, no flow, 1X	208.9	0.5	7.6	IWI (3X); Davisil 644 SiO_2
ZYQ006	0.39%Pt-15%Co/SiO_2	400ºC, no flow, 1X	200.7	0.6	7.7	IWI (3X); Davisil 644 SiO_2
ZYQ007	0.97%Pt-15%Co/SiO_2	400ºC, no flow, 1X	224.2	0.7	7.6	IWI (3X); Davisil 644 SiO_2
ZYQ008	1.93%Pt-15%Co/SiO_2	400ºC, no flow, 1X	169.6	0.5	4.4	IWI (3X); Davisil 644 SiO_2
ZYQ009	3.86%Pt-15%Co/SiO_2	400ºC, no flow, 1X	217.0	0.6	7.3	IWI (3X); Davisil 644 SiO_2
ZYQ010	0.5%K-15%Co/SiO_2	400ºC, no flow, 1X	210.9	0.5	7.9	IWI (3X); Davisil 644 SiO_2
ZYQ011	1.5%K-15%Co/SiO_2	400ºC, no flow, 1X	200.8	0.5	8.1	IWI (3X); Davisil 644 SiO_2
ZYQ012	3.0%K-15%Co/SiO_2	400ºC, no flow, 1X	168.6	0.4	8.9	IWI (3X); Davisil 644 SiO_2
ZYQ013	5.0%K-15%Co/SiO_2	400ºC, no flow, 1X	214.0	0.6	7.5	IWI (3X); Davisil 644 SiO_2
ZYQ014	15%Co/SiO_2	400ºC, flow, 1X	223.9	0.6	7.5	IWI (3X); Davisil 644 SiO_2
ZYQ015	15%Co/SiO_2	400ºC, flow, 1X	100.0	0.4	15.0	Excess H_2O Impreg (2X); Shell SiO_2 980F, 500 µm
ZYQ016	15%Co/SiO_2	400ºC, flow, 1X	103.4	0.4	15.2	Excess H_2O Impreg (1X); Shell SiO_2 980F, 500 µm
ZYQ017	15%Co/SiO_2	400ºC, no flow, 1X	84.7	0.3	17.3	Excess H_2O Impreg (2X); Shell SiO_2 980F, 500 µm
ZYQ018	15%Co/SiO_2	400ºC, flow, 1X	112.3	0.3	14.8	Excess H_2O Impreg (2X); Shell SiO_2 980F, 250 µm

Sample ID	Sample Composition	Calcination	BET SA (m_2/g)	+/-	Avg. Pore (nm)	Additional Comments
ZYQ019	15%Co/SiO_2	400ºC, flow, 1X	114.2	0.4	15.3	Excess H_2O Impreg (2X); Shell SiO_2 980F, 150 µm
ZYQ020	15%Co/SiO_2	400ºC, flow, 1X	105.5	0.4	15.8	Excess H_2O Impreg (2X); Shell SiO_2 980F, 50 µm
ZYQ021	15%Co/SiO_2	400ºC, flow, 1X	52.3	0.2	10.9	IWI (3X); S 980G 2.3, 60-200 mesh
ZYQ022	15%Co/Al_2O_3	400ºC, flow, 1X	171.3	0.7	2.0	IWI (3X); Condea Vista B, 100-200 mesh
ZYQ023	15%Co/SiO_2	400ºC, flow, 1X	231.9	0.8	7.2	IWI (3X); Davisil 952 SiO_2
ZYQ024	15%Co/TiO_2	400ºC, flow, 1X	41.8	0.2	12.3	IWI (3X); Degussa TiO_2 (P25), 100-200 mesh
ZYQ025	15%Co/SiO_2	400ºC, flow, interval 3X	226.0	0.7	9.1	IWI (3X); Davisil 952 SiO_2
ZYQ026	15%Co/SiO_2	400ºC, flow, 1X	229.3	0.5	7.3	IWI (3X); Davisil 644 SiO_2
ZYQ027	15%Co/SiO_2	400ºC, flow, 1X	240.1	0.7	9.3	Excess H_2O Impreg (2X); Davisil 952 SiO_2
ZYQ028	5%Co/SiO_2	400ºC, no flow, 1X	259.7	1.0	10.0	IWI (1X); Davisil 952 SiO_2, 60-80 mesh
ZYQ029	10%Co/SiO_2	400ºC, no flow, 1X	234.1	0.9	9.8	IWI (2X); Davisil 952 SiO_2, 60-80 mesh
ZYQ030	15%Co/SiO_2	400ºC, no flow, 1X	226.3	0.7	9.6	IWI (3X); Davisil 952 SiO_2, 60-80 mesh
ZYQ031	20%Co/SiO_2	400ºC, no flow, 1X	190.0	0.5	9.0	IWI (4X); Davisil 952 SiO_2, 60-80 mesh
ZYQ032	25%Co/SiO_2	400ºC, no flow, 1X	170.0	0.6	7.8	IWI (5X); Davisil 952 SiO_2, 60-80 mesh
ZYQ036	0.53%Pt-14.3%Co/Al_2O_3	400ºC, flow, 1X	161.6	0.2	4.1	IWI (3X); Condea Vista B, 100-200 mesh
ZYQ037	5%La-15%Co/Al_2O_3	400ºC, flow, 1X	155.1	0.2	3.9	IWI (3X); Condea Vista B, 100-200 mesh
ZYQ038	15%Zr-15%Co/Al_2O_3	400ºC, flow, 1X	160.9	0.1	4.1	IWI (3X); Condea Vista B, 100-200 mesh
ZYQ039	0.2%Re-15%Co/Al_2O_3	400ºC, flow, 1X	156.5	0.2	4.2	IWI (3X); Condea Vista B, 100-200 mesh
ZYQ040	0.5%Re-15%Co/Al_2O_3	400ºC, flow, 1X	136.7	0.2	3.8	IWI (3X); Condea Vista B, 100-200 mesh
ZYQ041	1.0%Re-15%Co/Al_2O_3	400ºC, flow, 1X	187.7	0.2	4.0	IWI (3X); Condea Vista B, 100-200 mesh
ZYQ042	20%Co/ZrO_2-SiO_2	400ºC, flow, 1X	200.0	0.6	8.8	IWI (3X); Davisil 952 SiO_2, 60-80 mesh

Sample ID	Sample Composition	Calcination	BET SA (m_2/g)	+/-	Avg. Pore (nm)	Additional Comments
ZYQ043	0.5%Ru-20%Co/ZrO_2-SiO_2	400ºC, flow, 1X	197.0	0.6	8.4	IWI (3X); Davisil 952 SiO_2, 60-80 mesh
ZYQ044	0.5%Pt-20%Co/ZrO_2-SiO_2	400ºC, flow, 1X	205.5	0.6	9.2	IWI (3X); Davisil 952 SiO_2, 60-80 mesh
ZYQ045	0.5%Re-20%Co/ZrO_2-SiO_2	400ºC, flow, 1X	191.9	0.6	8.9	IWI (3X); Davisil 952 SiO_2, 60-80 mesh
ZYQ050	0.5%Ru-15%Co/Al_2O_3	400ºC, flow, interval 3X	161.0	0.2	3.2	IWI (3X); Davisil 952 SiO_2, 60-80 mesh
ZYQ051	0.2%Re-15%Co/Al_2O_3	400ºC, flow, interval 3X	148.2	0.1	4.0	IWI (3X); Davisil 952 SiO_2, 60-80 mesh
ZYQ052	0.5%Re-15%Co/Al_2O_3	400ºC, flow, interval 3X	151.8	0.1	4.1	IWI (3X); Davisil 952 SiO_2, 60-80 mesh
ZYQ053	2%Re-15%Co/Al_2O_3	400ºC, flow, interval 3X	153.3	0.1	3.9	IWI (3X); Davisil 952 SiO_2, 60-80 mesh
ZYQ054	0.2%Ru-15%Co/Al_2O_3	400ºC, flow, interval 3X	153.8	0.1	4.0	IWI (3X); Davisil 952 SiO_2, 60-80 mesh
ZYQ055	1%Ru-15%Co/Al_2O_3	400ºC, flow, interval 3X	159.1	0.2	3.1	IWI (3X); Davisil 952 SiO_2, 60-80 mesh
LIJ001	10%Co/TiO_2	300ºC, no flow, 1X	---	---	---	IWI: Degussa TiO_2 P25
LIJ002	10%Co-0.1%B/TiO_2	300ºC, no flow, 1X	---	---	---	IWI: Degussa TiO_2 P25
LIJ003	10%Co-0.2%Ru/TiO_2	300ºC, no flow, 1X	---	---	---	IWI: Degussa TiO_2 P25
LIJ004	0.2%Ru-10%Co-0.1%B/TiO_2	300ºC, no flow, 1X	---	---	---	IWI: Degussa TiO_2 P25
LIJ005	10%Co-0.37%Re/TiO_2	300ºC, no flow, 1X	---	---	---	IWI: Degussa TiO_2 P25
LIJ006	10%Co-0.39%Pt/TiO_2	300ºC, no flow, 1X	---	---	---	IWI: Degussa TiO_2 P25

Table 2
Hydrogen Chemisorption and XRD Results

Sample ID	Sample Composition	H_2 Chemisorption % Dispersion	2θ	XRD Co_3O_4 (311) Jade (nm)	XRD Co_3O_4 (311) Winfit (nm)
ZYQ000	15%Co/Al_2O_3	2.40	37.0 (36.9)	18.3 (9.7)	10.3 (6.3)
ZYQ001	15%CoSiO_2	0.85	---	---	---
ZYQ007	0.97%Pt-15%Co/SiO_2	1.24	---	---	---
ZYQ022	15%Co/Al_2O_3	3.03	---	---	---
ZYQ036	0.53%Pt-14.3%Co/Al_2O_3	9.02	37.4 (17.3, 38.6)	13.7 (11.6, 24.5)	9.7 (6.2, 14.4)
ZYQ039	0.2%Re-15%Co/Al_2O_3	7.59 (spent 6.23)	37.0 (36.8, 38.4)	12.5 (6.1, ---)	10.2 (4.9, 20.1)
ZYQ040	0.5%Re-15%Co/Al_2O_3	9.07	---	---	---
ZYQ041	1.0%Re-15%Co/Al_2O_3	9.88 (spent 10.73)	37.1 (37.0, 38.5)	13.0 (8.4)	9.3 (3.3, 32.2)
ZYQ044	0.5%Pt-20%Co/ZrO_2-SiO_2	0.98	---	---	---
ZYQ050	0.5%Ru-15%Co/Al_2O_3	5.00	37.1 (37.1)	---	9.9 (3.0)
ZYQ052	0.5%Re-15%Co/Al_2O_3	5.59	---	---	---
ZYQ053	2%Re-15%Co/Al_2O_3	6.25	---	---	---
ZYQ054	0.2%Ru-15%Co/Al_2O_3	5.58	---	---	---
ZYQ055	1%Ru-15%Co/Al_2O_3	7.11	---	---	---
LIJ001	10%Co/TiO_2	3.64	---	---	---
LIJ002	10%Co-0.1%B/TiO_2	3.19	---	---	---
LIJ003	10%Co-0.2Ru/TiO_2	4.46	---	---	---
LIJ004	0.2%Ru-10%Co-0.1%B/TiO_2	5.12	---	---	---
LIJ005	10%Co-0.37%Re/TiO_2	4.78	---	---	---
LIJ006	10%Co-0.39%Pt/TiO_2	5.11	---	---	---

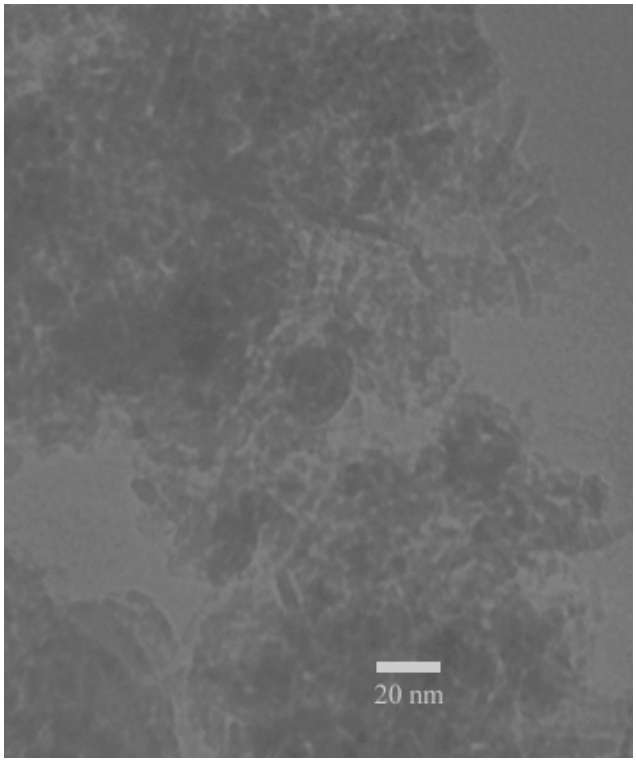

Figure 1a. TEM micrographs for a 0.5% Re promoted 15%Co/Al_2O_3 fresh catalyst.

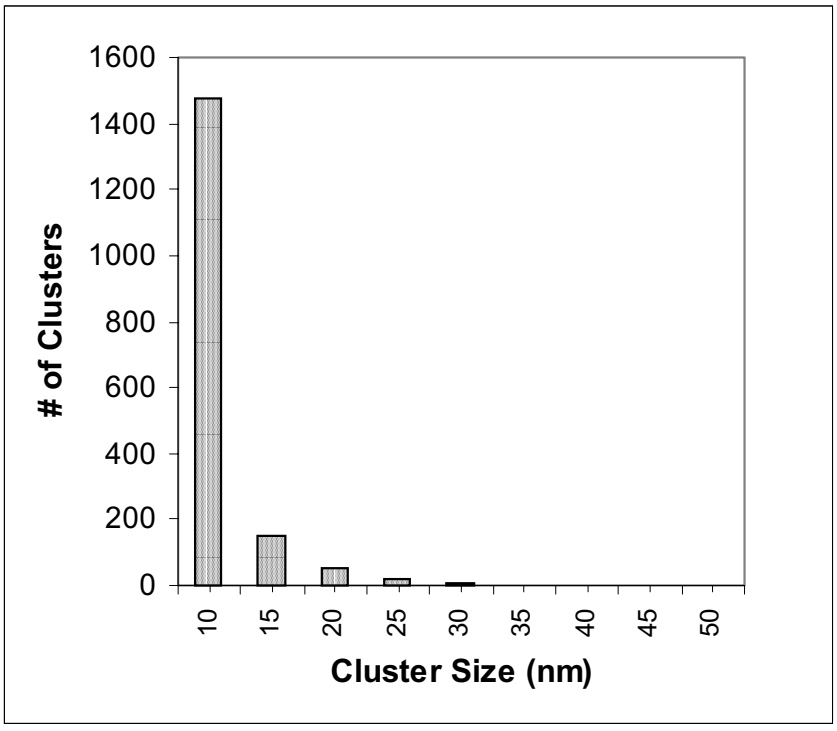

Figure 1b. Particle size distribution from analysis of TEM micrographs for a 0.5% Re promoted fresh 15%$CoAl_2O_3$ catalyst.

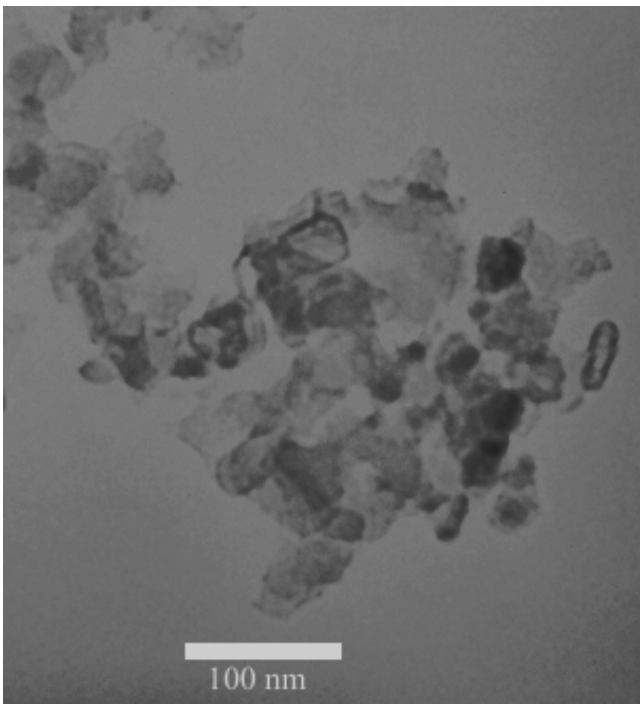

Figure 2a. TEM micrographs for a 0.2% Re promoted 15%Co/Al_2O_3 fresh catalyst.

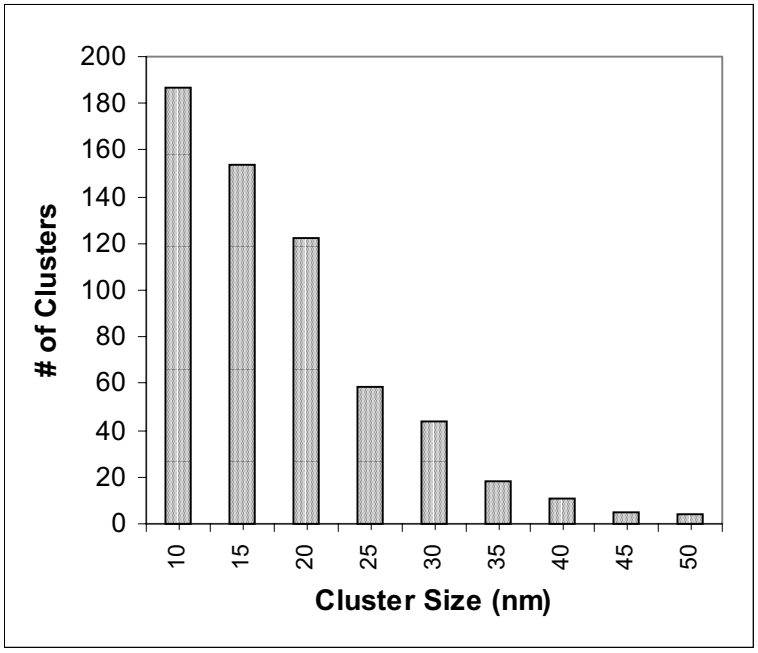

Figure 2b. Particle size distribution from analysis of TEM micrographs for a 0.2% Re promoted 15%Co/Al_2O_3 spent catalyst sampled after reaching a steady-state conversion in the CSTR.

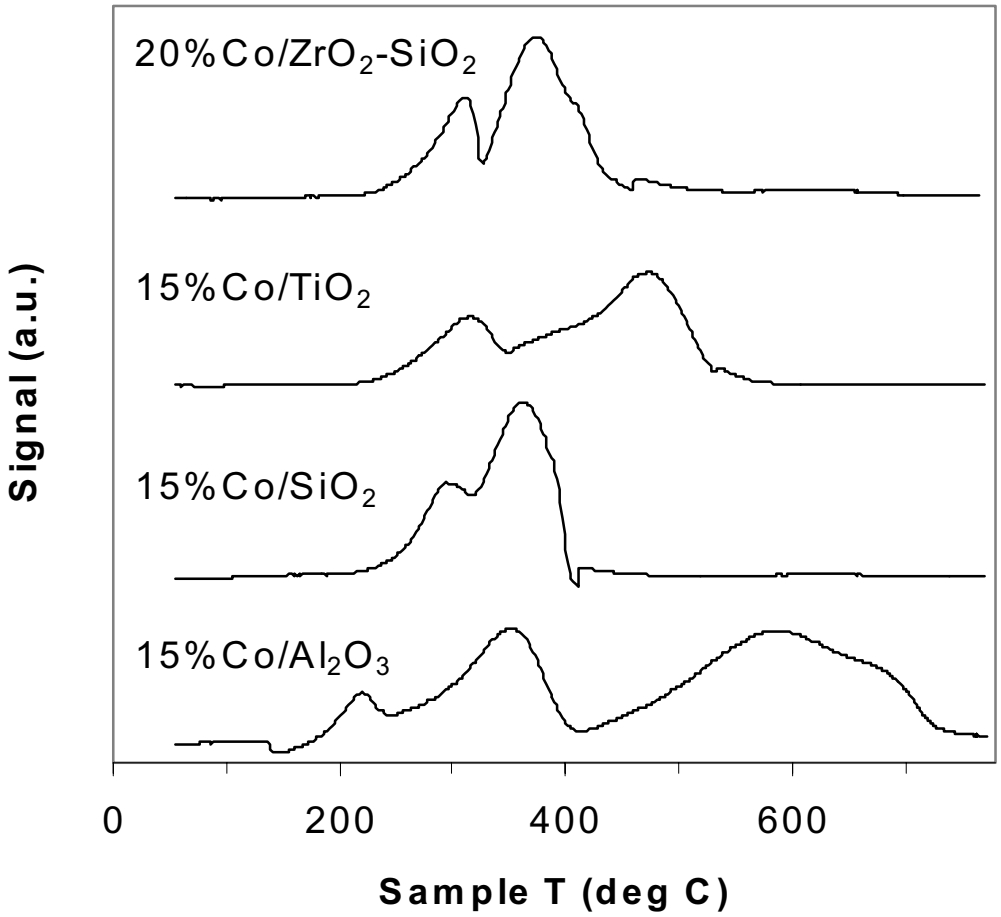

Figure 3. TPR of unpromoted Co catalysts.

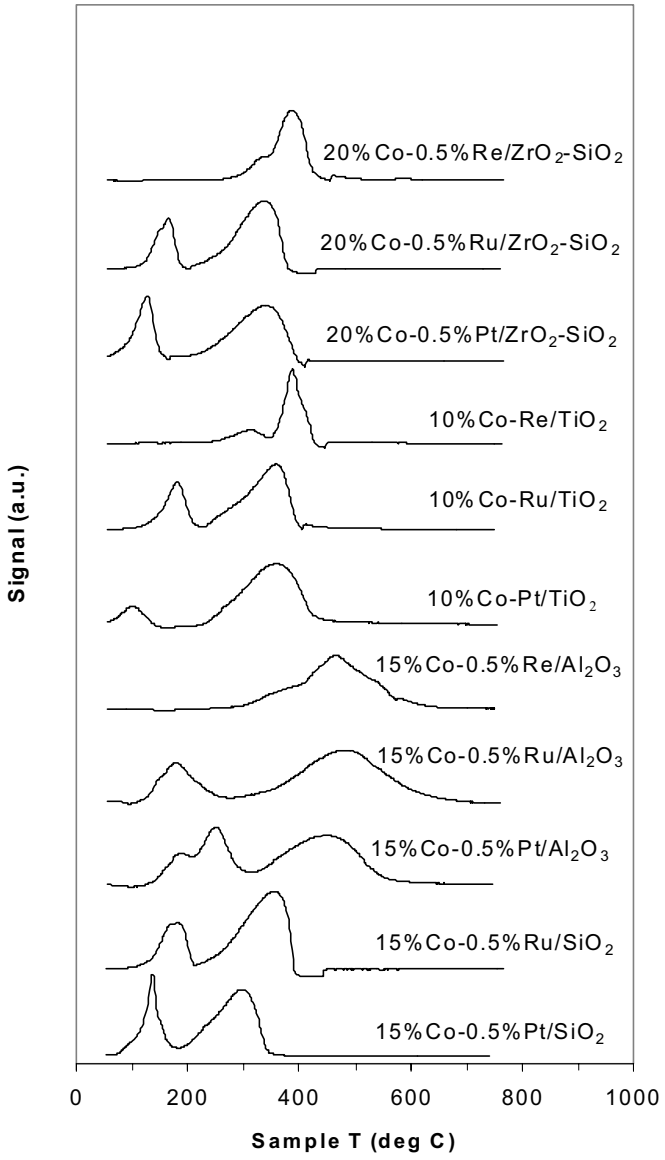

Figure 4. TPR of noble metal promoted Co catalysts.

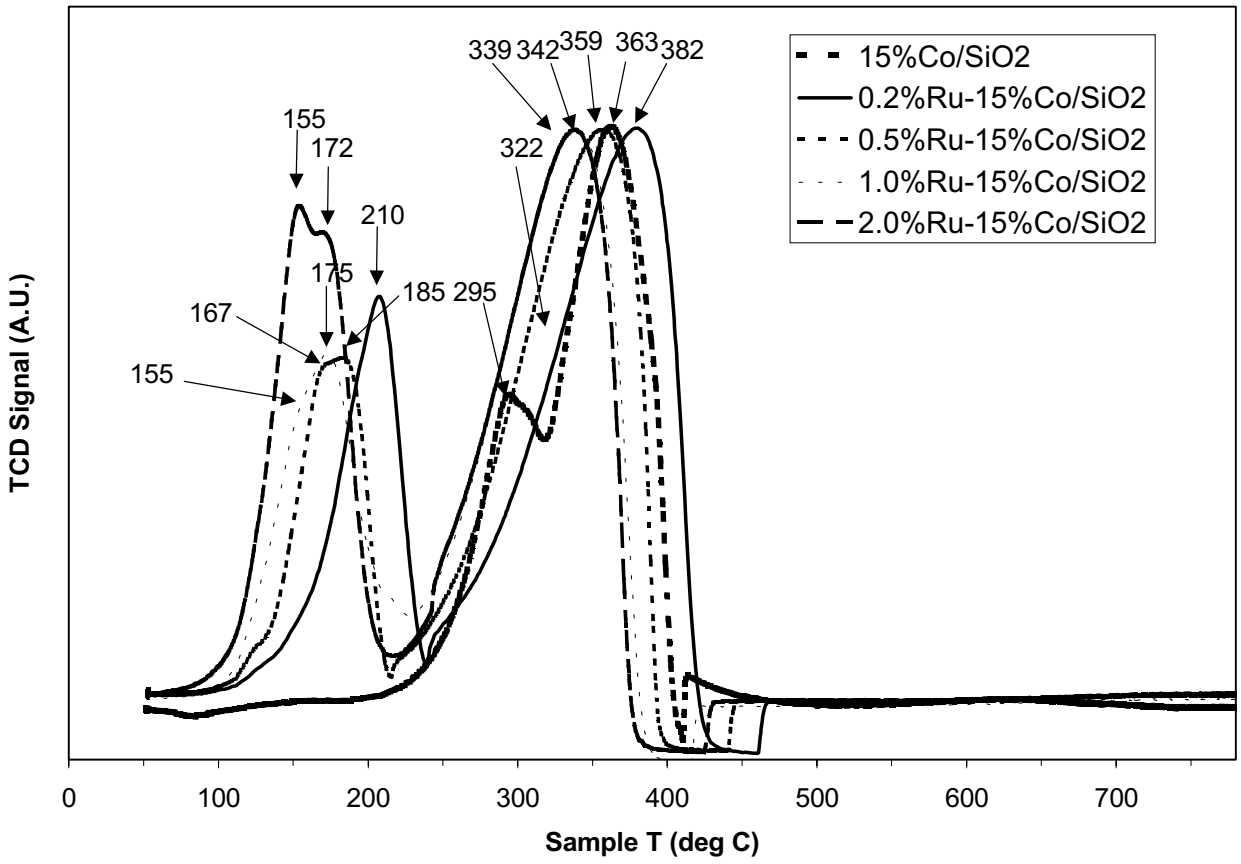

Figure 5. Effect of increasing Ru promoter loading on the reduction temperature of 15%Co/SiO_2.

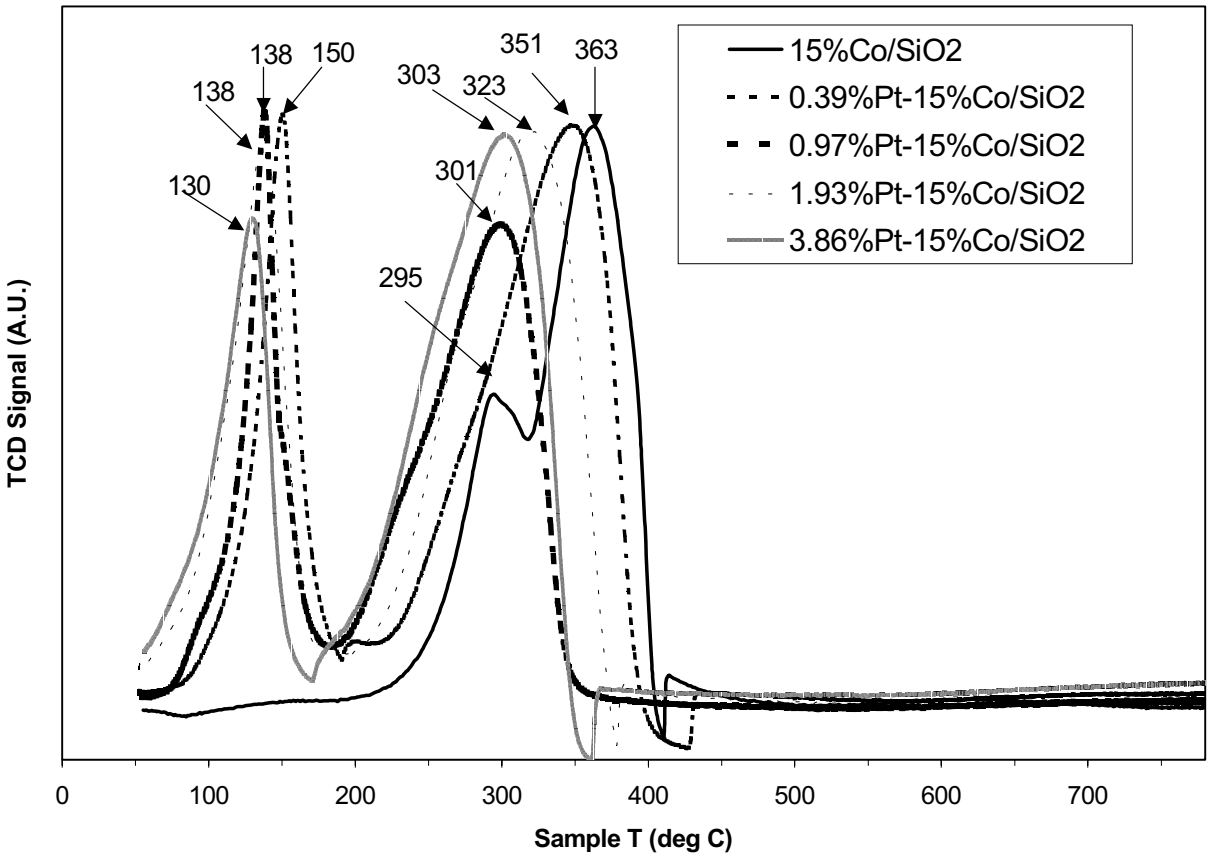

Figure 6. Effect of increasing Pt promoter loading on the reduction temperature of 15%Co/SiO_2.

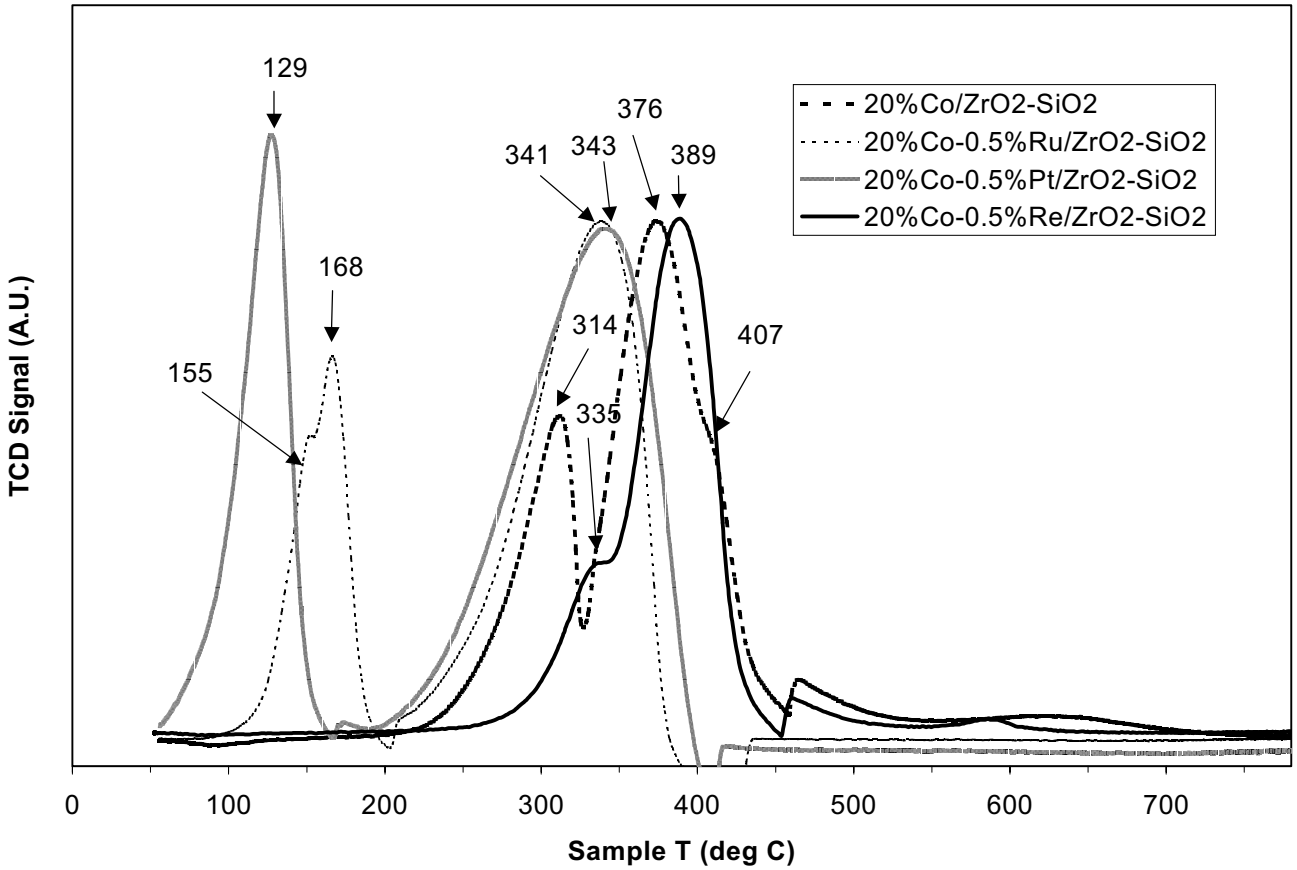

Figure 7. Effect of noble metal promoter type on the reduction temperature of 20%Co/ZrO_2-SiO_2.

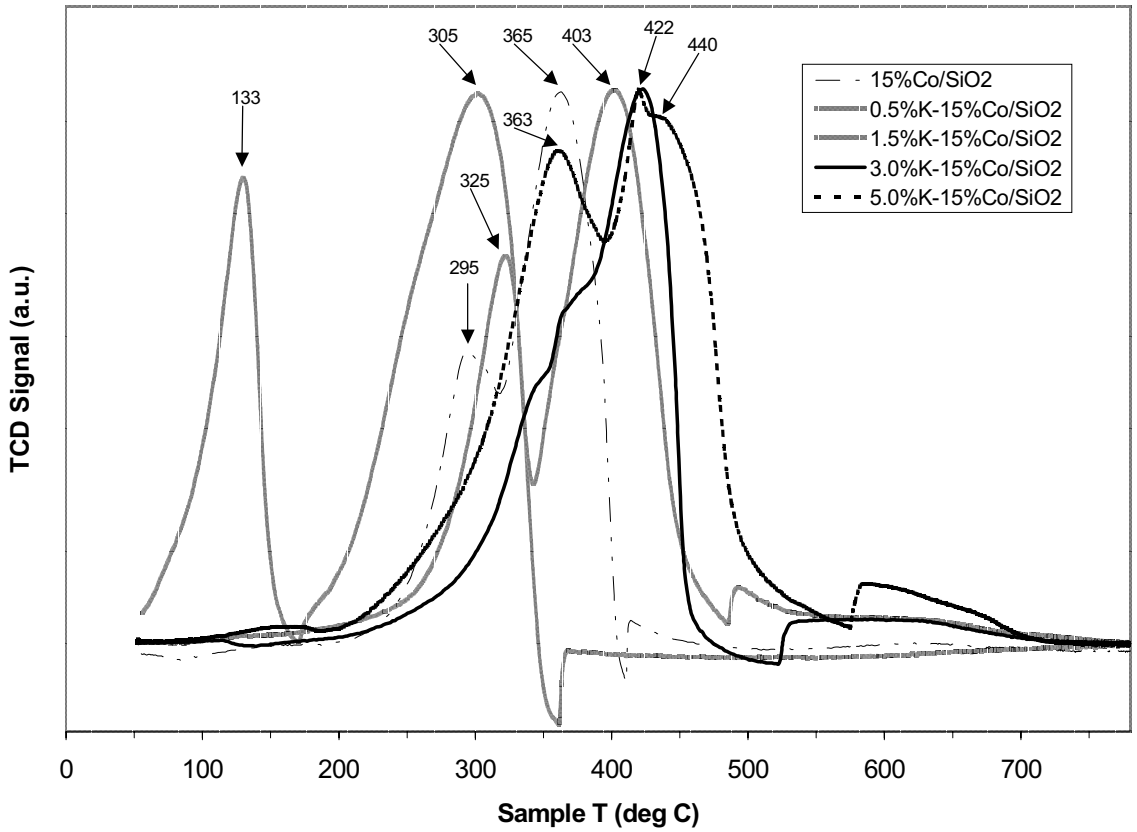

Figure 8. Effect of increasing K additive loading on the reduction temperature of 15%Co/SiO_2.

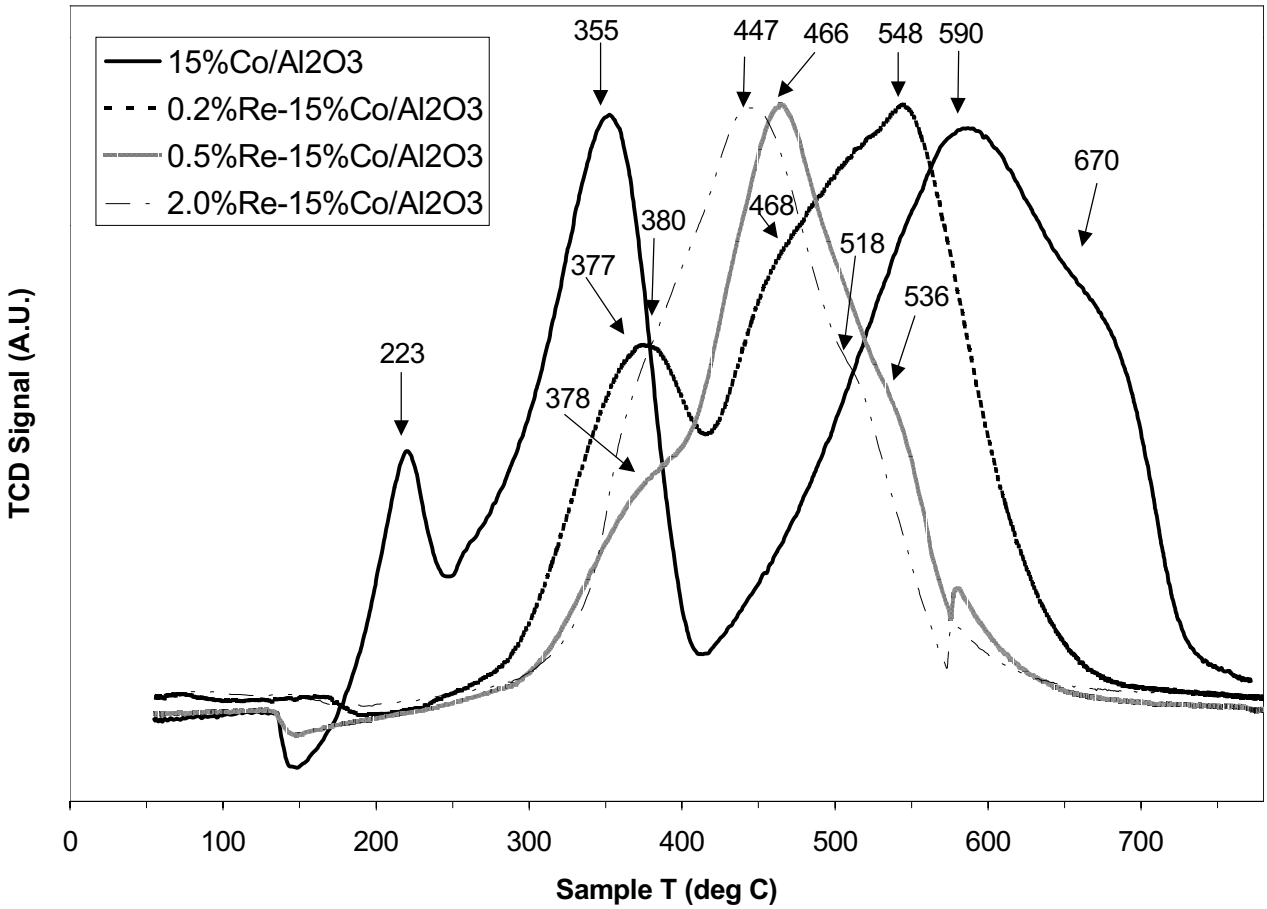

Figure 9. Effect of increasing Re promoter loading on the reduction temperature of 15%Co/Al_2O_3 (three interval drying steps and one final calcination step).

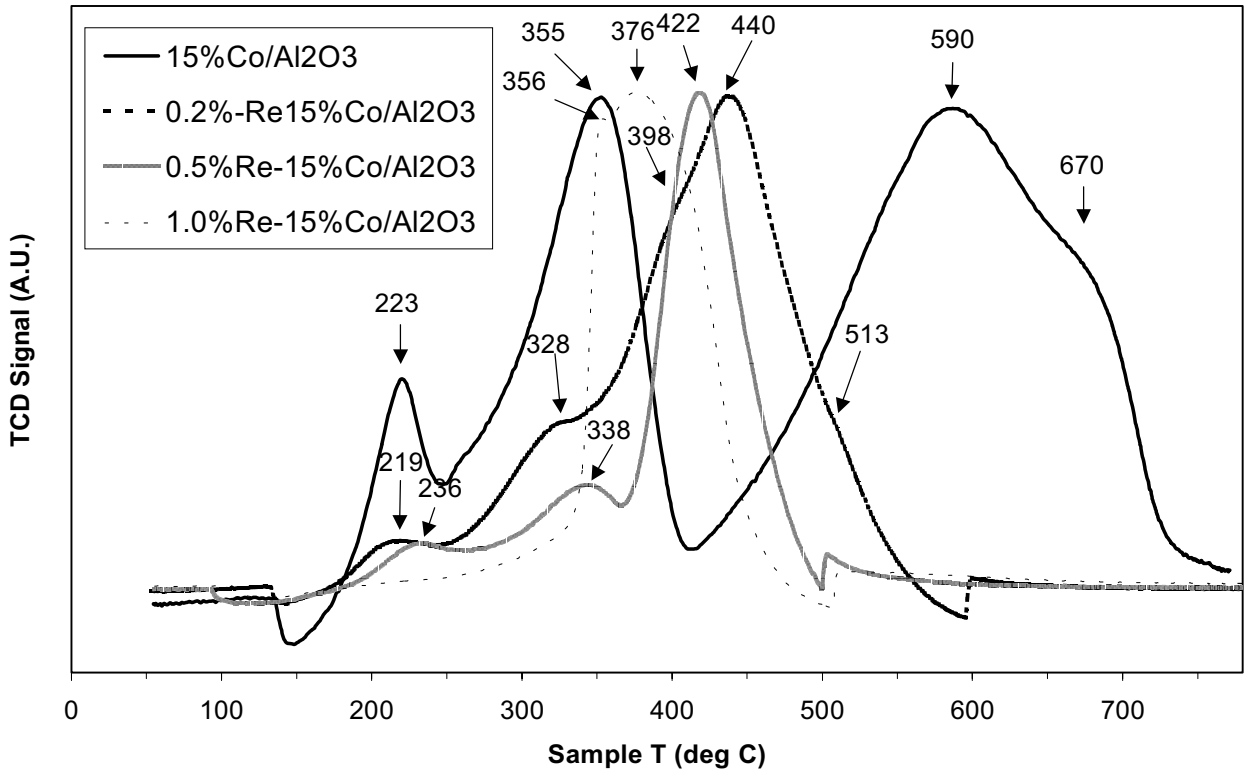

Figure 10. Effect of increasing Re promoter loading on the reduction temperature of 15%Co/Al_2O_3 (three interval drying steps and three interval calcination steps).

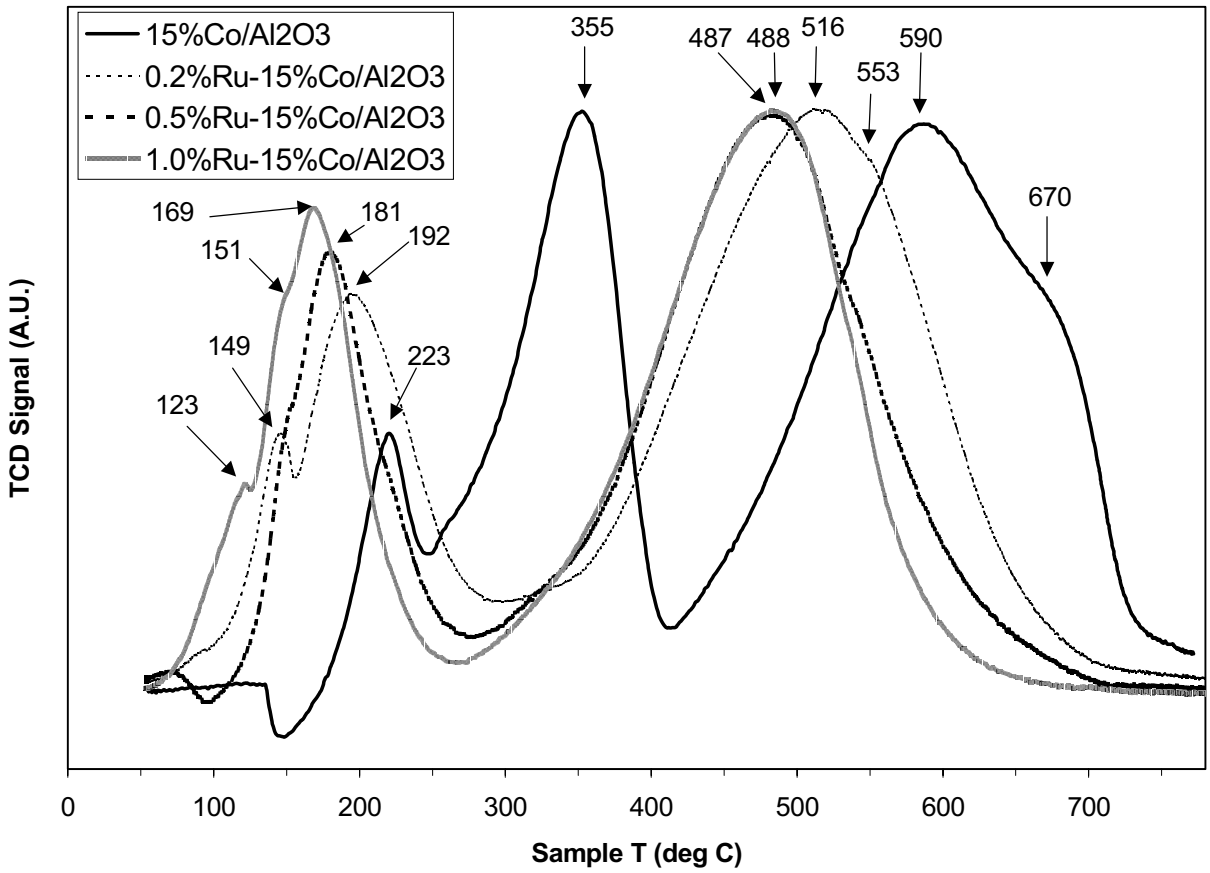

Figure 11. Effect of increasing Ru promoter loading on the reduction temperature of 15%Co/Al_2O_3.

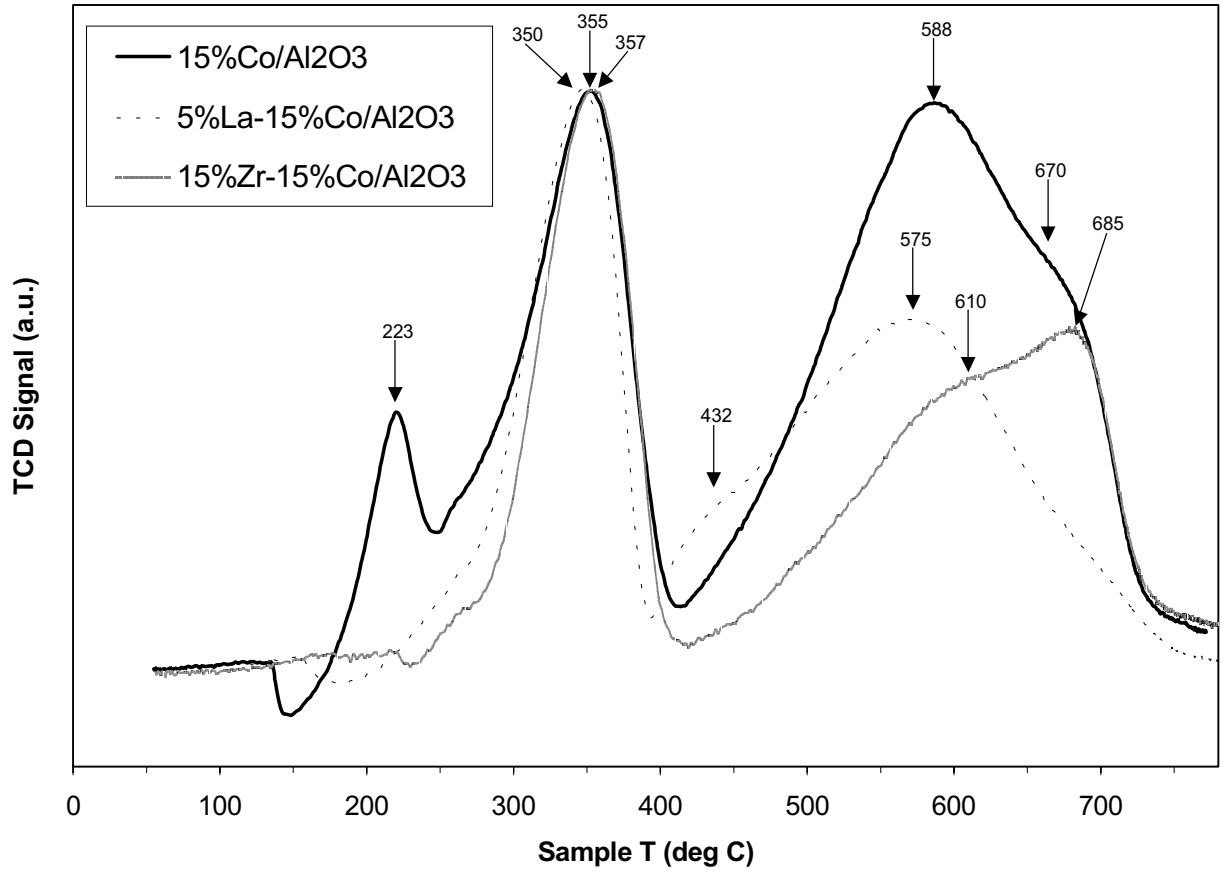

Figure 12. Effect of La or Zr additive on the reduction temperature of 15%Co/Al_2O_3.

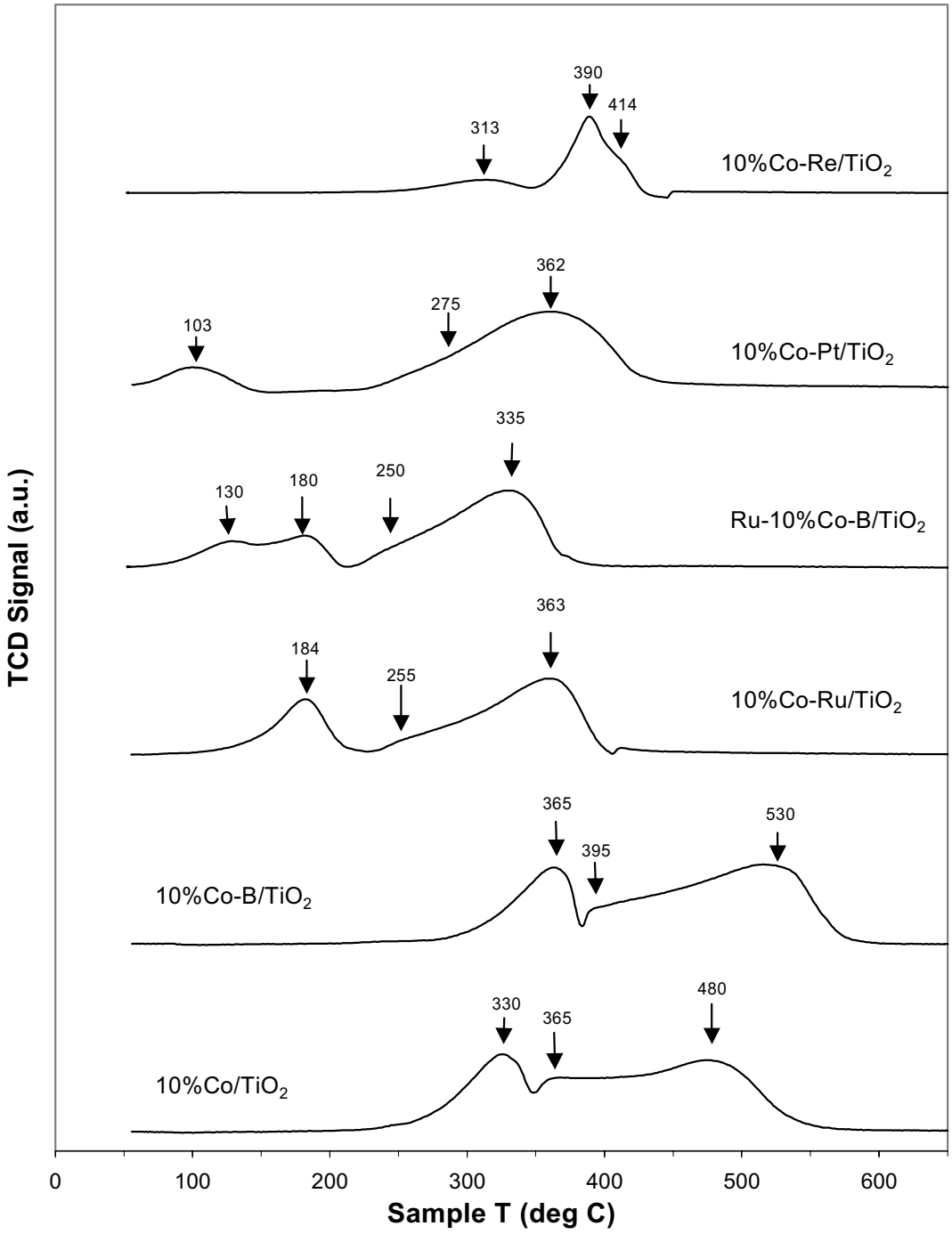

Figure 13. Effect of promoter addition on the reduction temperature of 10%Co/TiO_2.

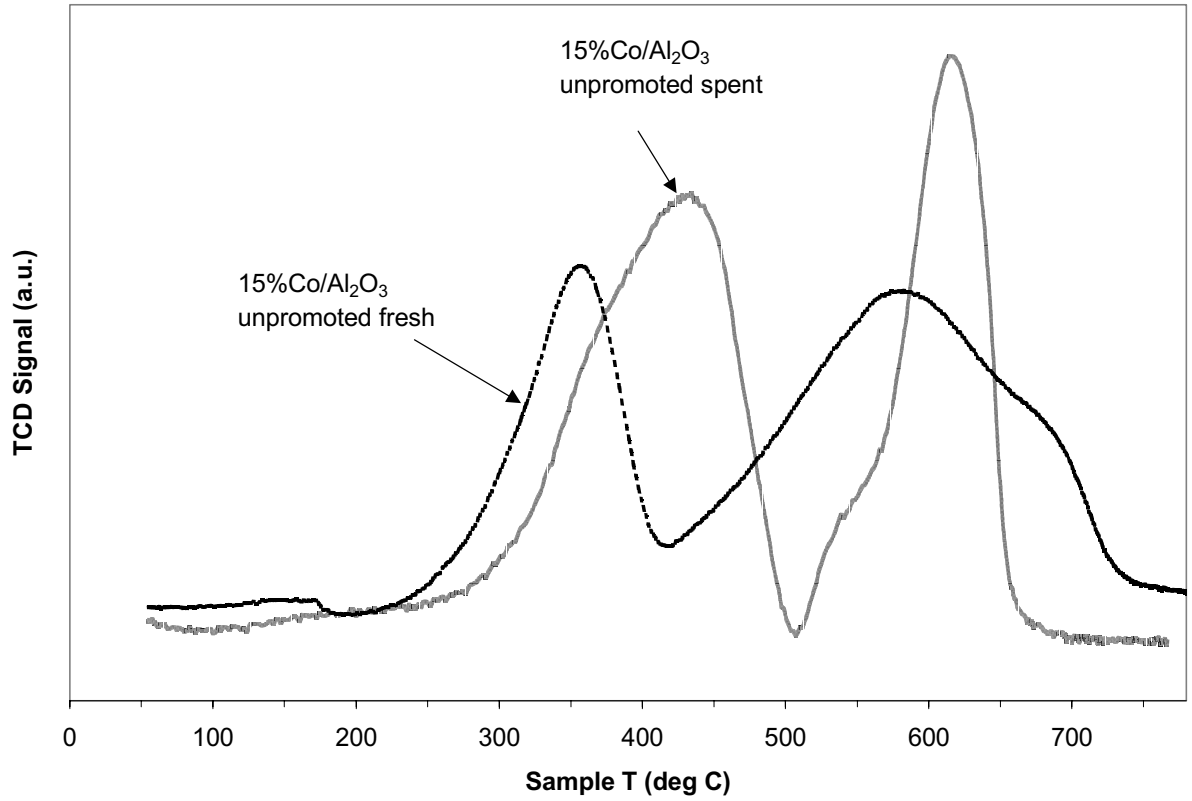

Figure 14. TPR profiles of fresh and spent unpromoted 15%Co/Al_2O_3 catalysts.

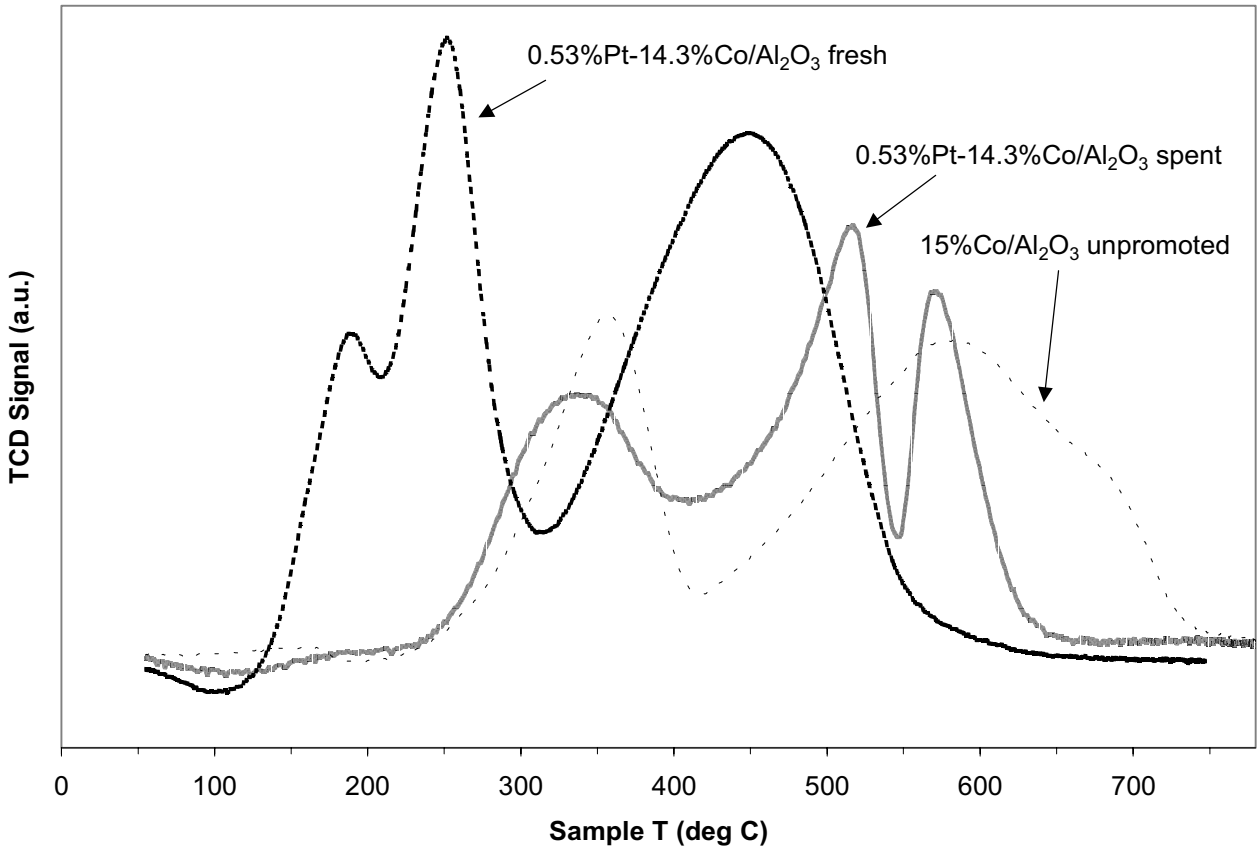

Figure 15. TPR profiles of fresh and spent 14.3%Co/Al_2O_3 catalysts promoted by 0.53% Pt referenced to the unpromoted fresh 15%Co/Al_2O_3 catalyst.

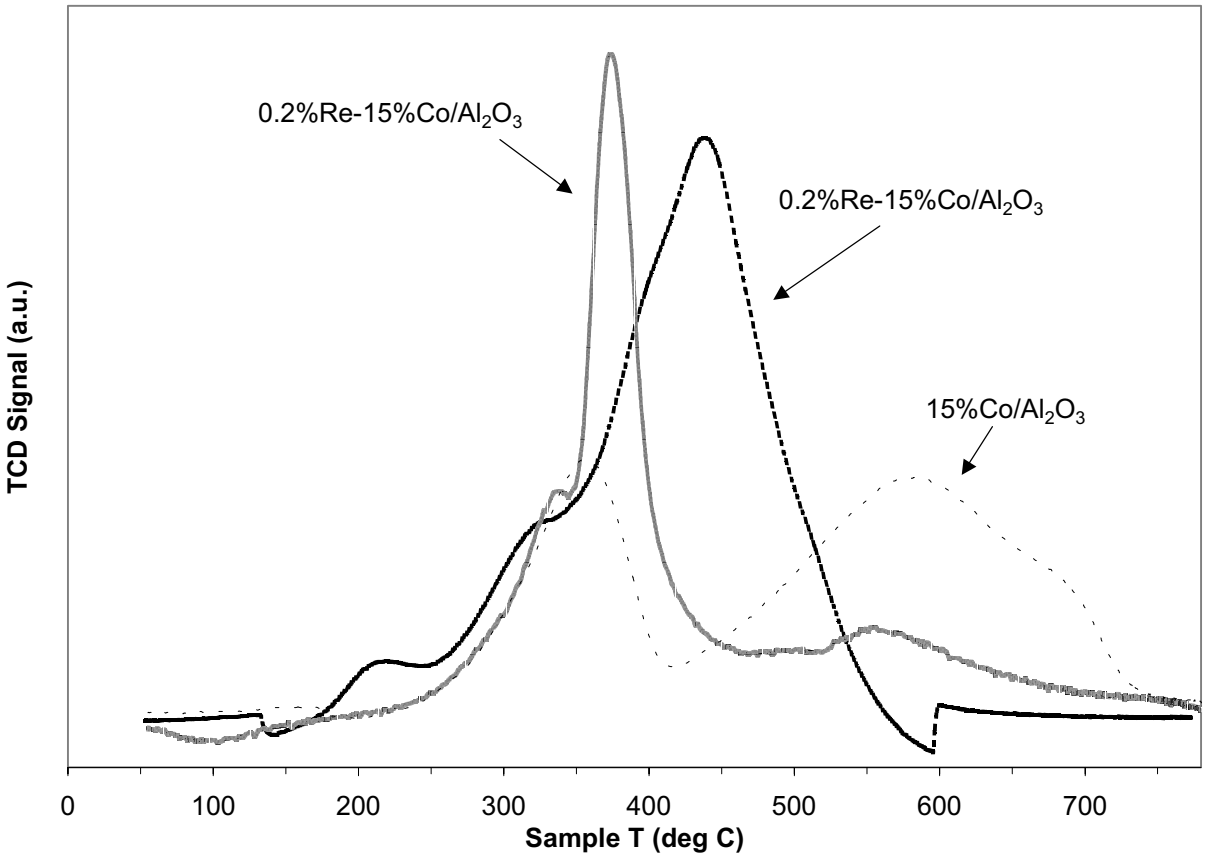

Figure 16. TPR profiles of fresh and spent 15%Co/Al_2O_3 catalysts promoted by 0.2% Re referenced to the unpromoted fresh 15%Co/Al_2O_3 catalyst.

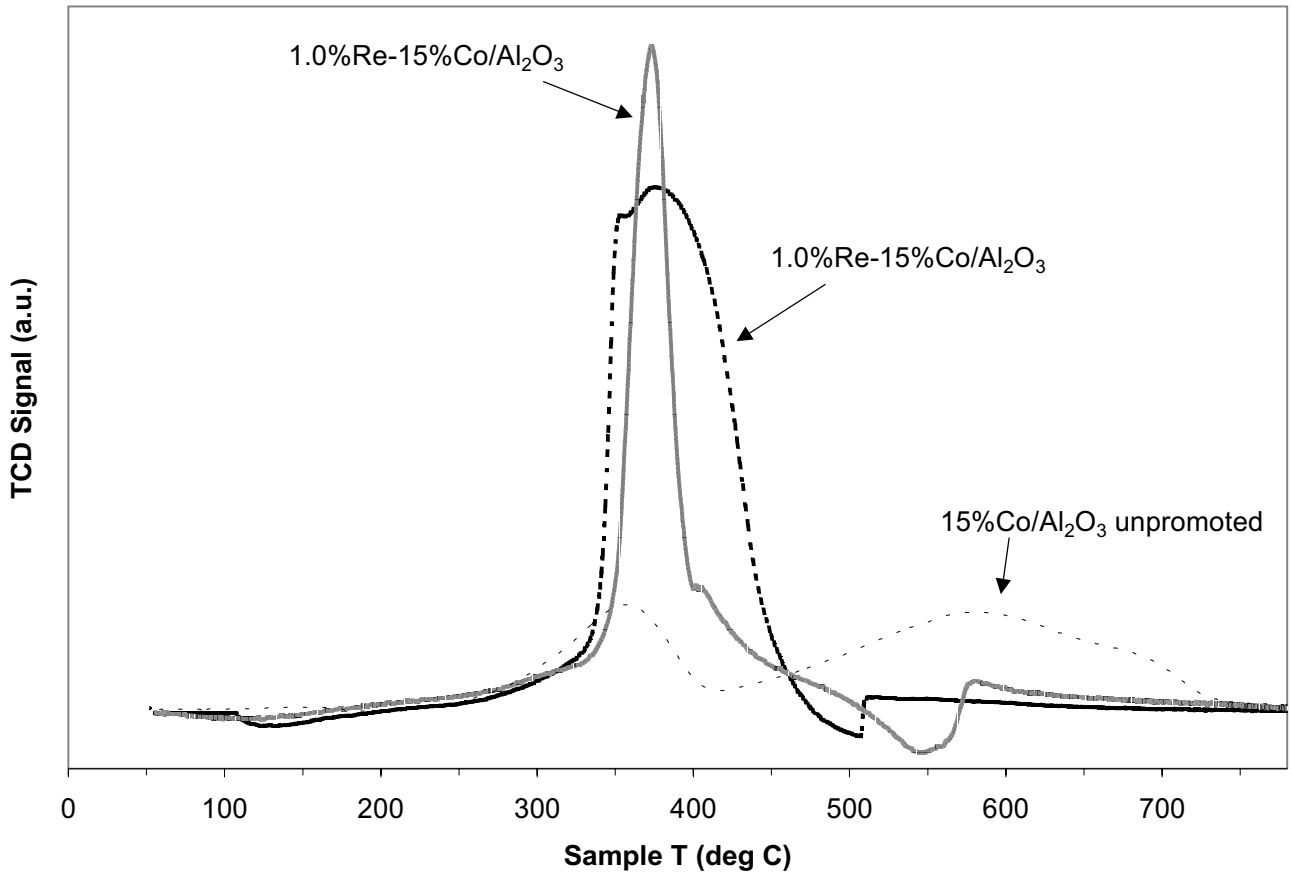

Figure 17. TPR profiles of fresh and spent 15%Co/Al_2O_3 catalysts promoted by 0.2% Re referenced to the unpromoted fresh 15%Co/al_2O_3 catalyst.

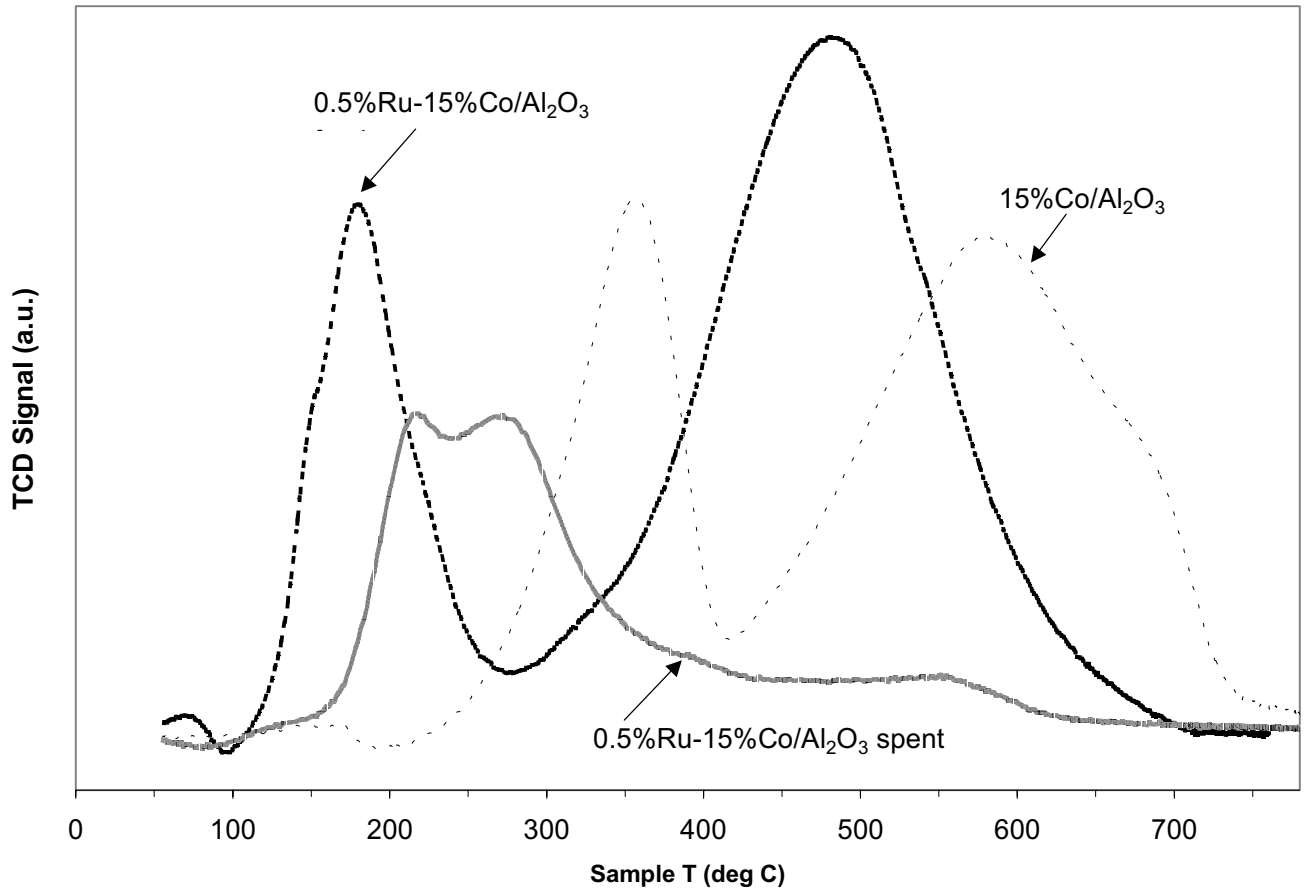

Figure 18. TPR profiles of fresh and spent 15%Co/Al_2O_3 catalysts promoted by 0.5% Ru referenced to the unpromoted fresh 15%Co/Al_2O_3 catalyst.

Task 4. Wax/Catalyst Separation

The objective of this task is to develop techniques for the separation of catalysts from FT reactor slurries.

A. Slurry Bubble Column Reactor (SBCR) Activities

Abstract

The following discussion describes the work done to enhance the CAER's SBCR system. A 5.08 cm diameter by 2 m tubular reactor had been modified to operate in a Fischer-Tropsch SBCR mode. The previous work had focused primarily on catalyst separation from the wax products. Problems with maintaining a constant catalyst inventory within the reactor have been addressed and design modifications are underway. Heat load/loss calculations have been performed to evaluate the need for cooling with high space velocities.

Introduction

Current SBCR Configuration

Currently, the CAER is utilizing the Prototype Integrated Process Unit (PIPU) system for scale-up research of the Fischer-Tropsch Synthesis (FTS).

The PIPU is a pilot plant system built in the early 1980s for studying a multitude of synthetic fuel/chemical processes. In the mid 1990s, a direct coal liquefaction reactor within the PIPU plant was reconfigured as a SBCR for FTS studies (see Figure 1.). The reactor was originally designed to operate with coarse catalyst pellets (>500 μm). Consequently, the reactor system did not contain a wax separation system sufficient for smaller catalyst particles that are typically used in FTS. Therefore, a slurry accumulator and a batch wax filtration system were installed.

The bubble column reactor has 5.08 cm diameter and a 2 m height with an effective reactor volume of 4 liters. The synthesis gas was passed continuously through the reactor. The product gas and liquid exit the top of the reactor and pass through a separation section to a hot condenser (230^{o}C), and a cold separator (3^{o}C). Product wax was batch filtered from the accumulator vessel. A dry flow meter for SBCR was used to measure the exit gas flow rate. A more detailed description of the SBCR was described in the previous final report (ref. 1).

Early attempts to operate the reactor in a F-T mode were successful in that a clear wax product could be obtained. The iron concentration in the wax collected after passing the separation system in the SBCR was about 10 ppm. The initial activity observed in the bubble column was about 10% less than that of comparable CSTR runs. In addition, the rate of conversion decline in the SBCR was much greater than that observed in the CSTR.

This apparent increased deactivation rate in the SBCR may be due to the nature of the wax/catalyst separation system and the physical limitations for controlling the distribution of the catalyst particles between the reactor and a slurry receiver vessel placed overhead. The volume of the overhead receiving vessel (18 L), containing unfiltered wax, is relatively large as compared with the reactor vessel volume (about 4 L). Gas and entrained slurry exit the top of the reactor and are collected in the 18 L vessel. Unfiltered slurry recirculates via a natural convection loop through a dip-tube located inside the reactor. At least 8 liters of slurry must accumulate in the receiver vessel before the wax could be batch-filtered from the catalyst using a Mott sintered-metal filtration tube. This effectively lowers the concentration of catalyst in the reactor slurry phase and thereby increases the space velocity over the course of a run.

Proposed SBCR Modifications

Since we focused primarily on small-scale 1-liter CSTR reactor studies in the last five years, solving the above-mentioned problem with the SBCR had not been a priority. Recently however, industrial involvement regarding catalyst attrition studies, catalyst/wax separation, and bulk wax sample production has renewed interest in operating the SBCR system. Therefore, we are currently making design changes to the catalyst/wax separation system so that the volume of slurry within the SBCR remains at equilibrium. In addition, we are modifying the filtration system to accept a variety of filter elements.

Based on our analysis of previous SBCR runs, the following design objectives were decided upon for enhancing the operation of the SBCR:

1. The level of slurry in the overhead tank should be controlled and quantified so that the amount of catalyst inside the reactor can be accurately estimated;
2. The volume of unfiltered slurry outside the reactor should be minimized; and
3. The modified system should be able to accept a variety of commercially available filter systems.

The proposed design modifications for meeting these objectives are shown schematically in Figure 2. Gas and slurry exit through a port near the top of the reactor column. The slurry will be disengaged from the gas phase in an overhead receiver with a volume of about 4 liters. The level or volume of the slurry within the receiver will be continuously monitored by measuring the differential pressure across the height of the vessel. An argon purge of both pressure legs will keep the lines free of slurry. The volume of slurry within the receiver will be controlled to be no more than 1 liter by removing wax from the reactor system via a control valve. Filtered wax will be held in a heated 18 liter storage vessel. The unfiltered slurry will flow back to the reactor via

a natural convection loop through a dip-tube exiting near the bottom of a reactor. The filter assemble will be located outside the overhead receiver so that changes in the filter media can be made on-line, without aborting or interrupting the reactor run.

Heat Loss Analysis Results

Previously, the SBCR was operated with a slurry catalyst concentration less than 20% and space velocities lower than 5 slpm/g. Since the current reactor configuration does not include a heat removal system, the heat load at higher space velocities (and slurry concentration > 20 wt%) may exceed the heat loss to the surroundings. This is a concern since the small reactor diameter (5.08 cm) limits the placement of internal heat transfer surfaces.

The system heat load due to the heat of reaction was calculated based on a $CO+H_2$ conversion ranging from 70 to 80%. The heat loss was estimated by considering both radiative and convective cooling using the method of Kern (ref.2) for the ideal case of an well-insulated vertical pipe. Results of the heat transfer analysis for operating with a 30 wt% slurry are shown in Figure 3. The point of zero heat load (i.e., when the heat generation is equal to the convective and radiative heat losses) occurs at a space velocity of 2 slpm/g. Therefore, for space velocities greater than 2 slpm/g, heat must be removed and conversely for space velocities less than 2 slpm/g, the heat must be added to the SBCR to maintain a constant temperature.

In reality, the SBCR heat loss may be greater than that of a well-insulted pipe since the reactor is only partially covered with the heating mantel. Thus, the above analysis should be considered a conservative estimate. However, the analysis does indicate that some means of cooling the reactor may be required for high space velocities and conversions. Cooling the reactor vessel shell is not practical because the coils would interfere with the heating mantel used during the initial start-up periods. Cooling surfaces mounted between the mantel and the reactor

could result in localized hot-spots and potentially ruin the heating elements. Since internal cooling is not practical in this case, external cooling of the slurry is being considered. One practical option is to cool the slurry in the overhead accumulator before returning the SBCR.

Conclusions

Once the proposed modifications are implemented, the overall performance of the CAER SBCR will be improved. The reactor slurry level control system will improve the stability of long-duration catalyst deactivation experiments. External slurry filtration will allow for changes in filter media during reactor runs with minimal process upsets. In addition, the design improvements will allow for a more accurate comparison of catalyst performance in the bubble column and CSTR reactors.

References

1. Davis, B. H., Technology Development for Iron Fischer-Tropsch Catalysis, Final Report, DE-AC22-94PC94055, 1997.
2. Kern, D., *Process Heat Transfer*, McGraw-Hill Book Company, 1950.

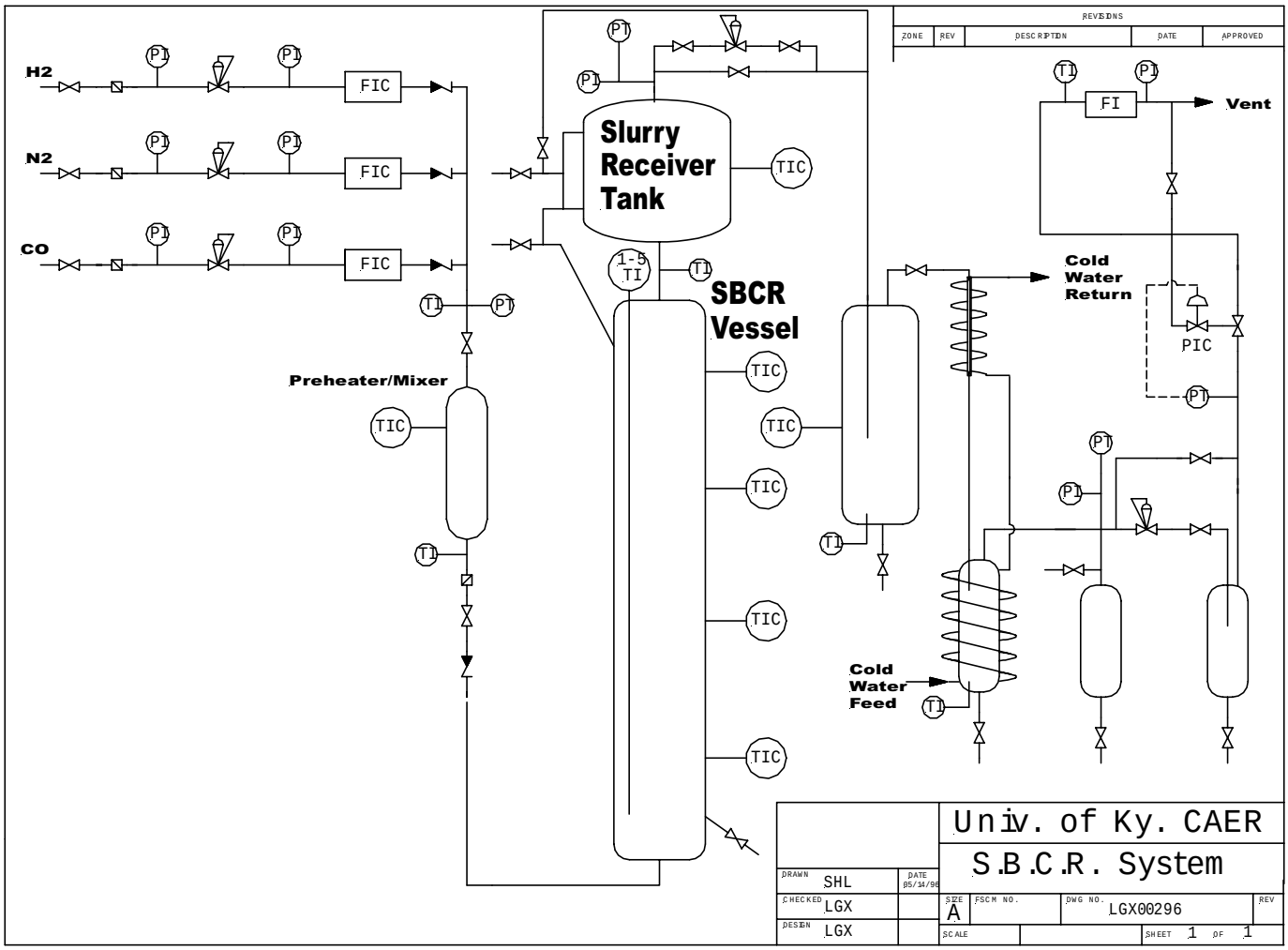

Figure 1. CAER 2" i.d. slurry bubble column reactor system.

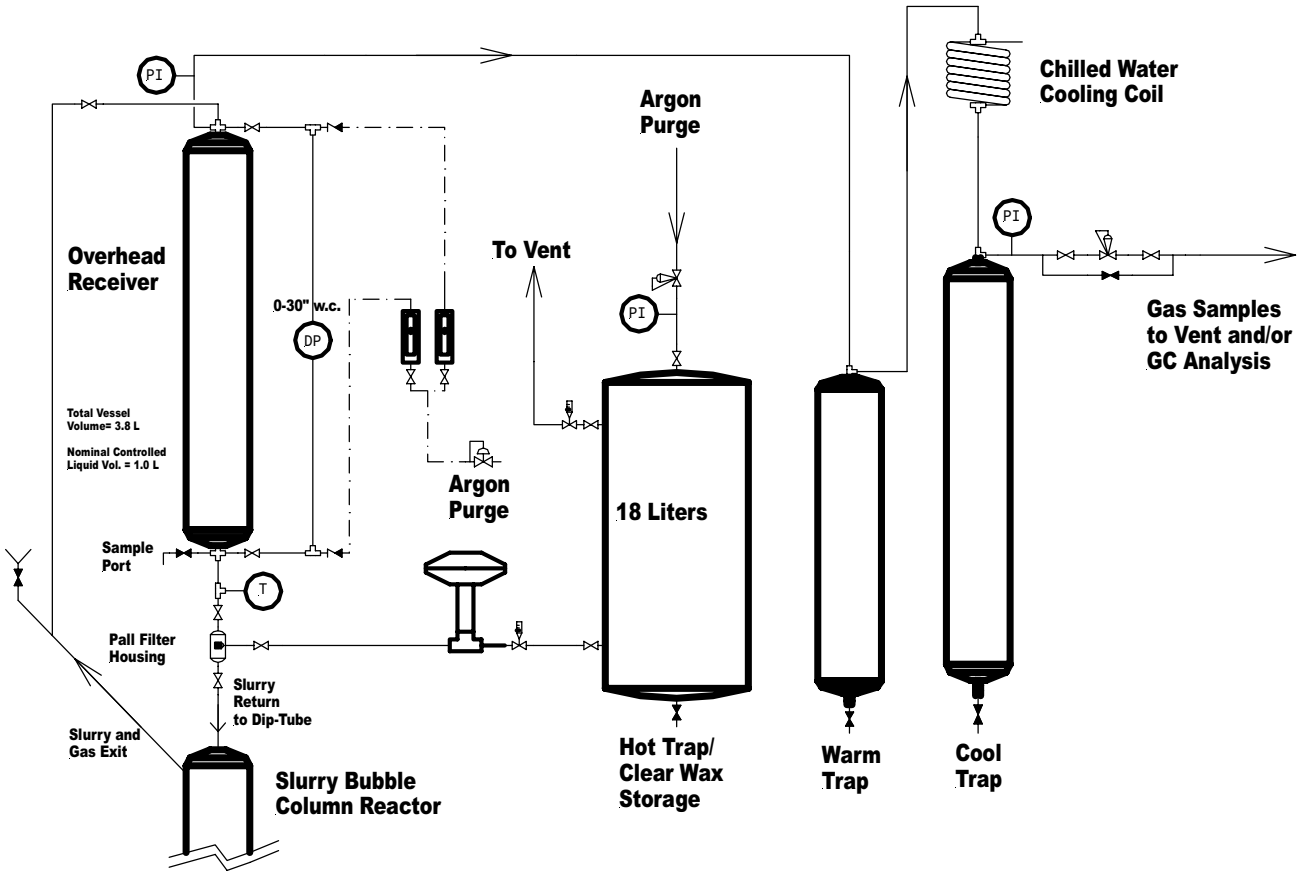

Figure 2. Modified SBCR wax/catalyst separation and sample collection systems.

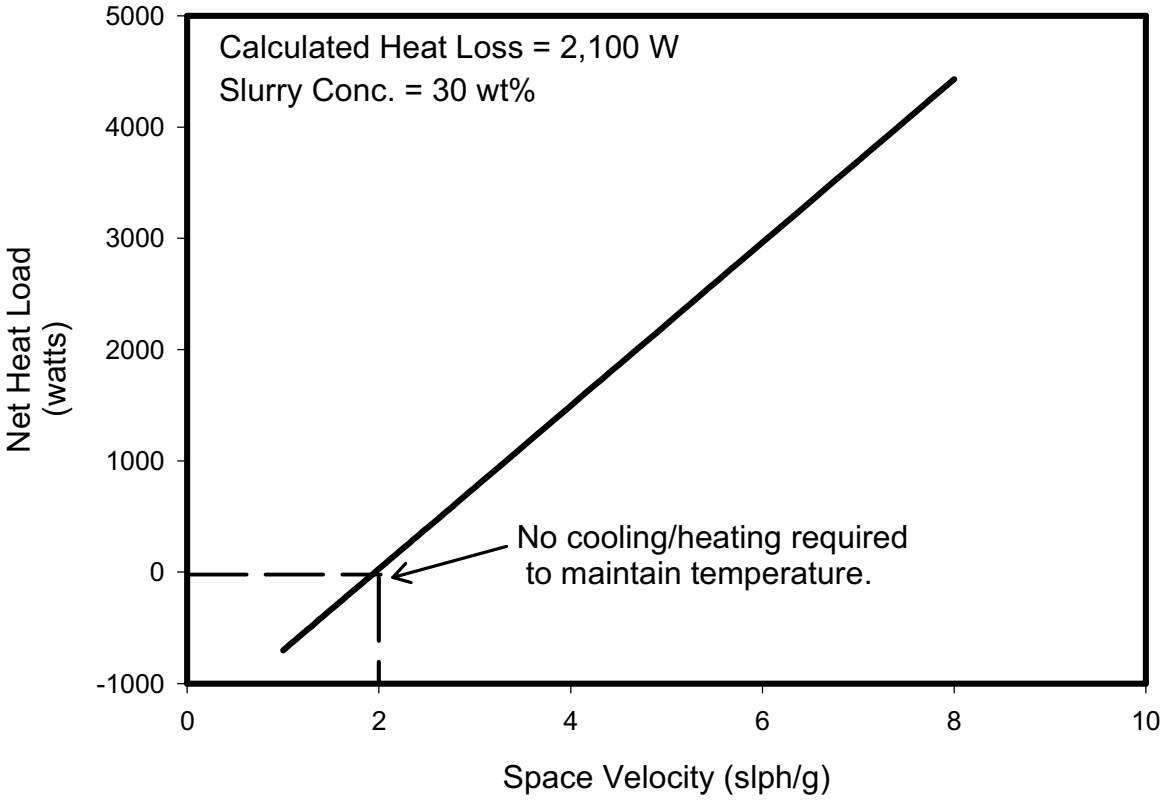

Figure 3. CAER 2" (5.08 cm) i.d. SBCR: effect of space velocity on net heat load.

Task 5. Oxygenates

The objective of this task is to obtain a better understanding of the factors that affects catalyst selectivity toward oxygenates for iron-based Fischer-Tropsch catalysts.

No scheduled activity to report.

Task 6. Literature Review of Prior Fischer-Tropsch Synthesis with Co Catalysts

The objective of this task is to prepare a critical review of prior work on cobalt Fischer-Tropsch catalysts.

Work is continuing on an extensive review of FTS kinetics.

Task 7. Co Catalyst Preparation

The objective of this task is to prepare a limited number of cobalt-based Fischer-Tropsch catalysts that can be used to obtain baseline data on cobalt-based Fischer-Tropsch synthesis.

See Task 8.

Task 8. Cobalt Catalyst Testing for Activity and Kinetic Rate Correlations

The objective of this task is to conduct initial screening of the cobalt catalysts prepared in Task 7 to select three baseline catalysts that will then be used to generate a data base on the performance of cobalt-based Fischer-Tropsch catalysts in slurry reactors.

A. CO and CO_2 Hydrogenation over Co-Pt/Al_2O_3 Catalyst

Introduction

The feed syngas from natural gas contains a small amount of CO_2, the effect of CO_2 therefore should be studied to determine the necessity of separation of CO_2 from syngas. Study of CO_2 hydrogenation will also help us understand the mechanism for methane formation. CO_2 methanation is important in production of substitute natural gas, since it contributes additional methane needed to meet heating value specifications. Two categories of mechanisms for CO_2

hydrogenation has been proposed based on the early work done on nickel catalysts, (1) conversion of CO_2 to CO via the reverse water gas shift reaction followed by CO methanation, and (2) direct hydrogenation of CO_2 to methane by a mechanism distinct form CO methanation.

Previous works on CO and CO_2 hydrogenation of our group leads to the conclusion that CO hydrogenation rate is much higher than CO_2 over cobalt catalyst and CO_2 methanation goes through methanol as an intermediate.

The purpose of this investigation is to determine the deactivation rate for CO_2 hydrogenation at different H_2:CO ratio and different conversion level, as well as the deactivation rate of CO hydrogenation. We would probably have a better understanding of the mechanism of deactivation.

Experimental

Preparation of Co-Pt/Al_2O_3

Condea vista B alumina with a surface area of 300m^2/g, pore volume of 1.15m^3/g was used as support materials and the cobalt loading was 15%. A multi-step incipient wetness impregnation method was used to add cobalt nitrate solution to alumina with a drying procedure after each impregnation at 80^{0}C in a rotary evaporator. Following cobalt addition, tetramineplatinum nitrate solution was e added by an incipient wetness impregnation method and the platinum loading was 0.5%. The catalyst was then dried in a rotary evaporator at 80^{0}C again and calcined at 400^{0}C for 4hrs.

Fixed-bed Fischer-Tropsch Synthesis Study

3g of Co-Pt/Al_2O_3 catalyst was diluted by 15g of glass bead and then loaded in a two inch diameter reactor, a three zone furnace was used to control the temperature of the reactor. Four Brooks mass flow controllers were used to control the flow rate of CO, CO_2, H_2 and He. Fischer-

Tropsch synthesis was conducted at 210^0C, 350psig with H_2:CO=2:1 and GHSV=5.0SL/hr/gcatalyst(H_2:CO:He=2:1:2). CO_2 hydrogenation was tested at same temperature and pressure but with H_2:CO ratio of both 2:1(H_2:CO:He=2:1:2) and 4:1(H_2:CO_2:He=4:1:4). The space velocity was changed from 9.0SL/hr/gcatalyst to 5.0 SL/hr/gcatalyst.

Results and Discussion

Since we use H_2:CO ratio of 2:1 as the feed gas, the highest CO_2 conversion is 50%. At time on stream 48hr, CO_2 conversion observed was 45% which is close to equilibrium. The fact that the conversion decreased at 0.81% CO_2 conversion per day indicated that the catalyst is reasonably stable for CO_2 hydrogenation. In order to investigate the stability of catalyst far from equilibrium, we increased the flow rate from 5.0SL/hr/gcatalyst to 9.0SL/hr/gcatalyst. The deactivation rate became even lower(from 0.81% to 0.69% CO_2 conversion per day) and the activity range maintained at about 20% CO_2 conversion range.

One of the assumptions for the deactivation mechanism of cobalt Fischer-Tropsch synthesis catalyst is the oxidation of surface cobalt to oxide or cobalt aluminate by water. Our assumption of the oxidation mechanism is that when H_2O/H_2 partial pressure ratio goes up to certain point, the oxidation of the cobalt cluster starts to occur. For CO_2 hydrogenation when the conversion level is at 40%, the H_2O/H_2 partial pressure ratio is about 2.0 and is much higher than CO hydrogenation (0.3 at 40% CO conversion). But for CO_2 hydrogenation, the deactivation is not so obvious (figure 1 is the CO_2 conversion as a function of time on stream). One explanation is that the oxidation only occurs to the small clusters and the methanation of CO_2 is catalyzed by the larger cobalt clusters. The other explanation is that the surface oxidation did not occur as fast as CO hydrogenation. That makes the assumption of H_2O/H_2 partial pressure ratio as the decisive factor for the oxidation invalid. It also brings up another explanation of the deactivation of CO

hydrogenation, which is H_2O/CO ratio is a more important factor. One possibility is that the adsorption of H_2O and CO are competitive and since more H_2O has been formed, the less CO can been adsorbed. But the results of CO_2 hydrogenation eliminate that possibility; therefore, one can conclude that H_2O and CO has formed some kind of intermediate which caused the oxidation or crystal growth of cobalt clusters.

Since the methanation of CO_2 requires H_2:CO ratio of 4:1, we adjusted the feed gas to this ratio to further study the stability of the catalyst and the results are shown in figure 2. When the conversion level is 42%, the catalyst did not deactivate after 24hrs, then the flow rate was decreased to achieve a conversion of about 55%; the catalyst started to deactivate slowly but leveled off at about 40% CO_2 conversion. It can been concluded that during CO_2 hydrogenation, deactivation is slower than for CO hydrogenation even at high conversion levels.

After 504 hours of using CO_2 as a feed gas, CO hydrogenation was studied with a H_2:CO ratio of 2:1 and space velocity of 5SL/hr/gcatalyst. Figure 3 shows the results of CO conversion as a function of time on stream, and figure 4 is CO and CO_2 conversion as a function of time on stream when CO was used as the feed gas first. It can been concluded that CO_2 hydrogenation did cause deactivation of the catalyst for subsequent CO hydrogenation since, after 504 hours of time on stream, CO conversion decreased from 52.5% to 28.7%. However, it can been seen from figure 3 that the deactivation rate of CO hydrogenation is much faster than CO_2 hydrogenation at 30% CO conversion. If the feed gas is CO and the conversion is 60%, the deactivation rate could have been much higher and after 504 hours of time on stream, CO conversion rate would have been much lower than 28.7%. From figure 3, it seems that the CO conversion stayed at about 20% and it agrees with our CSTR data that the deactivation rate is a function of CO conversion level; the lower the CO conversion, the lower the deactivation rate.

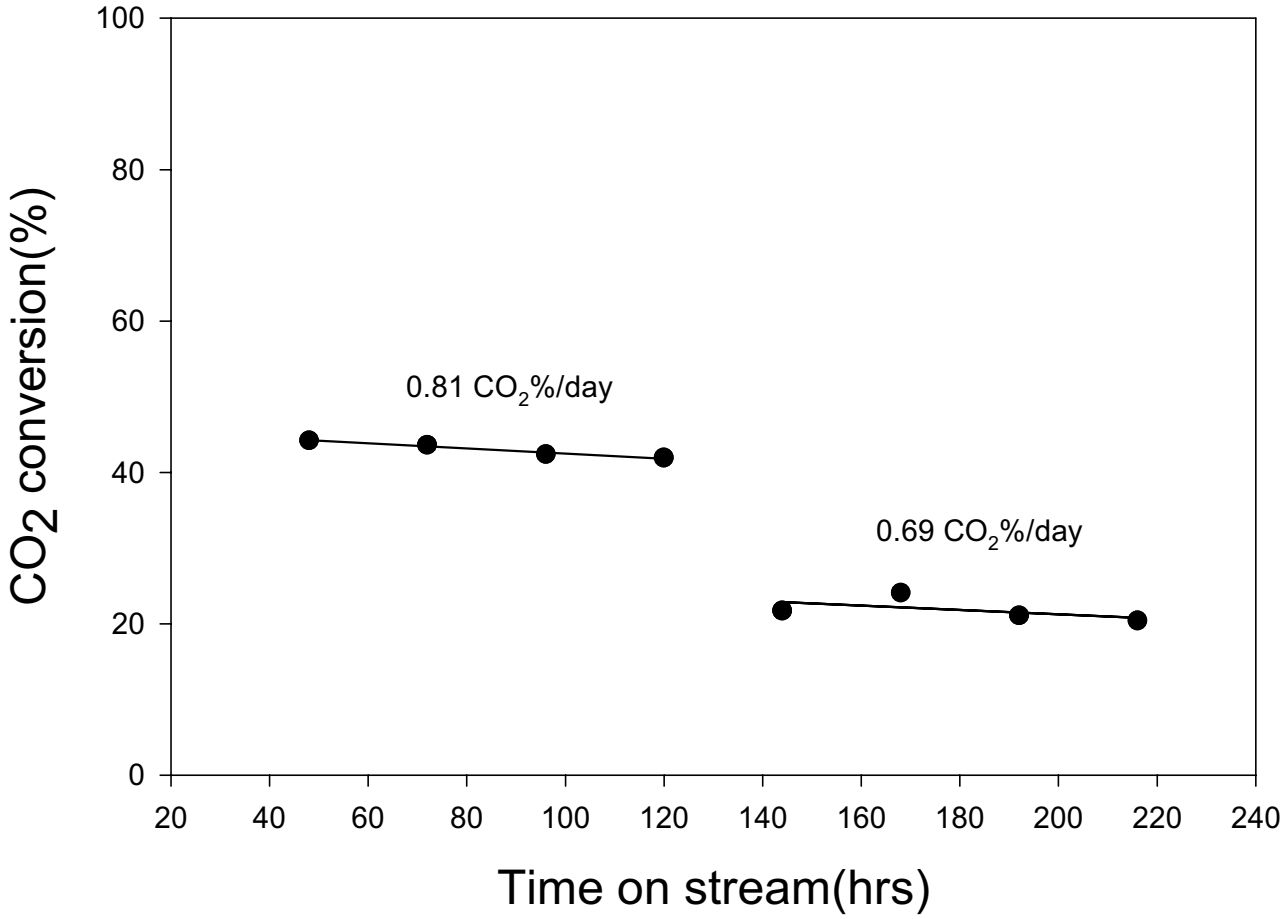

Figure 1. CO_2 hydrogenation over Co-Pt/Al_2O_3, 210^oC, 350psig, H_2:CO=2:1, GHSV=5.0SL/hr/gcatalyst.

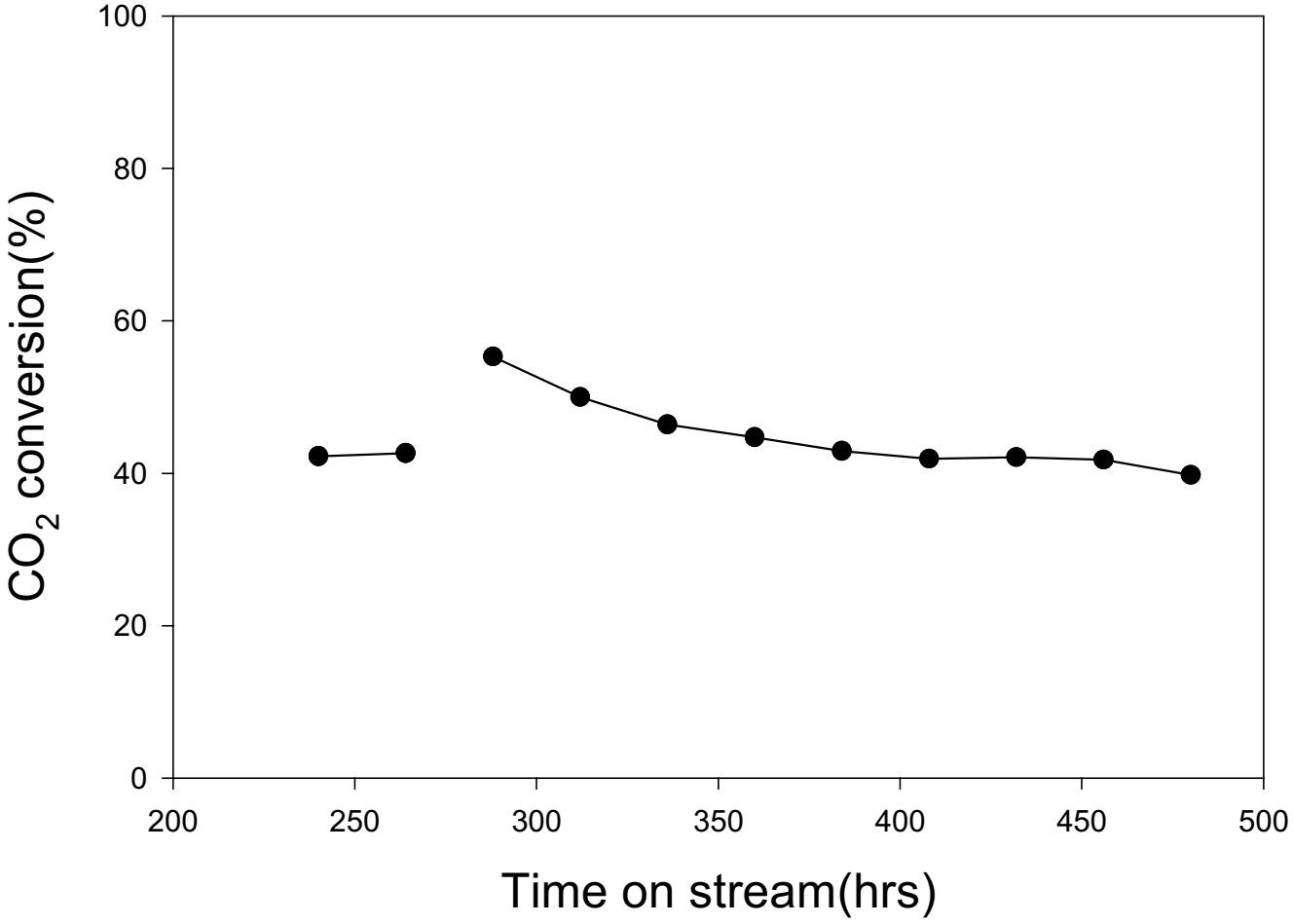

Figure 2. CO_2 hydrogenation over Co-Pt/Al_2O_3 at 210^oC, 350psig, H_2:CO=4:1, GHSV=9.0 and 5.0SL/hr/gcatalyst.

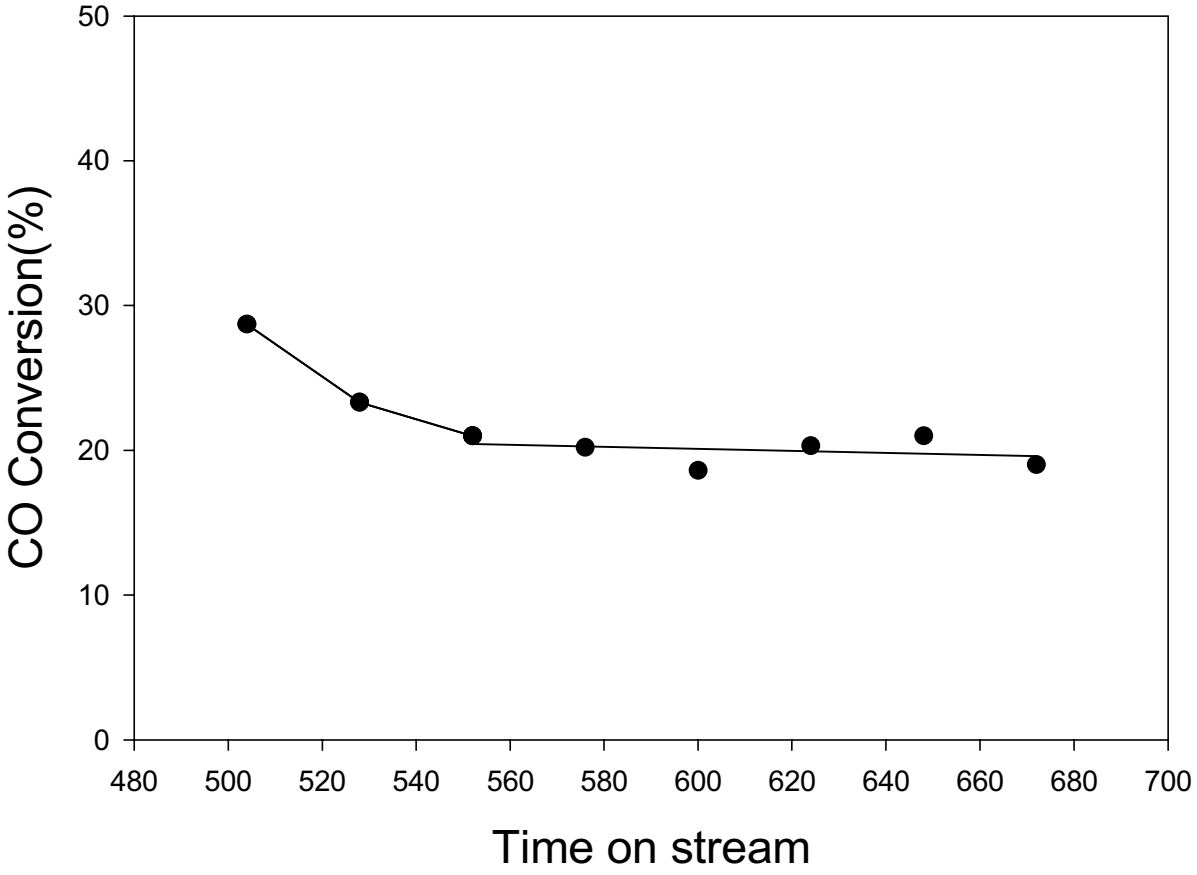

Figure 3. CO hydrogenation over Co-Pt/Al_2O_3 at 210^oC, 350psig, H_2:CO=2:1, GHSV=5.0SL/hr/gcatalyst.

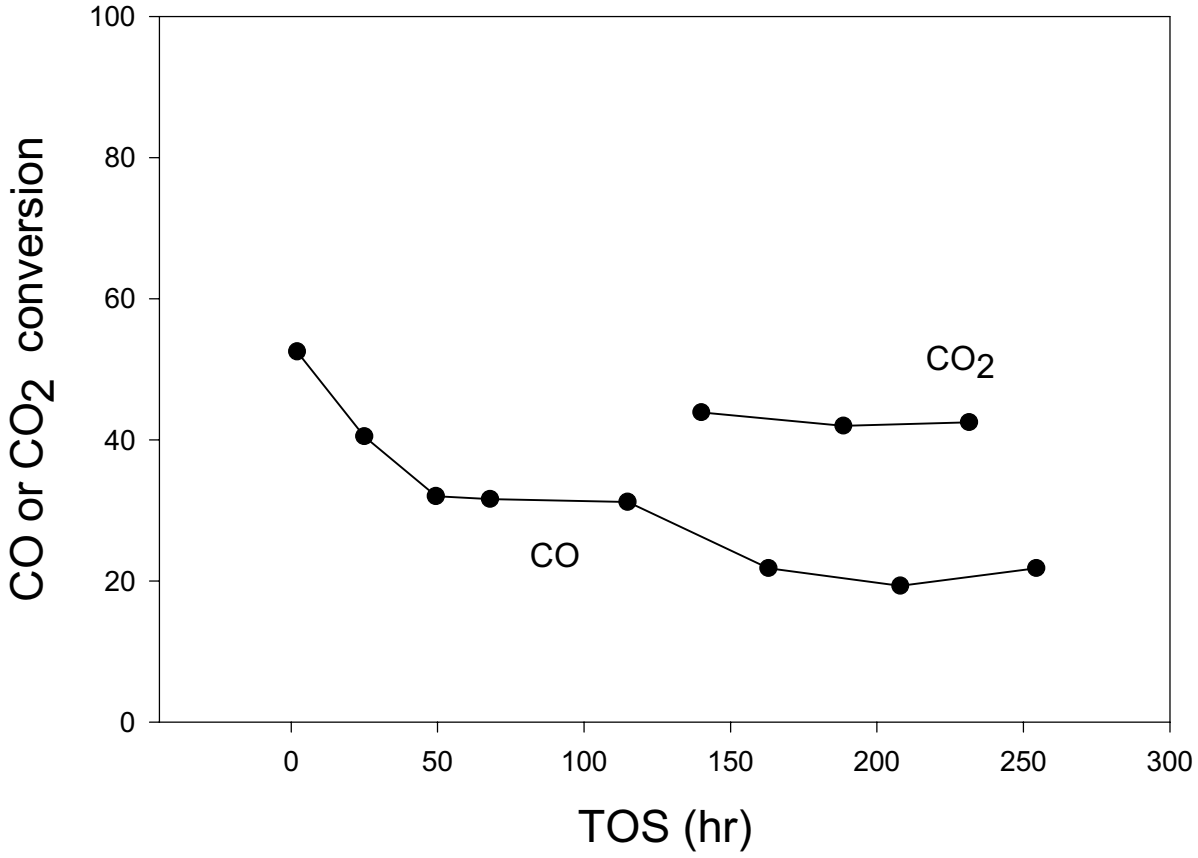

Figure 4. CO or CO_2 conversion as a function of time on stream

Task 9. Cobalt Catalyst Life Testing

The objective of this task is to obtain life data on baseline cobalt Fischer-Tropsch catalysts.

A. Deactivation Rates for Co Catalysts

Introduction

In comparison with low cost Fe FTS catalysts, cobalt catalysts may work at relatively low reaction temperatures and pressures with higher yields of linear paraffins in the C_{5+} range and do not convert water by water gas shift reaction. The cobalt catalysts are believed to deactivate less than the Fe-based catalyst. The major drawback of cobalt catalyst is it high cost. Therefore, the present studies focused on improving the deactivation rates of these catalysts.

Experimental

Preparation of Cobalt Catalysts

The Co/Al_2O_3 catalyst was prepared by incipient wetness impregnation of Al_2O_3 (Condea Vista B alumina, BET surface area 200 m^2/g, pore volume 0.4 cm^3/g) with cobalt nitrate solution. The preparation procedure includes three step impregnations of cobalt salt and then followed by impregnation of promoter. Finally, calcined the sample at 400°C in the flow Air and Helium.

Pretreatment of the catalysts

The catalysts were pretreated first ex-situ and then in-situ, according to the following procedure. The catalysts were reduced ex-situ using 30% H_2 and 70% He (V/V) in a fixed bed reactor at a space velocity of 10,000 GHSV at 350°C. The temperature was ramped to 350°C at 1°C/min and held at 350°C for 10 hours. This reduced catalysts were transferred to CSTR in inert atmosphere. This was accomplished by over pressuring the fixed bed reactor that contain the reduced catalyst and then opening the appropriate valves to force the entire catalyst volume

into the CSTR containing startup solvent. The reduction reactor was weighed prior to and after catalyst transfer to ensure that a quantitative transfer of catalyst had been accomplished. The catalyst was then reduced in-situ in the CSTR; the hydrogen was introduced to reactor at atmospheric pressure with the flow rate of 30 SL/hr. The reactor temperature was increased to 230°C at the ramp rate 1°C for 12 hours.

Reaction conditions

Approximately 20 g of catalyst was transfer into a 1 liter stirred autoclave which had been charged with 300 g of C_{30} oil(decene trimer obtained from Ethyl Corp.). The catalyst was reduced at 230°C in-situ in atmospheric pressure for 10 hours in the flow of hydrogen. After reduction, the reactor temperature was lowered to 180°C and synthesis gas was introduced into the reactor. Then the reactor was pressurized to 275 psig and temperature was slowly increased to 220°C during 3 hours. The feed gas used in the reaction was H_2 : CO ratio of 2:1.

Results and Discussion

Unpromoted 15%Co/Al_2O_3 catalysts

The activity and rate of loss of activity of the unpromoted Co/Al_2O_3 catalyst are shown in Fig. 1. The initial CO conversion, at space velocity 5 SL/hr/g catalyst, is 18%. The deactivation rate of unpromoted Co/Al_2O_3 catalyst is low (1.56% CO conversion/week) compared to Re or Ru promoted catalysts.

FT-Kinetic Studies of 15%Co/Al_2O_3 Catalysts

Typically, the activity of the fresh catalyst decreases with time on stream and then levels off in 5-7 days. After this period, the deactivation is slow and linear. The kinetic study was performed during the steady state. Two sets of kinetic studies were carried out with constant CO partial pressure (table 1) and constant H_2 partial pressure (table 2). Four H_2/CO ratios and five

space velocities has been used to determine the rates. Argon gas used as the makeup gas to adjust the space velocity. The CO conversion with different space time at different H_2/CO ratio presented in Fig. 2 and Fig. 3. However, the additional calculations are required to determine the reaction rate and that will be done during the next quarter.

To determine the Activation Energy, we have carried out FT runs at four temperatures. The Arhenius plots are presented in Fig. 4 and Fig. 5. The activation energy, calculated from CO conversion and H_2 conversion from Figs. 4 and 5, respectively, is approximately 17 Kcal/mole in both cases.

Pressure Effect over 0.2%Re-15%Co/Al_2O_3 catalyst

The effect pressure on CO conversion of the 0.2%-Re-15%Co/Al_2O_3 and space velocity 2 SL/hr/ g catalyst is shown in Fig. 6. The CO conversion increases with increasing pressure. The CO conversion increased significantly from 100 psig to 300 psig. The effect of pressure on methane selectivity and CO_2 selectivity is shown in Fig. 7. The methane selectivity decreases slightly with increase in pressure but the CO_2 selectivity remain almost same with increases in pressure.

Activity of 0.5%Ru-15%Co/Al_2O_3 and 0.5%Ru-20%Co/ZrO_2-SiO_2 Catalysts

The objective of this task is to find the stable Co-based Fischer-Tropsch catalysts. In this study, our aim was to determine the effect of support to the deactivation rate of the catalyst in comparison with the unpromoted Co/Al_2O_3 catalyst. The activities of 0.5%Ru-15%Co/Al_2O_3 and 0.5%Ru-20%Co/ZrO_2-SiO_2 Catalysts are shown in Fig. 8 and Fig. 9, respectively. Initial CO conversion of 0.5%Ru-15%Co/Al_2O_3 catalyst is two times greater than the initial activity of unpromoted 15%Co/Al_2O_3 catalyst at a space velocity of 5 SL/hr/g. However, the rate of deactivation is greater for the promoted Ru catalyst. While for the unpromoted catalyst, the CO

conversion dropped by 18% of the initial activity after 85 h, and remained stable after that, the CO conversion dropped by 42% of the initial value after 1000 h for the Ru promoted catalyst. The activity of Ru-promoted ZrO_2-SiO_2 catalyst also showed a higher activity than the unpromoted catalyst. However, the deactivation rate is lower (3.53% CO conversion/week) than for the Ru-promoted Al_2O_3 catalyst (4.2% CO conversion/week) at space velocity of 5 SL/hr/g. Similar studies are continuing .

Activity of 0.5%Pt-15%Co/Al_2O_3 Catalyst

The activity tests performed in CST and Fixed-bed reactor are presented in Fig. 10 and Fig.11, respectively. The initial activity of Pt-catalyst is about the same as the Ru-promoted catalyst at space velocity 5 SL/hr/g. The CO conversion in the fixed-bed reactor at 210°C is ~30.0% after 500 hrs time on stream (Fig. 11).

Table 1 : Inlet gas composition for the kinetic studies (constant CO partial pressure)

H_2/CO ratio	1.0	1.5	2.0	2.4
CO%	25	25	25	25
H_2%	25	37.5	50	60
Ar%	50	37.5	25	15

Table 2 : Inlet gas composition for the Kinetic studies (constant H2 partial pressure)

H_2/CO ratio	1.0	1.5	2.0	2.4
CO%	25	16.7	12.5	10.4
H_2%	25	25	25	25
Ar%	50	58.3	62.5	64.6

Fig. 1 : Time on Stream vs CO conversion over Co/Al_2O_3 at 220°C and 275 psig

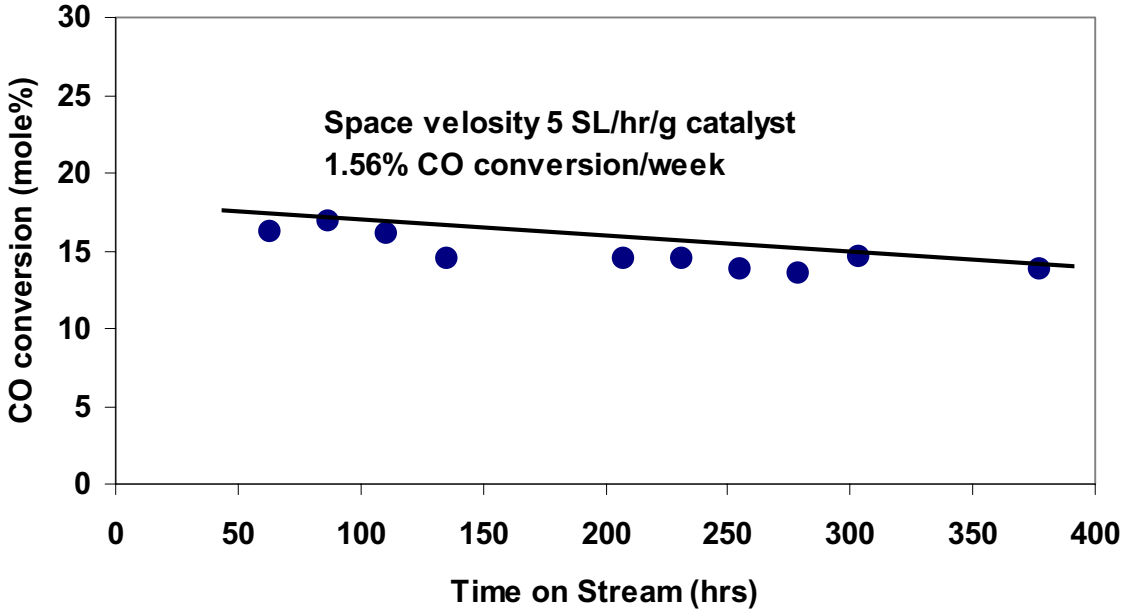

Fig. 2 : Kinetic of 15%Co/Al_2O_3 at 220°C and 275 psig pressure (constant CO partial press.)

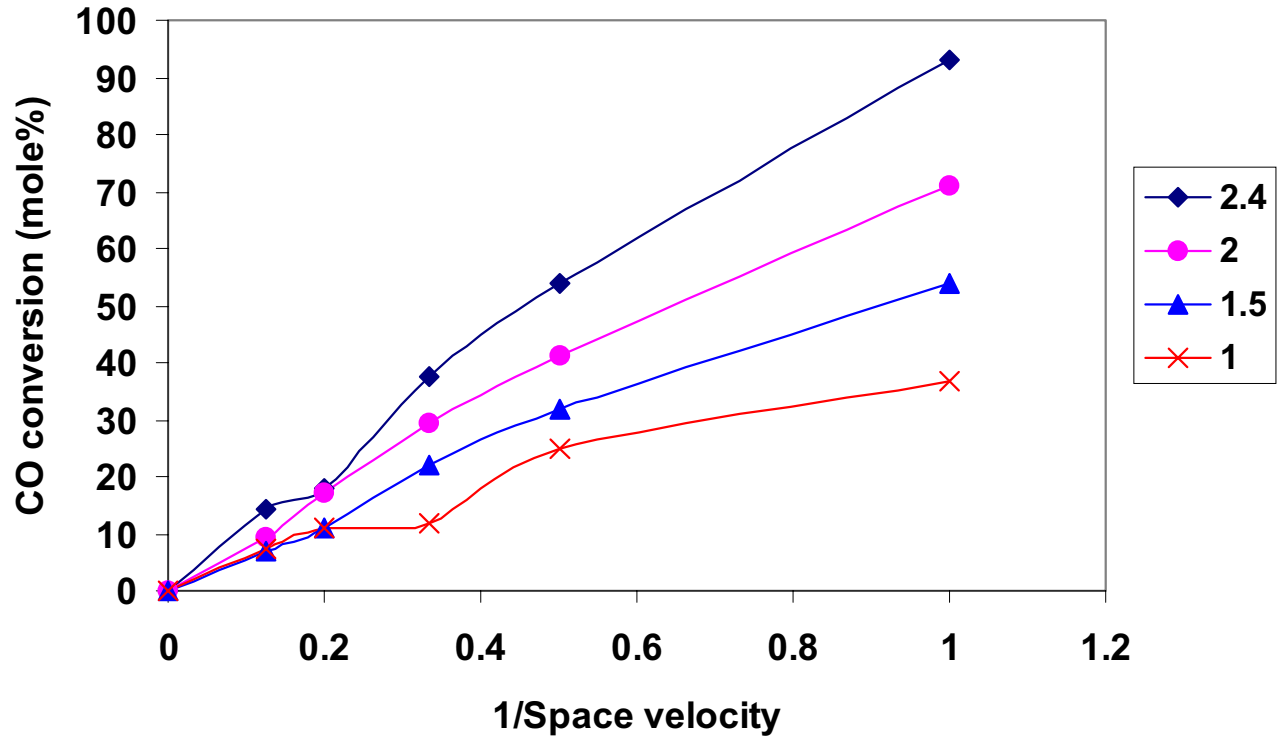

Fig. 3 : Kinetic of CO/Al_2O_3 catalyst at 220°C and 275 psig pressure (contant H_2 partial Press.)

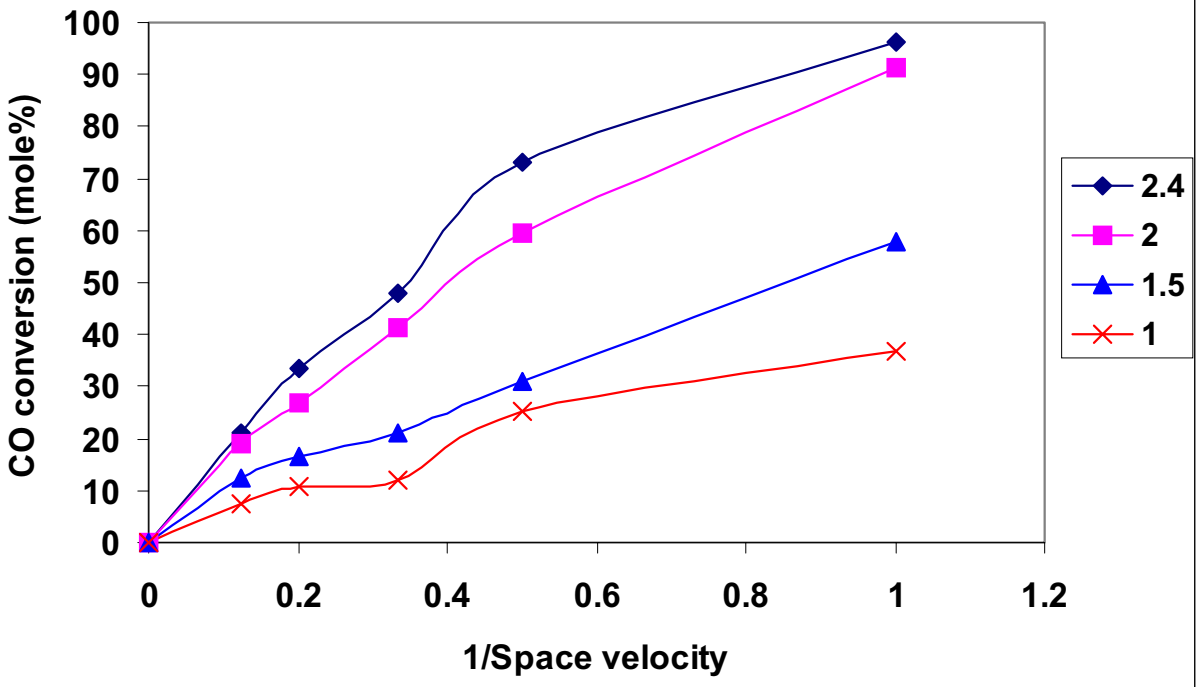

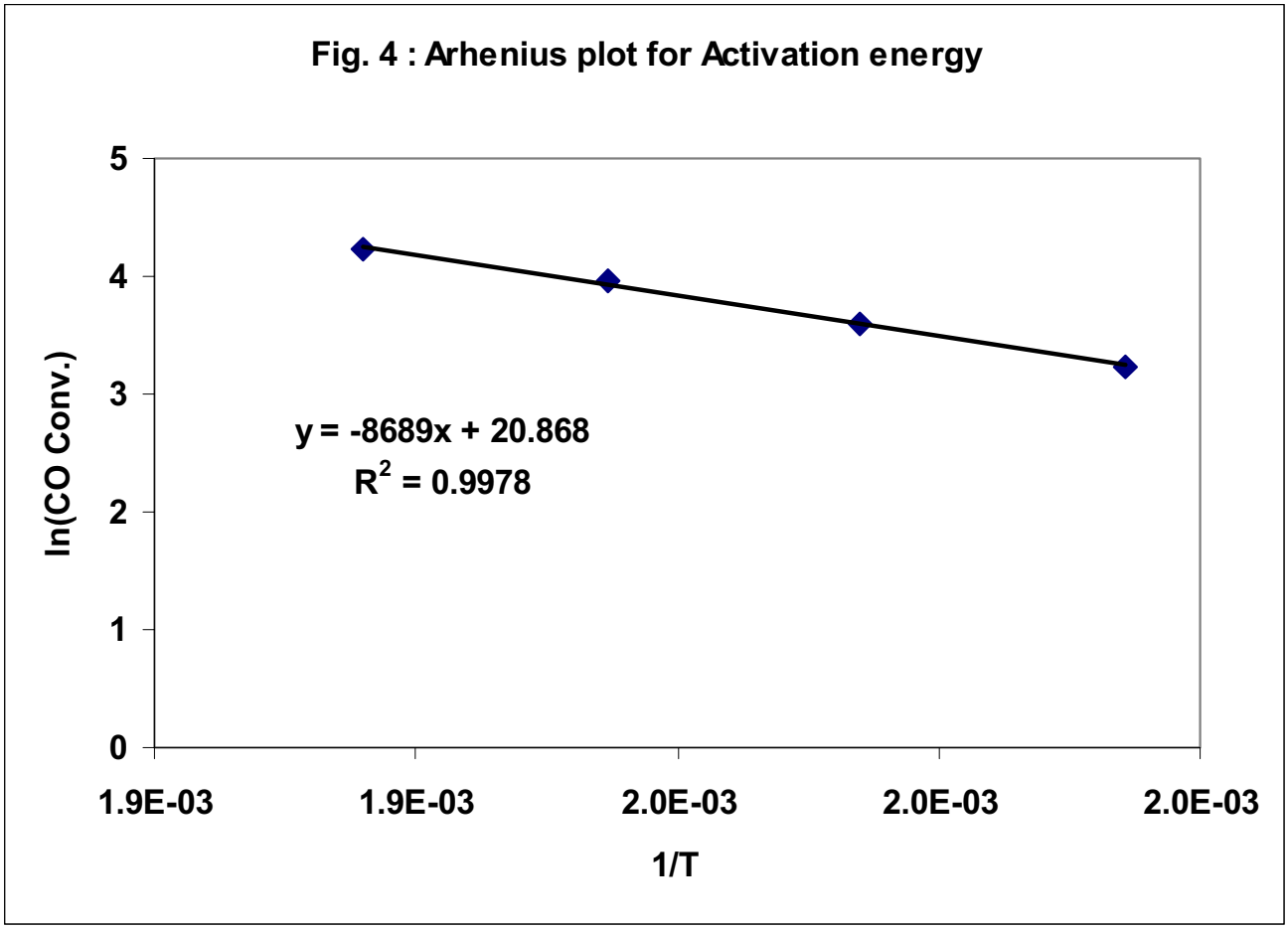
Fig. 4 : Arhenius plot for Activation energy
5
4
3
2
1
0
ln(CO Conv.)
y = -8689x + 20.868
R2 = 0.9978
1.9E-03
1.9E-03
2.0E-03
2.0E-03
2.0E-03
1/T

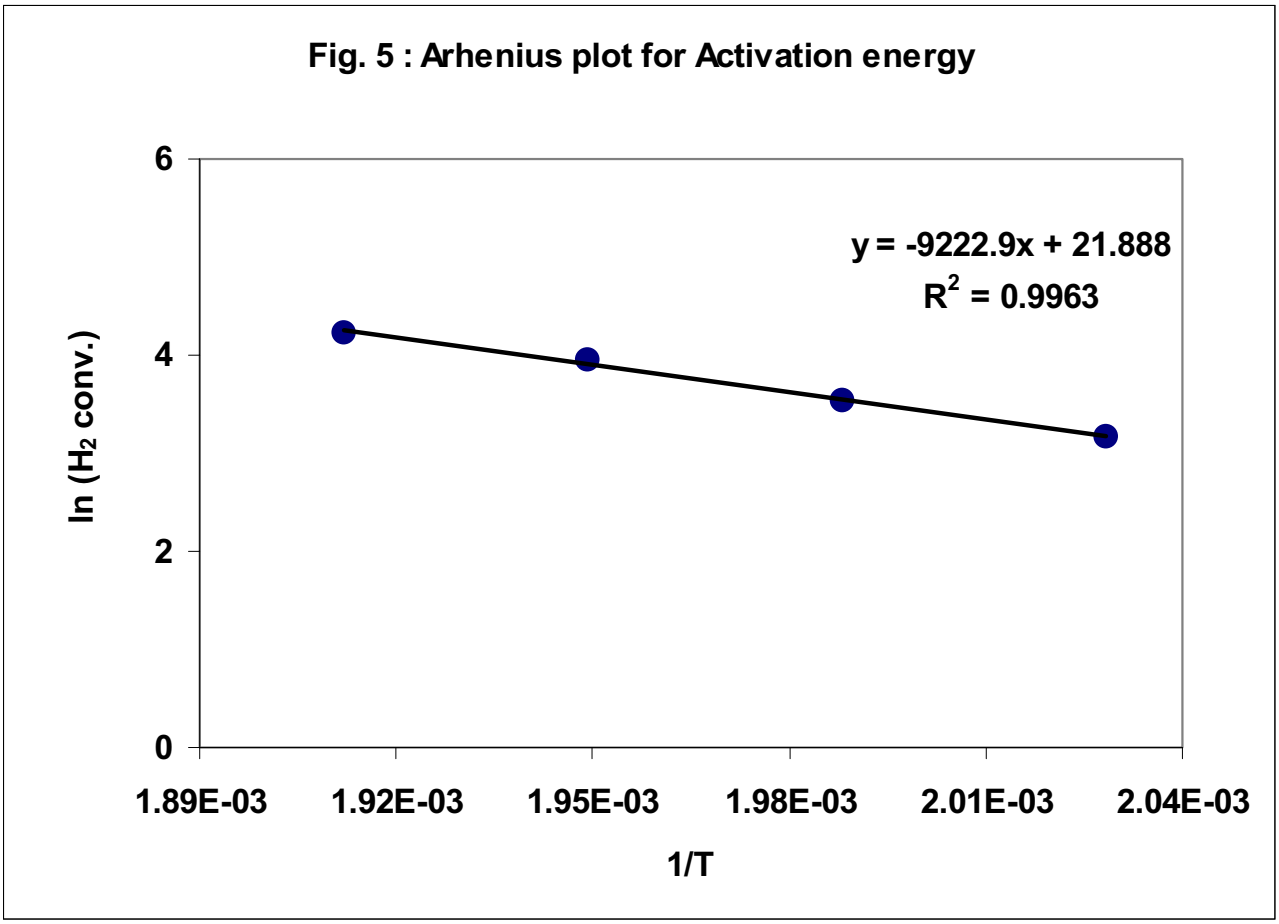
Fig. 5 : Arhenius plot for Activation energy
y = -9222.9x + 21.888
R2 = 0.9963
ln (H2 conv.)
6
4
2
0
1.89E-03
1.92E-03
1.95E-03
1.98E-03
2.01E-03
2.04E-03
1/T

Fig. 6 : Pressure effect on CO conversion over 0.2%Re-%Co $_2O_3$ at 230°C

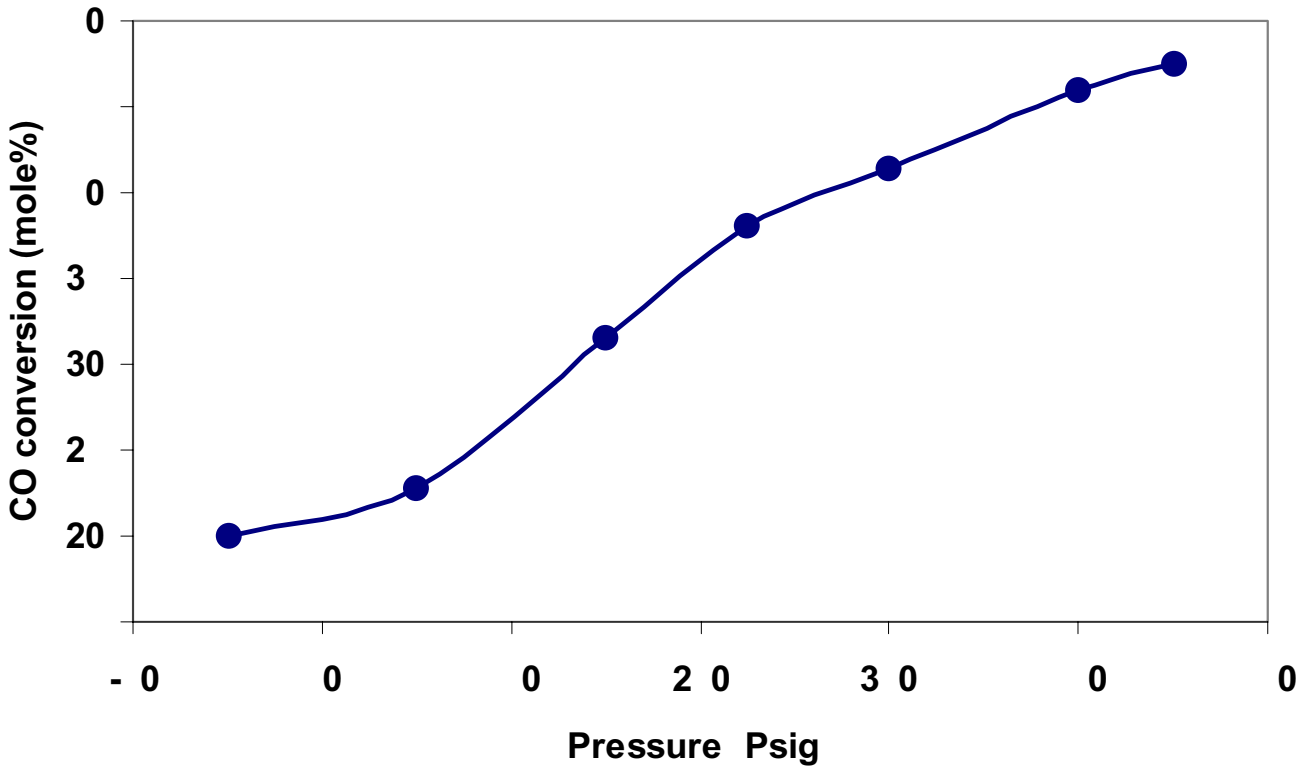

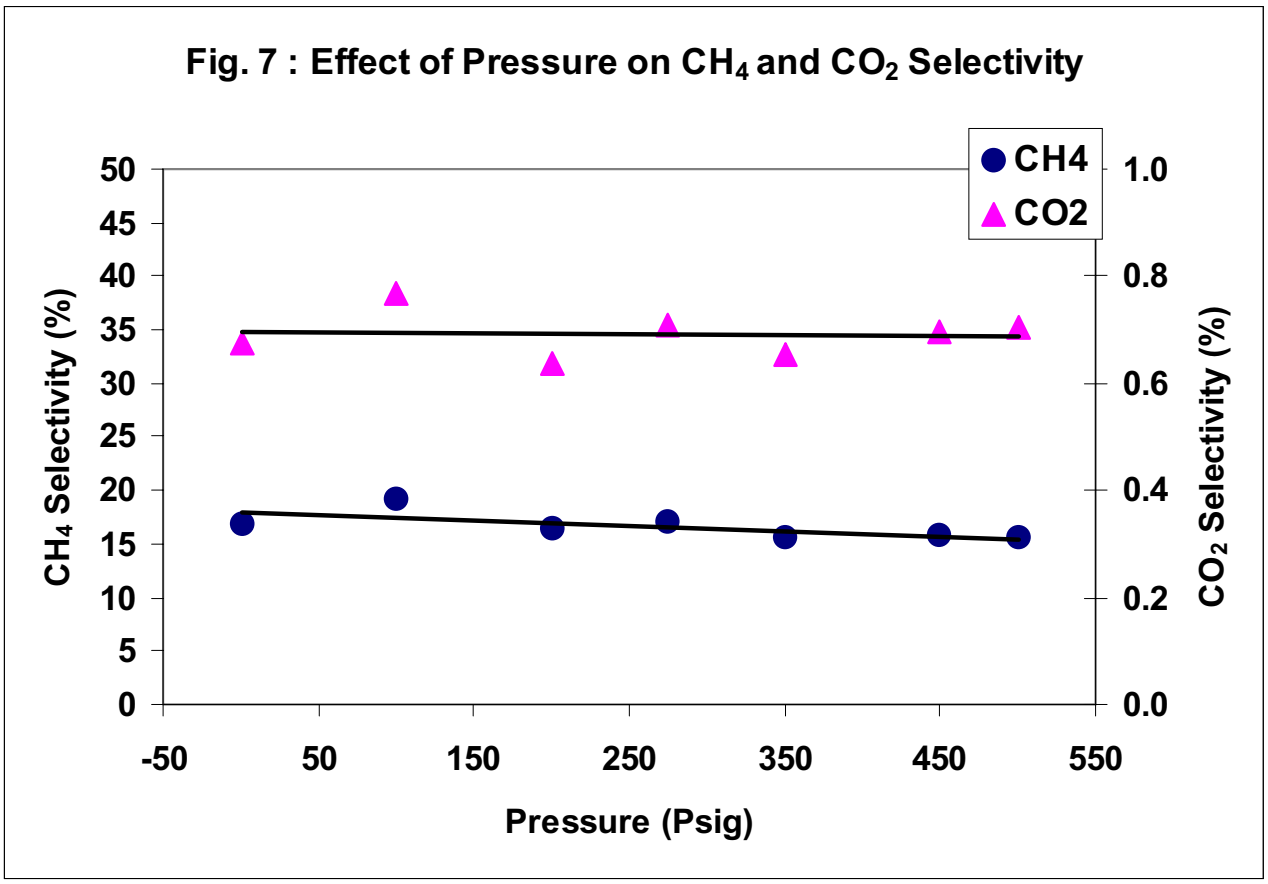
Fig. 7 : Effect of Pressure on CH_4 and CO_2 Selectivity
CH4
CO2
50
45
40
35
30
25
20
15
10
5
0
1.0
0.8
0.6
0.4
0.2
0.0
-50
50
150
250
350
450
550
CH_4 Selectivity (%)
CO_2 Selectivity (%)
Pressure (Psig)

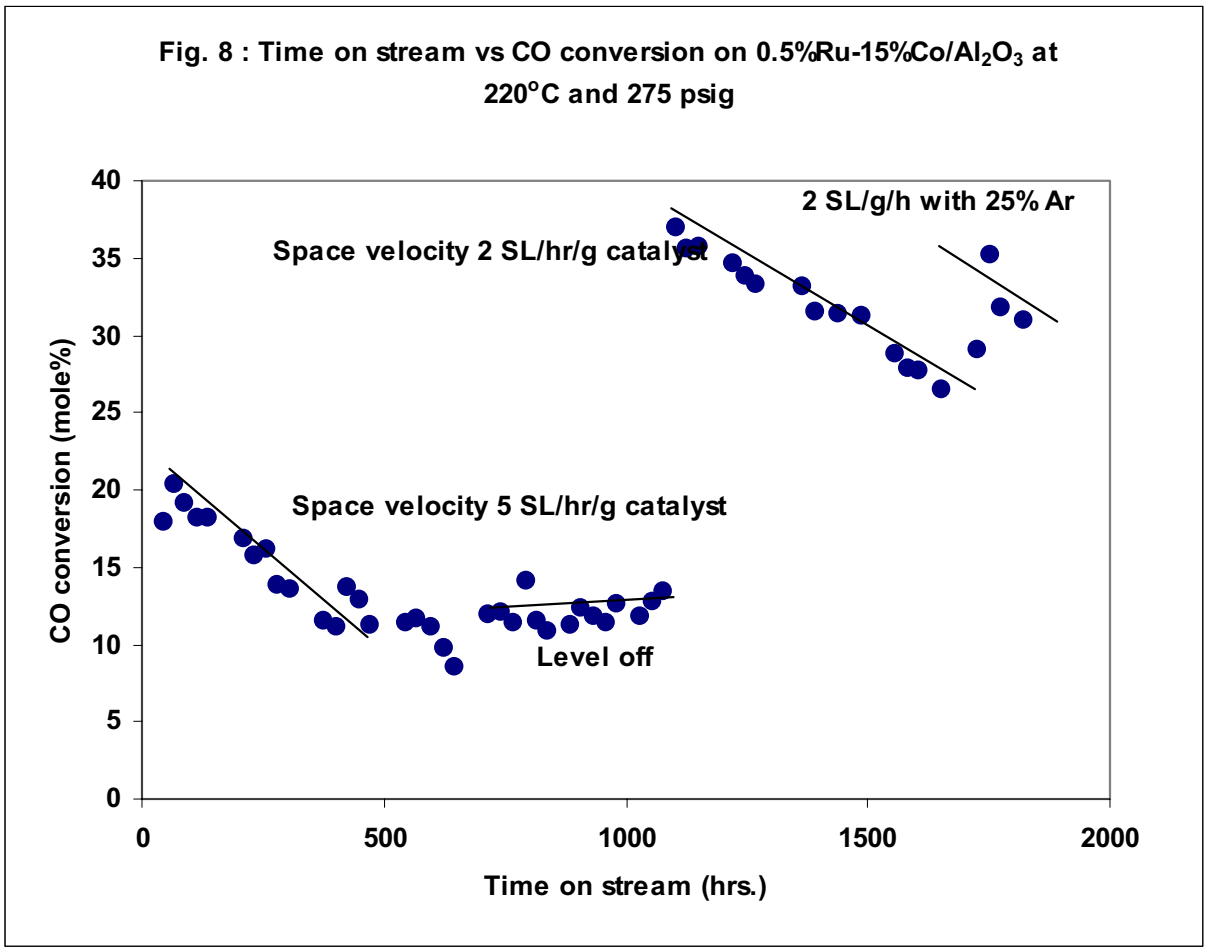
Fig. 8 : Time on stream vs CO conversion on 0.5%Ru-15%Co/Al2O3 at 220°C and 275 psig
2 SL/g/h with 25% Ar
Space velocity 2 SL/hr/g catalyst
Space velocity 5 SL/hr/g catalyst
Level off
CO conversion (mole%)
Time on stream (hrs.)
0
5
10
15
20
25
30
35
40
0
500
1000
1500
2000

Fig. 9 : Time on stream vs CO conversion over 0.5%Ru-20%Co/ZrO_2-SiO_2 at 220°C and 275 psig

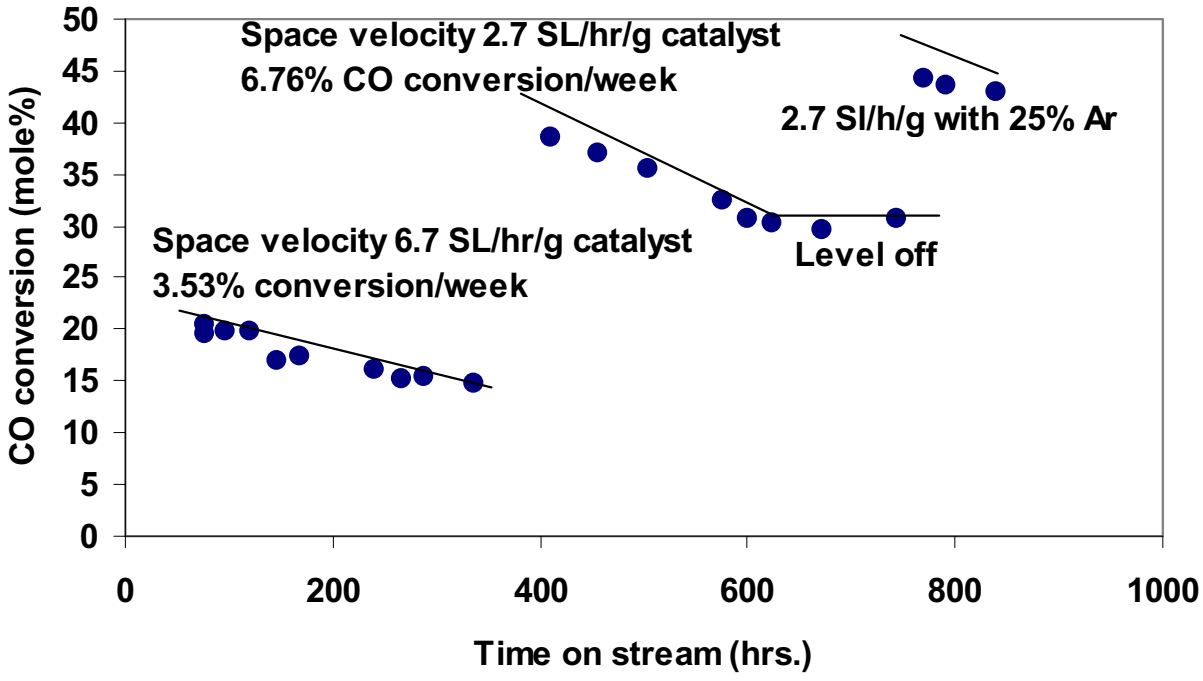

Fig. 10 : Time on stream vs CO conversion on 0.5%Pt-15%Co $_2O_3$ at 220°C and 275 psig

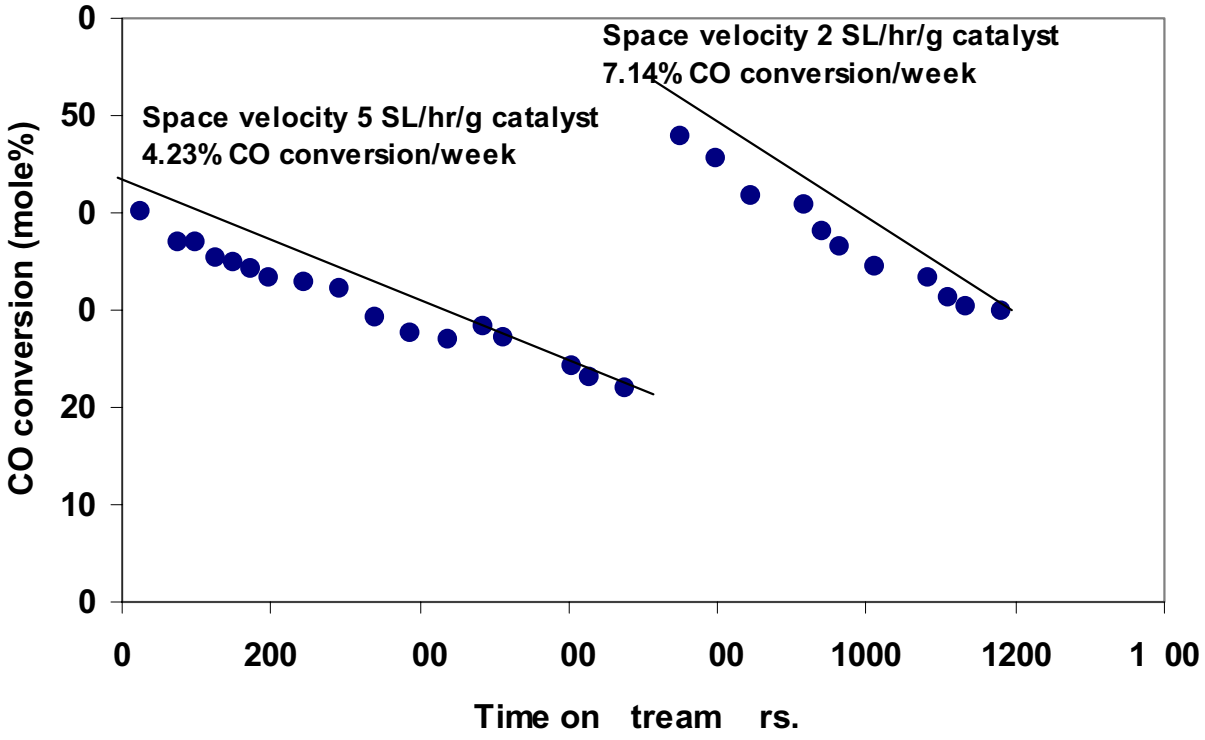

Fig. 11 : Time on stream vs CO conversion over 0.5% Pt-15% Co/Al_2O_3 at 210°C, 350 psig, H_2:CO = 2:1, GHSV = 5 SL/hr/g catalysts in Fixed-bed

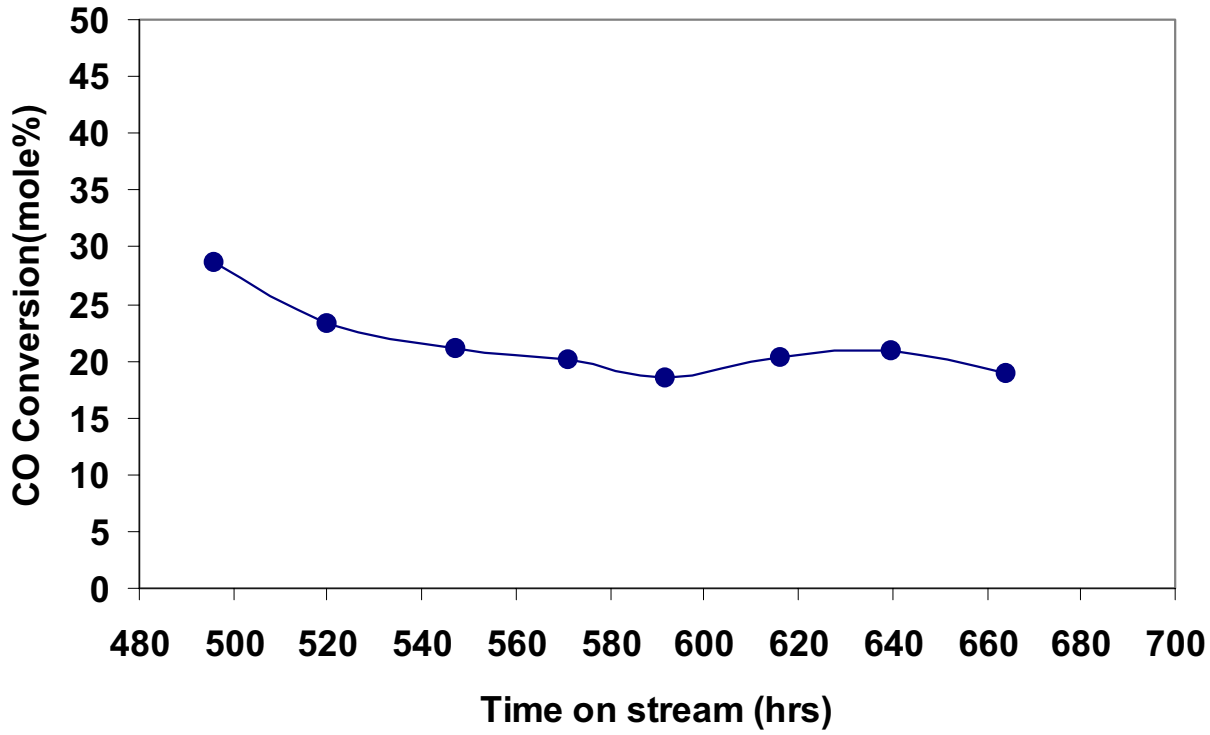

Task 10. Cobalt Catalyst Mechanism Study

The objective of this task is to determine the impact of secondary reactions on the relationship of cobalt Fischer-Tropsch catalysts under conditions appropriate to slurry bubble column reactors.

No scheduled activity to report.

Task 11. University of California, Berkeley (Subcontract)

The objective of this task is the characterization of the structure and function of active sites involved in the synthesis of high molecular weight hydrocarbons from CO and H_2 on multi-component catalysts based on Fe as the active component.

Table Of Contents

I. FISCHER-TROPSCH SYNTHESIS ON IRON CATALYSTS

1. Background

1.1. Structure and Function of Active Phases in Fischer-Tropsch Synthesis

Fe-based oxides have been used as commercial catalysts for Fischer-Tropsch synthesis (FTS) to produce a wide range of paraffin and olefin products, ranging from methane to high molecular weight waxes [1]. During activation in synthesis gas and subsequent FTS reaction, several phases including metallic iron, iron carbides and iron oxides can co-exist at steady-state conditions [2-5]. The relative amounts of these phases depend on various activation and reaction conditions, which also lead to different catalytic performance. Some researchers [6] have proposed that surface iron atoms are responsible for FTS activity, while others have considered surface carbides or a mixture of carbides [7,8] with metallic iron [9] to be the active phase. There are also some reports that suggest that magnetite Fe_3O_4 is the active FTS phase [10-12]. Although these studies have each provided some evidence to support its specific proposal about the active phase, the available information remains phenomenological and sometimes contradictory, and a direct method to identify the active phase during reaction and to count the number of active sites has remained elusive.

Based on our previous studies of the active phases and catalytic activity on Fe-Zn-K-Cu oxides [23], we have started in this reporting period the preparation of a new series of high surface area Fe-Zn catalysts and investigated the reduction and carburization process and catalytic activity in our search for alternate and superior catalysts for FTS reactions.

1.2. Effects of Zn, Ru (Cu) and K on Fe Oxides

Many components have been incorporated into Fe catalysts in order to improve their mechanical and catalytic properties. Our previous studies have shown that Zn, K and Cu [13-15] promote the catalytic properties of Fe oxides. Zinc oxide, as a non-reducible oxide at FTS conditions, appears to stabilize the surface area of Fe oxide precursors. Alkali, as a modifier of the adsorption enthalpies of H_2 and CO, has been reported to increase the selectivity to desired C_{5+} products. Copper promotes the carburization processes and decreases the temperature required for the activation of iron oxide precursors. According to our previous optimum composition of Fe-Zn-K-Cu (Zn/Fe=0.1, K/Fe=0.02, Cu/Fe=0.01), we have prepared a series of Zn and Fe co-precipitated oxides with constant Zn/Fe and K/Fe atomic ratios (Zn/Fe=0.1, K/Fe=0.02) and varying amounts of Ru (Ru/Fe=0-0.01). Ru is a very active FTS catalyst. Ru was chosen in order to improve the catalytic activity and to minimize unfavorable water gas shift reactions, which can be catalyzed by the Cu component on Fe catalysts. Also, K was added in order to increase wax and alkene yields, while decreasing the production of undesirable methane products. The same effects of K are expected on Fe-Zn-Ru-K catalysts. We have examined the surface area, bulk structure, required reduction and carburization temperatures, as well as the catalytic behavior of these catalysts, in order to identify optimum Ru contents that give maximum site densities and FTS reaction rates.

2. Synthesis Procedures

2.1 Higher Surface Area Fe-Zn-K-Cu Oxides

Fe-Zn-K-Cu catalysts were prepared by co-precipitation of iron and zinc nitrates following the procedure described in our previous report [18]. In order to produce high surface area samples, alcohol (isopropanol or ethanol) instead of water was used to wash the precipitates before drying the precipitates. Isopropanol or ethanol was employed to reduce the pore mouth pinching caused by the surface tension of intrapore liquids during drying processes. The subsequent impregnation procedure of an aqueous solution of potassium carbonate and copper nitrate using incipient wetness methods was the same as previously described [18].

2.2. Fe-Zn-Ru-K Oxides

All catalysts were prepared by co-precipitation of iron and zinc nitrates (Aldrich, 99+%) at a constant pH of 7.0 in order to form porous mixed oxides. Then, these oxide precursors were impregnated with a ruthenium (III) nitrosyl nitrate [$Ru(NO)(NO_3)_x(OH)_y$ (x+y=3)] (Aldrich, solution in dilute nitric acid, Ru 1.5%) and with an aqueous solution of potassium carbonate (Aldrich, 99+%) and copper nitrate (Aldrich, 99+%) using incipient wetness methods. The Zn/Fe oxide precursors were prepared first. Fe nitrate (1.4 M) and Zn nitrate (3.0 M) solutions were mixed at a given Zn/Fe atomic ratio (Zn/Fe=0.1). A solution of ammonium carbonate (Aldrich, 98%) (1 M) was prepared separately. Deionized water (~ 50 ml) was added into a large flask, which was heated on a hot plate with a magnetic stirrer and held at 353 K throughout the synthesis. The mixed Zn/Fe solution was added at 2 cm^3/min flow into the flask using a rotary pump. At the same time, the ammonium carbonate solution was fed separately, and its flow was controlled to maintain the slurry pH at 7±0.1, as monitored by a pH meter. The resulting precipitates (~20 g) were washed several times with about 1 *l* water per gram of catalyst, dried at 393 K overnight, and then treated in dry air at 623 K for 1 h. The air-treated powder was promoted with a ruthenium (III) nitrosyl nitrate solution [$Ru(NO)(NO_3)_x(OH)_y$ (x+y=3)] (Aldrich, solution in dilute nitric acid, Ru 1.5%) using incipient wetness protocols and then dried at 373 K. The dried material was treated in dry air at 623 K for 4 h. A similar process was used in order to promote samples with 2 at.% K using a K_2CO_3 solution (0.16 M). Finally, the dried material was treated again in dry air at 623 K for 4 h. These catalysts were pressed into pellets at 440 MPa, lightly crushed, and then sieved in order to retain the 80-140 mesh (100~180 μm) fraction used for FTS reactions and for all subsequent characterization studies.

3. Catalyst Characterization

3.1. Protocols for the Characterization of Fe-based FTS Catalysts

This research program addresses the synthesis and the structural and catalytic characterization of active sites in Fe-based catalysts for FTS. We have designed a matrix of samples consisting of a systematic range of multicomponent catalysts in order to

determine the number and type of surface sites present on fresh catalysts and on samples during and after FTS reaction (Table 1.1). Our objective is to develop rigorous relationships between the synthesis methods, the resulting catalyst structures, and their function in FTS reactions.

Table 1.1. Matrix of samples and characterization methods for FTS reaction

<table>
<tr><th colspan="3">Nominal Composition of the Catalysts</th><th rowspan="2">Characterization Before and After FTS</th><th rowspan="2">FTS reaction</th></tr>
<tr><th>Zn/Fe mole ratio</th><th>K/Fe (at.%)</th><th>Cu/Fe (at.%)</th></tr>
<tr><td rowspan="8">0</td><td rowspan="2">0</td><td>0</td><td rowspan="24">XRD

Surface area

In-situ XAS

H_2-TPR

CO-TPR</td><td rowspan="24">Effect of reaction condition

220 °C 21.4 atm

235 °C 21.4 atm

270 °C 5 atm

Effect of CO_2 addition

Isotopic studies</td></tr>
<tr><td>1</td></tr>
<tr><td rowspan="3">2</td><td>0</td></tr>
<tr><td>1</td></tr>
<tr><td>2</td></tr>
<tr><td>4</td><td>1</td></tr>
<tr><td rowspan="3">0.05</td><td>0</td><td>0</td></tr>
<tr><td>2</td><td>1</td></tr>
<tr><td>4</td><td>2</td></tr>
<tr><td rowspan="6">0.1*</td><td rowspan="2">0</td><td>0</td></tr>
<tr><td>1</td></tr>
<tr><td rowspan="3">2</td><td>0</td></tr>
<tr><td>1</td></tr>
<tr><td>2</td></tr>
<tr><td rowspan="2">4*</td><td>1</td></tr>
<tr><td>2*</td></tr>
<tr><td rowspan="3">0.2</td><td>0</td><td>0</td></tr>
<tr><td>2</td><td>1</td></tr>
<tr><td>4</td><td>2</td></tr>
<tr><td rowspan="6">0.4</td><td rowspan="2">0</td><td>0</td></tr>
<tr><td>1</td></tr>
<tr><td rowspan="3">2</td><td>0</td></tr>
<tr><td>1</td></tr>
<tr><td>2</td></tr>
<tr><td>6</td><td>1</td></tr>
<tr><th>Zn/Fe</th><th>Ru/Fe (at.%)</th><th>K/Fe (at.%)</th></tr>
<tr><td rowspan="4">0.1</td><td>0.5</td><td rowspan="2">0</td></tr>
<tr><td>1</td></tr>
<tr><td>0.5</td><td rowspan="2">2</td></tr>
<tr><td>1</td></tr>
</table>

* Samples treated by water and alcohol wash.

3.2. Crystal Structure

Figure 1 shows the X-ray diffraction patterns of the Fe-Zn oxide precursors prepared using different washing process and treated at different temperatures. At 534 K, Fe_2O_3 formed in water-washed Fe-Zn precursors as indicated by the sharp diffraction peaks matching those of standard patterns of Fe_2O_3. However, only broad Fe_2O_3-like diffraction peaks were detected on alcohol-washed Fe-Zn precursors, indicating that alcohol-washed Fe-Zn oxides consist of more finely dispersed Fe_2O_3. As the treatment temperatures increased to 623 K, the diffraction peaks become sharper on alcohol-washed Fe-Zn oxides, indicating the formation of larger crystallites of Fe_2O_3.

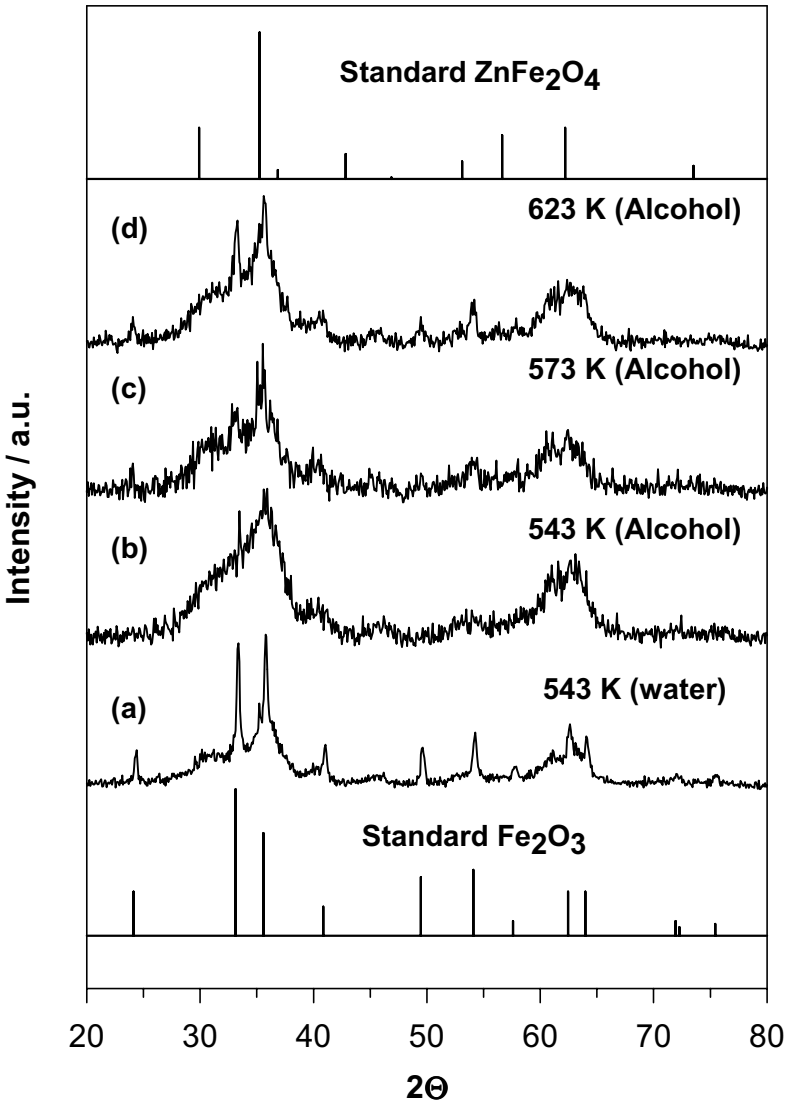

Figure 1. X-ray diffraction patterns of Fe-Zn oxide precursors. (a) water-washed precipitates, treated at 543 K for 4 h, (b) alcohol-washed precipitates, treated at 543 K for 4 h, (c) alcohol-washed precipitates, treated at 573 K for 4 h, (d) alcohol-washed precipitates, treated at 623 K for 4 h.

Figure 2 shows the X-ray diffraction patterns on Fe-Zn-K-Cu oxides after FTS reaction for 1 h. Fe_3O_4 was the only crystal phase detected on Fe-Zn, Fe-Zn-K2-Cu and Fe-Zn-K2-Cu1 oxide samples. No Fe carbides were detected on these samples. Since the conversion of Fe_3O_4 to Fe carbides is facile, it is expected that Fe carbides exist in an amorphous form on these samples, and that the compact Fe carbide layers covering over the Fe_3O_4 cores inhibit the carburization of Fe_3O_4. Substantial amount of χ-$Fe_{2.5}C$, despite poorly crystallized, was detected along with Fe_3O_4 crystallites on Fe-Zn-K4-Cu2 sample. This indicates that higher concentrations of K and Cu increase the extent of Fe_3O_4 carburization and also increases the formation rate of Fe carbide crystallites.

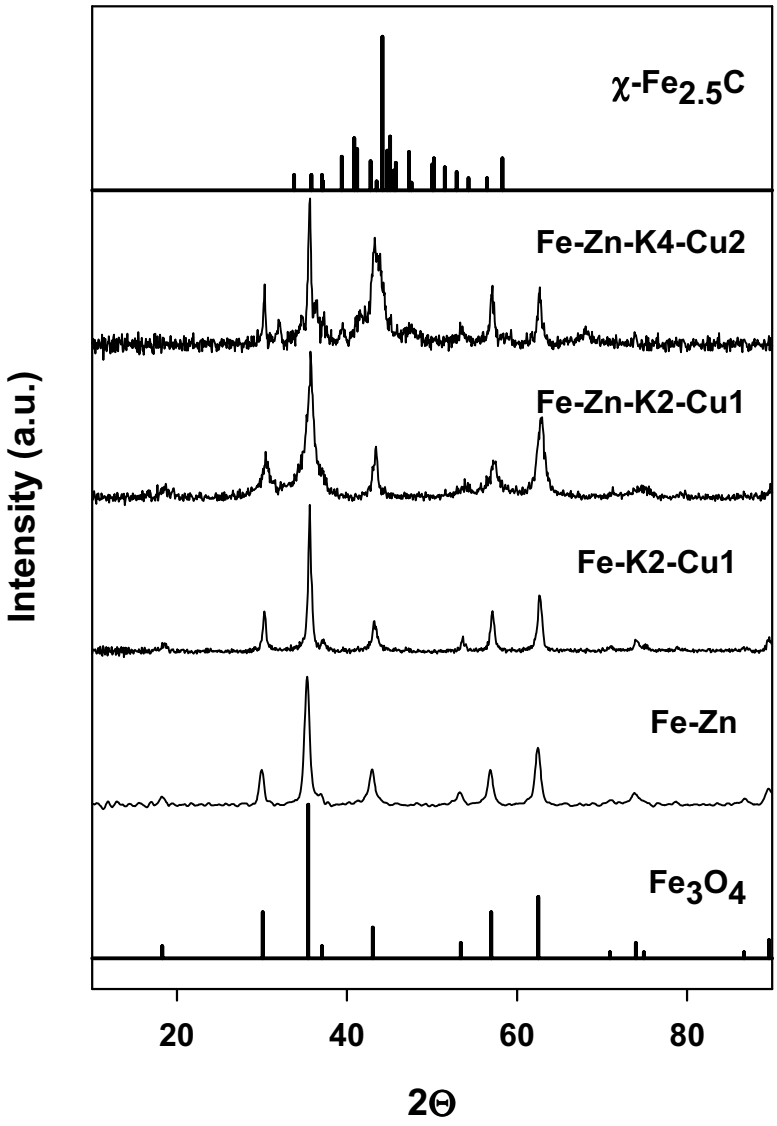

Figure 2. X-ray diffraction patterns of Fe-Zn-K-Cu oxides after FTS reaction at 250 ^oC for 1 h. (0.2 g sample, $H_2/CO=2$, flow rate 100 cm^3/min)

3.3. BET Surface Area

Many factors, including precipitate drying, treatment temperature and time, and the promoter impregnation, influence the surface area of the precursors. In this reporting period, these factors were systematically examined in order to increase the surface area of catalysts and to improve their catalytic performance.

3.3.1. Precipitate Drying Process and Treatment Temperature

Several approaches have been used to increase the surface area of the catalyst precursors. One attempt was the use of alcohol instead of waster to wash the precipitates in order to reduce the surface tension of the intrapore liquids during drying process. Ethanol or isopropanol was used, because they have much lower surface tension than water (20 vs. 60 nL/m). The precipitates were washed after precipitation with excess amount of alcohol in order to replace the water trapped in the intrapores of the precipitates.

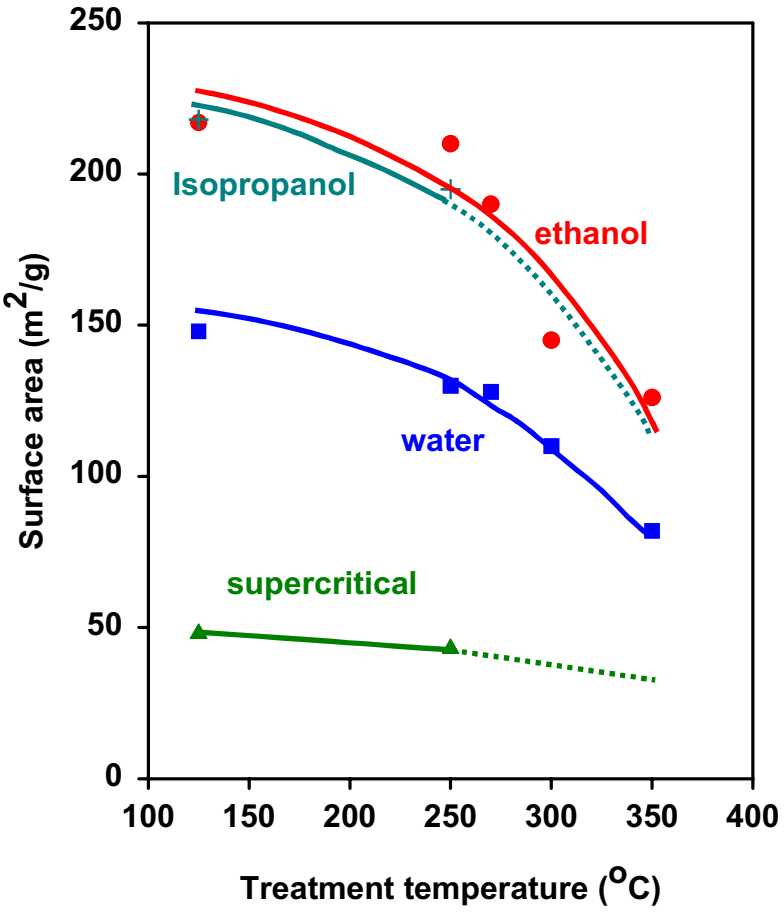

Figure 4. Surface area of Fe-Zn precipitates dried in different liquids and the surface area of the Fe-Zn precursors as a function of treatment temperature. Ethanol-washed (circle), isopropanol-washed (cross), water-washed (square), supercritical (triangle). (All the samples were treated at the give temperatures for 4 h).

Figure 4 shows the surface area of Fe-Zn precursors that pretreated in different liquids as a function of treatment temperature. Ethanol or isopropanol-washed precipitates showed higher Fe hydroxide surface areas than water-washed precipitates (215 vs 148 m^2/g). Alcohol fills the precipitate pores and prevents pore mouth pinching during drying by decreasing the surface tension of the intrapore liquids. The resemblance of the surface area for isopropanol-washed and ethanol-washed samples is consistent with their similar surface tensions. Isopropanol-containing precipitates treated at the critical conditions for isopropanol (235 ^oC, 48 atm) gave a surface area of only 48 m^2/g. Apparently H_2O from the decomposition of Fe hydroxides at these supercritical conditions led to sintering of the resulting Fe oxides. It appears that replacing water from the precipitates with low surface tension liquids during drying process is a key factor in increasing the surface area of the hydroxide and the subsequent oxide precursors.

After drying the precipitates at 125 ^oC for 12 h, the hydroxide powders were treated in dry air at different temperatures in order to examine the effect of treatment temperature on the surface area of the samples. The surface areas of resulting oxides decreased with increasing treatment temperature on both alcohol-washed and water-washed hydroxides, but the alcohol-washed hydroxides were more sensitive to the treatment temperatures. It appears that a treatment temperature of ~300 ^oC is suitable for decomposing hydroxide while not decreasing markedly the surface area of Fe oxides. Since water forms during hydroxide decomposition and it causes catalyst sintering, a high space velocity flow of dry air is required in order to minimize sintering during hydroxide decomposition (>2000 h^{-1}).

3.3.2. Promoter Impregnation

There are two different ways to impregnate promoters. One way is to impregnate promoters on Fe-Zn hydroxide precursors and then treat the sample at higher temperatures; the other way is to impregnate promoter on pretreated Fe-Zn oxide precursors. We are interested in learning whether the promoter impregnation or the sequence of impregnation influences the surface area of the samples. Figure 5 shows the surface areas of Fe-Zn hydroxides and oxides promoted with Ru and K as a function of treatment temperature. The addition of Ru to Fe-Zn hydroxide precursors decreased its surface area (220 vs 192 m^2g^{-1}), apparently because of the pore mouth pinching caused by the high surface tension of water during drying. Additional impregnation of K further decreased the surface area of Fe-Zn-Ru for the same reason. Each impregnation decreases the surface areas of the samples by ~10-20%.

These K and/or Ru-promoted Fe-Zn hydroxides were subsequently treated at different temperature in order to examine the effect of treatment temperature on their surface areas. Here, similar temperature effects were observed on promoted Fe-Zn oxides. The surface areas of K- and/or Ru-promoted Fe-Zn oxides decreased by ~50% by increasing the treatment temperature from 250 to 350 ^oC. Therefore, for the Fe-Zn based catalysts, the treatment temperature strongly influences their surface areas. Impregnating Ru onto Fe-Zn oxides, which were pretreated at 350 ^oC for 4 h, and subsequently treating the samples at 250, 300 and 350 ^oC respectively, showed almost identical surface area as that of the precursor Fe-Zn oxides. This indicates that once treated at higher temperatures, the

structure of Fe-Zn oxides is strong enough to prevent it from pore mouth pinching and further sintering. Also it implies that the length of treatment does not influence the surface areas of Fe-Zn oxides at given treatment temperatures.

Impregnation of promoters decreases the surface area of Fe-Zn oxide; the sequence of impregnation, however, appears not to influence the surface area of the resulting promoted Fe-Zn oxides at given treatment temperatures. It appears to be more efficient to impregnate promoters on Fe-Zn hydroxide precursors than on the Fe-Zn oxides obtained by thermal treatment of such precursors before impregnation.

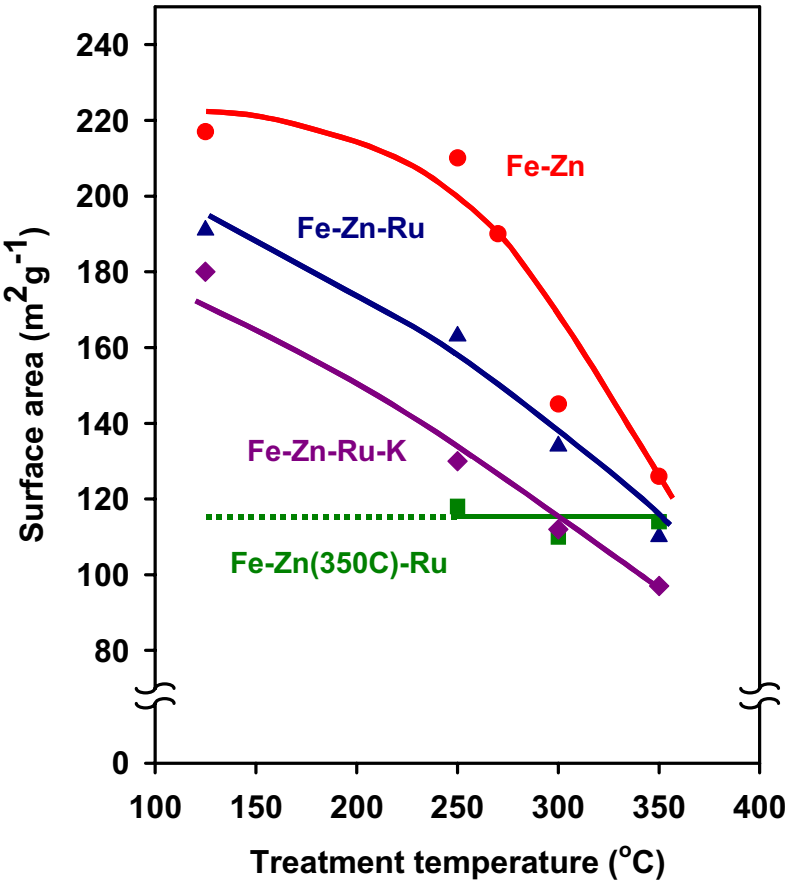

Figure 5. Surface area of Fe-Zn oxides promoted with Ru and K as a function of treatment temperature. (a) Fe-Zn oxide (circle), (b) Ru promoted on Fe-Zn hydroxide (triangle), (c) K and Ru promoted on Fe-Zn hydroxide (diamond), (d) Ru-promoted on Fe-Zn oxide pretreated at 350 °C for 4 h (square). (Zn/F=0.1, Ru/Fe=0.05, K/Fe=0.02, all samples were treated at given temperatures for 4 h)

3.4. Temperature-Programmed Reduction and Carburization of Fe-Zn-K-Cu Oxides

3.4.1. Reduction in H_2

Figure 6 shows the oxygen removal rate as a function of temperature for the reduction of Fe-Zn-K-Cu oxides in H_2. The reduction of K and Cu promoted Fe-Zn oxides started at

~100 K lower temperatures but finished at ~40 K higher temperatures than that on Fe-Zn oxide. This is apparently because Cu provides H_2 dissociation sites that decrease the reduction temperature, and K inhibits the reduction of Fe oxide in H_2 and thus prolongs their reduction processes. Fe-Zn-K2-Cu1 oxide started to reduce at almost identical temperatures but completed the reduction at ~40 K lower temperatures than the sample without Zn (Fe-K2-Cu1 oxide). Since K can titrate ZnO, especially at higher temperatures, the presence of Zn appears to weaken the inhibition effects of K on the reduction of Fe oxides. The Fe-Zn oxides promoted with higher concentrations of K and Cu (Fe-Zn-K4-Cu2) reduced at slightly higher temperatures than Fe-Zn-K2-Cu1. This suggests that the surface K/Cu ratio is probably slightly higher on Fe-Zn-K4-Cu2 than on Fe-Zn-K2-Cu1 sample.

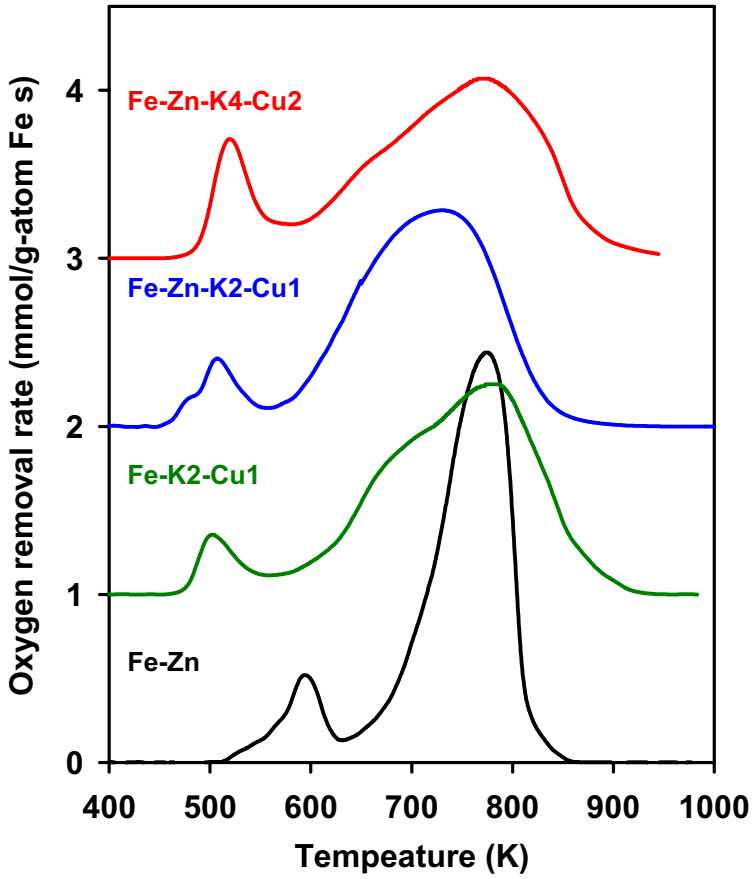

Figure 6. Oxygen removal rate as a function of temperature for the reduction of Fe-Zn-K-Cu oxides in H_2. (0.05 g sample, 10 ^{o}C/min ramping rate, 20 % H_2 in Ar, total flow rate 100 cm^3/min).

3.4.2. Reduction and Carburization in CO

Figure 7 shows oxygen removal and carbon introduction rates as a function of temperature during temperature-programmed reduction and carburization of Fe-Zn-K-Cu oxides in CO. K and Cu promoted Fe-Zn oxides reduced and carburized at ~30-50 K lower temperature than Fe-Zn oxides, apparently because K increases CO dissociation rates on Fe. The reduction and carburization profile of Fe-Zn-K4-Cu2 oxide in CO showed that the initial reduction/carburization temperature for Fe_3O_4 was lower and the carburization rates were slightly higher on Fe-Zn-K4-Cu2 than on Fe-Zn-K2-Cu1. These results again suggest that the surface K/Cu ratio probably is slightly higher on Fe-Zn-K4-Cu2 oxides than on the Fe-Zn-K2-Cu1 oxide. The increases in reduction and carburization rates on Fe-Zn-K4-Cu2 oxides imply its higher dispersion of Fe carbides, which in turn lead to higher reaction rates in FTS.

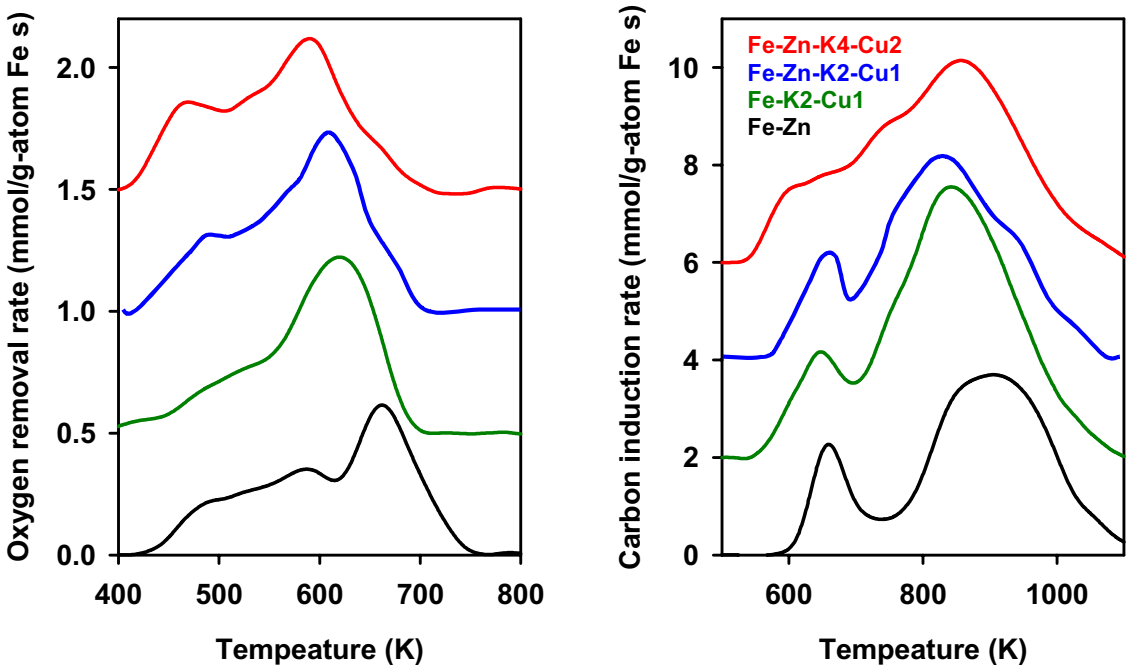

Figure 7. Oxygen removal and carbon introduction rates as a function of temperature during treatment of Fe-Zn-K-Cu oxides in CO. (0.05 g sample, 10 ^{o}C/min ramping rate, 20 % CO in Ar, total flow rate 100 cm^3/min)

3.5 CO chemisorption on Fe-Zn-K-Cu Oxides

Precipitated Fe oxides (0.2 g) were treated in flowing He (100 cm^3/min) at temperatures up to 573 K and then cooled down to 523 K. The He stream was switched to a flow of 60% synthesis gas (H_2/CO=2) in Ar (total flow rate 100 cm^3/min) at 523 K. After exposure to synthesis gas for 1 h, the synthesis gas stream was switched back to He and maintained at 523 K for an additional 1 h before cooling the sample to ambient temperature. The cooling process was accomplished by removing the furnace from the reactor and letting the reactor cool to ambient temperature. A flow of 20% CO in Ar

(total flow rate 100 cm^3/min) was passed through the samples for 0.5 h in order to carry out the adsorption. Physisorbed species were removed in flowing Ar (flow rate 100 cm^3/min) for 0.5 h at room temperature and the chemisorbed species evolved during temperature-programmed desorption (TPD) (10 K/min) and were measured using mass spectrometry.

In our previous quarterly report [22], our mass spectroscopy and X-ray absorption spectroscopy studies of the samples during the FTS reaction showed that these samples consist of bulk Fe_3O_4 and surface Fe carbides after FTS reaction at 523 K for 1 h. The He treatment at 523 K for 1 h removed most of the hydrocarbons formed during FTS reactions as no hydrocarbons were detected by the subsequent TPD in Ar. After CO chemisorption at ambient temperature and subsequent, H_2, CO and CO_2 were the only detectable desorption species. The amount of H_2O or CH_4 formed was negligible during temperature-programmed desorption in Ar, indicating that there is no interaction between adsorbed CO and hydrogen atoms during temperature-programmed desorption.

Table 3 Quantitative analysis of desorption species on Fe-Zn-K-Cu oxides during TPD in Ar at temperatures up to 820 K.

Desorbed species	Condi-tions	Amount desorbed (mmol/g-atom Fe)			
		Fe-Zn	Fe-K2-Cu1	Fe-Zn-K2-Cu1	Fe-Zn-K4-Cu2
H_2	(a)	12.4	48.3	51.1	74.4
	(b)	13.7	52.2	49.5	76.7
CO	(a)	3.0	33.6	40.2	47.3
	(b)	16.0	57.3	63.3	76.7
CO_2	(a)	1.4	23.3	25.0	27.9
	(b)	3.1	38.4	46.6	64.4
CO Chemisorption*		14.7	38.8	44.6	65.9

(a) TPD in Ar After FTS reaction at 523 K for 1 h.
(b) TPD in Ar after FTS reaction at 523 K for 1 h and CO chemisorption for 0.5 h at ambient temperature.
* CO chemisorption = $[(CO+CO_2)]_{(b)} - [(CO+CO_2)]_{(a)}$

All the samples were characterized by CO chemisorption in order to examine the effect of promoters on the CO adsorption behavior. Figures 8, 9 and 10 shows the H_2, CO and CO_2 desorption rates as a function of temperature after chemisorption of CO on Fe-Zn-K-Cu oxides after FTS reaction at 523 K for 1 h. Table 3 shows the quantitative analysis of the amounts desorbed H_2, CO and CO_2 during TPD in Ar up to temperatures of 820 K.

3.5.1. H_2 desorption

Figures 8a shows the H_2 desorption rates as a function of temperature after chemisorption of CO on the samples without adsorbing any titrants after FTS reaction at 523 K for 1 h. A broad H_2 desorption peak appeared at 500-800 K. This suggests that some hydrogen atoms (10-80 mmol H_2/g-atom Fe) remained strongly adsorbed on Fe carbide surfaces, and that they were not removed by flowing He at 523 K. The presence of promoters appeared not to influence the H_2 desorption temperatures but they significantly increased the amount of adsorbed H atoms. The presence of K and Cu increased the amount of absorbed H atoms four-fold over the sample without these promoters (51 mmol H_2/g-atom Fe on Fe-Zn-K2-Cu1 vs 12 mmol H_2/g-atom Fe on Fe-Zn), and higher concentrations of K and Cu gave even higher amount of absorbed H atoms. This reflects the fact that K and Cu increase the reduction and carburization rates on Fe oxides and produced higher surface area Fe carbides, which in turn provide more sites for H adsorption. Zn also slightly increased the density of adsorbed H species (51 mmol H_2/g-atom Fe on Fe-Zn-K2-Cu1 vs 48 mmol H_2/g-atom Fe on Fe-K2-Cu1). This is apparently because Zn as a structural promoter increases the surface area of Fe carbides despite the fact that Zn present as $ZnFe_2O_4$ also titrates part of Fe oxides. After adsorbing CO at ambient temperature for 0.5 h, the subsequent TPD shows that the H_2 desorption peak (Figure 8b) is unchanged, suggesting that these adsorbed H-atoms are not accessible by CO at ambient temperature.

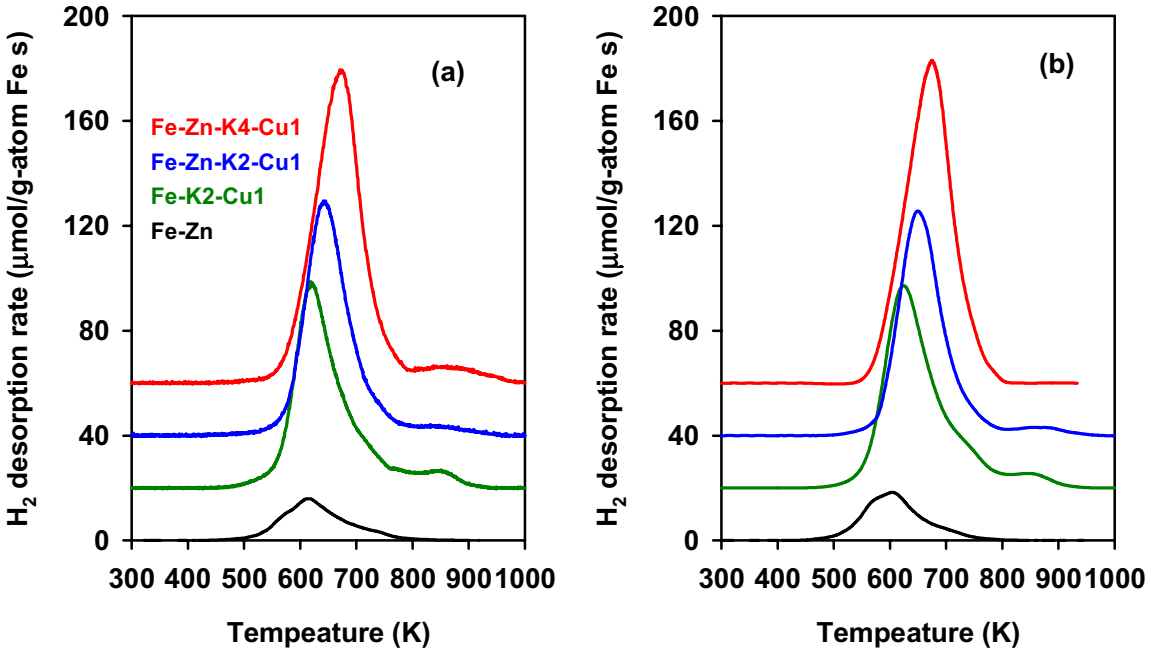

Figure 8. Temperature-programmed desorption of H_2 after FTS reaction and CO chemisorption. (0.2 g sample, K/Fe=0-0.04, Cu/Fe=0-0.02; FTS condition: 523 K, H_2/CO=2, total flow rate 100 cm^3/min; CO chemisorption: 20% CO in Ar, total flow rate 100 cm^3/min) (a): FTS at 523 K for 1 h, cooled in He, TPD in Ar; (b): FTS at 523 K for 1 h, cooled in He, CO chemisorption at room temperature for 0.5 h, TPD in Ar.

3.5.2 CO and CO_2 desorption

Figures 9 and 10 show the CO and CO_2 desorption rates as a function of temperature after chemisorption of CO on Fe-Zn-K-Cu oxides after FTS reaction at 523 K for 1 h. CO and CO_2 desorb simultaneously, implying that the desorption of CO is the rate-determining step. When CO desorbs, it may react readily with distant adsorbed O species, forming CO_2. Figures 9a and 10a show the desorption peaks of CO and CO_2 immediately after FTS reaction and before chemisorption. The asymmetric CO and CO_2 desorption peaks show that they consist of a small amount of weakly adsorbed C species, which can be attributed to the molecular desorption at 550-700 K, and a large amount of strongly adsorbed C species, which resulted from a recombination process of C and O at 700-800 K. The desorption peaks at temperatures higher than 800 K can be ascribed to the surface graphite deposits left behind by the Boudouard reaction. The presence of promoters resulted in greater CO or CO_2 desorption uptakes than the samples without them but they did not influence the desorption temperature. This suggests that the presence of K or Cu increases the density but not the type of the adsorption sites for FTS. Figures 9b and 10b show the desorption of CO and CO_2 after CO chemisorption. Compared with Figure 9a and Figure 10a, the amount of desorbed CO and CO_2 are both higher after CO chemisorbed than before CO chemisorption. The difference between these two curves is the amount of CO chemisorbed on the Fe carbides, which also reflects the total amount of accessible adsorption sites on Fe carbides.

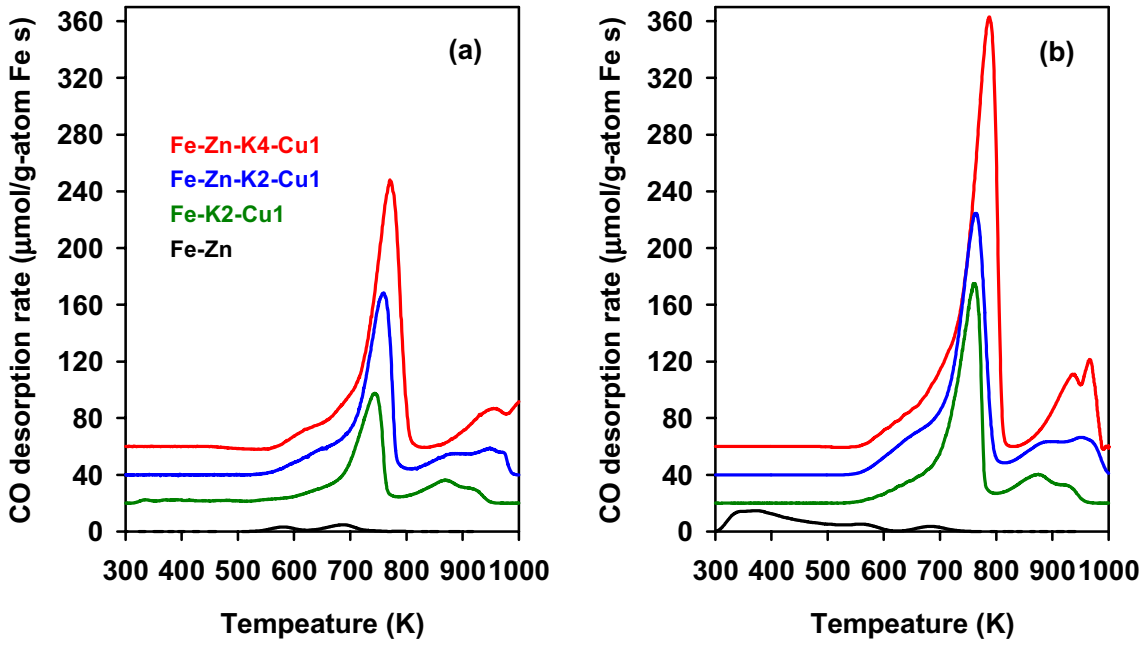

Figure 9. Temperature-programmed desorption of CO_2 after FTS reaction and CO chemisorption. (0.2 g sample, K/Fe=0-0.04, Cu/Fe=0-0.02; FTS condition: 523 K, H_2/CO=2, total flow rate 100 cm^3/min; CO chemisorption: 20% CO in Ar, total flow rate 100 cm^3/min) (a): FTS at 523 K for 1 h, cooled in He, TPD in Ar; (b): FTS at 523 K for 1 h, cooled in He, CO chemisorption at room temperature for 0.5 h, TPD in Ar.

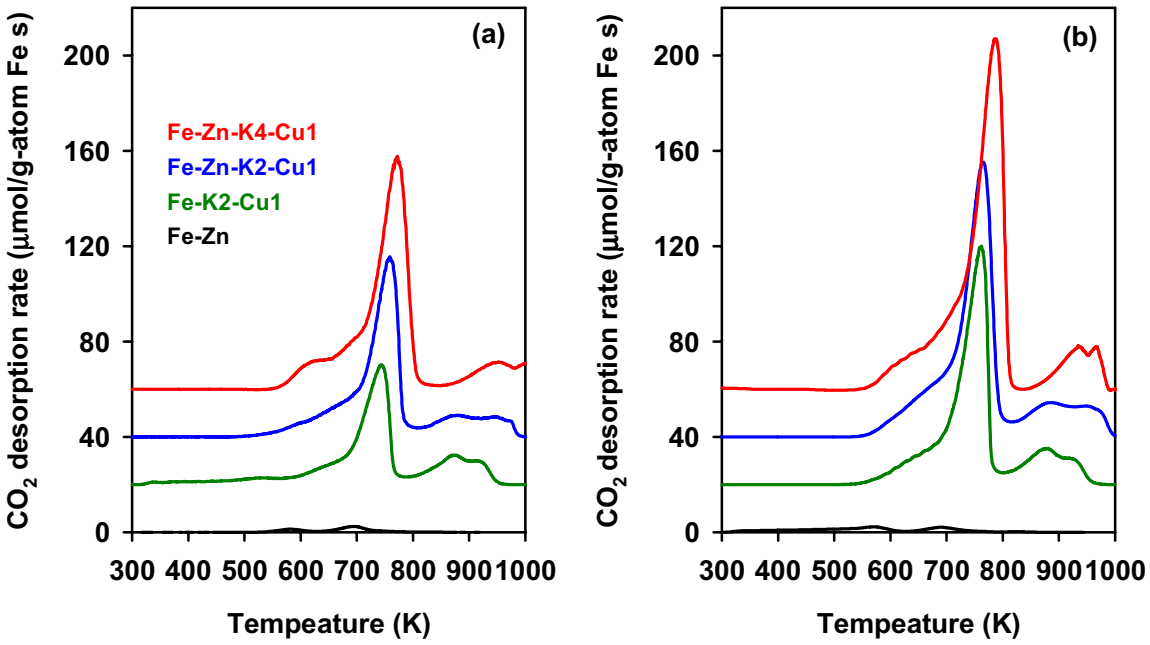

Figure 10. Temperature-programmed desorption of CO_2 after FTS reaction and CO chemisorption. (0.2 g sample, K/Fe=0-0.04, Cu/Fe=0-0.02; FTS condition: 523 K, H_2/CO=2, total flow rate 100 cm^3/min; CO chemisorption: 20% CO in Ar, total flow rate 100 cm^3/min) (a): FTS at 523 K for 1 h, cooled in He, TPD in Ar; (b): FTS at 523 K for 1 h, cooled in He, CO chemisorption at room temperature for 0.5 h, TPD in Ar.

As shown in Table 3, K and Cu promoted Fe-Zn oxides show much larger amounts of adsorbed CO than Fe-Zn oxides (44.6 vs. 14.7 mmol C/g-atom Fe), indicating that the presence of K and Cu increase the density of adsorption sites for FTS reaction. Higher concentrations of K and Cu on Fe-Zn-K4-Cu2 sample led to even higher density of CO chemisorption sites (65.9 mmol C/g-atom Fe). Comparing the amount of CO chemisorbed on Fe-K2-Cu1 (38.8 mmol C/g-atom Fe) with that on Fe-Zn-K2-Cu1 (44.6 mmol C/g-atom Fe), the amount of CO chemisorbed is slightly higher on the Zn-containing sample, reflecting the structural promotion effect of ZnO. It appears that the presence of K, Cu, or Zn increases the extent of reduction and carburization of Fe oxide, leading to higher surface area of Fe carbides, which consequently provides more sites for CO chemisorption and for FTS reactions.

3.5.3. Surface Area of Fe-Zn-K-Cu Oxides after FTS Reaction

Surface area measurements were performed on Fe-Zn-K-Cu oxides after FTS reaction but immediately before CO chemisorption studies in order to establish a correlation between the surface area of the catalysts and the adsorption site densities. The surface areas of all samples decreased significantly after exposure to synthesis gas at 523 K for 1 h, suggesting the shrinkage of Fe oxide particles after carbide formation. The higher surface area oxide precursors (50-120 m^2/g) tend to have higher surface areas after FTS reaction for 1 h (20-40 m^2/g). The amount of CO adsorbed correlates well with the

surface area of the catalysts on K and Cu promoted samples. In contrast, the amount of CO adsorbed is relatively low on Fe-Zn sample, but the surface area is relatively high compared with K and Cu containing samples. This is probably because Zn titrates some of the Fe oxides despite its structural promotion effect on increasing the surface area of Fe oxides. The relatively high surface area may not all be available for CO chemisorption and FTS reactions.

Table 4. Surface areas (m^2g^{-1}) of Fe-Zn-K-Cu (Zn/Fe=0.1) samples after FTS in synthesis gas up to 250 ^oC for 1 h

Sample	Fe-Zn	Fe-K2-Cu1	Fe-Zn-K2-Cu1	Fe-Zn-K4-Cu2
Before FTS	115	52	65	120
FTS 1 h	39	23	30	42

In conclusion, CO chemisorption can be used as a useful measure of the site density of catalysts. The amount of CO chemisorbed on the catalysts is in good agreement with their surface areas. The presence of K and Cu significantly increases the reduction and carburization rates on Fe oxides, leading to higher surface area Fe carbides, which in turn provide more sites for CO chemisorption and FTS reactions. Zn also increases the site density on Fe oxides, but it does not increase the number of sites in proportion to its increase in surface because of its apparent ability to block some Fe-derived active sites.

4. FISCHER-TROPSCH SYNTHESIS ON IRON CATALYSTS

4.1. FTS reactions on a high surface area Fe-Zn-Cu-K catalyst

During this reporting period, FTS reactions were carried out on a high surface area Fe-Zn-Cu-K sample (Zn/Fe=0.1, Cu/M=0.02, K/M=0.04), the synthesis procedure of which has been described in Section 2 (surface area for the precarburized samples being 120 m^2/g compared to 65 m^2/g earlier). The aim was to compare the behavior of the two samples for the FTS reaction and to determine the effects of surface area on FTS performance.

The activity and selectivity on the high surface area Fe-Zn-Cu-K sample is compared in this section with that of the low surface area Fe-Zn-Cu-K sample (Zn/Fe=0.1, Cu/M=0.02, K/M=0.04) reported earlier [18-20]. The CO conversion on the two catalysts is shown as a function of reciprocal space velocity in Figures 11; the CO consumption rate is shown as a function of the CO conversion in Figure 12. The CO conversion and CO rates are significantly higher on the high surface area catalyst than on the low surface area sample indicating an increase in the number of active sites available for the FTS reaction.

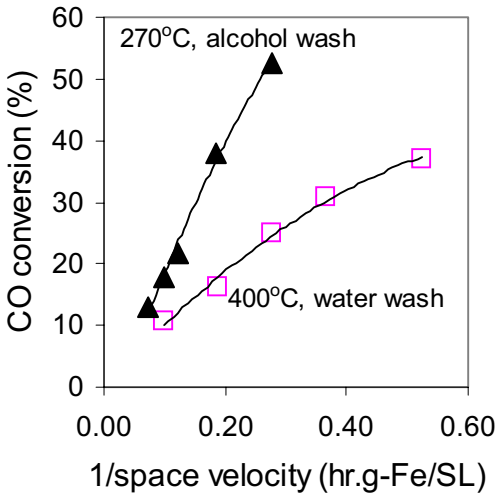

Figure 11. CO conversion as a function of reciprocal CO space velocity on the Fe-Zn-Cu-K catalyst samples (Calcined at 400°C, water wash; and Calcined at 270°C, alcohol wash), 220°C, 31.6 atm, $H_2/CO=2$.

A summary of the FTS data obtained on the two samples is presented in Table 4. The hydrocarbon productivity is approximately 2.3 times higher on the high surface area sample, consistent with the two-fold increase in surface area. Hence the increase in activity is likely to an increase in the number of available sites rather than a change in the activity per site (Figure 13). CO_2 selectivities are almost identical in the two cases. The higher surface area sample has a slightly higher selectivity to light hydrocarbons and a lower C_{5+} selectivity. It is possible that the concentration of Cu and K atoms per Fe is

smaller on the high surface area sample than the low surface area sample and this may account for the observed small decrease in product molecular weight and in olefin content as exemplified by the difference in the *1*-hexene/*1*-hexane ratio.

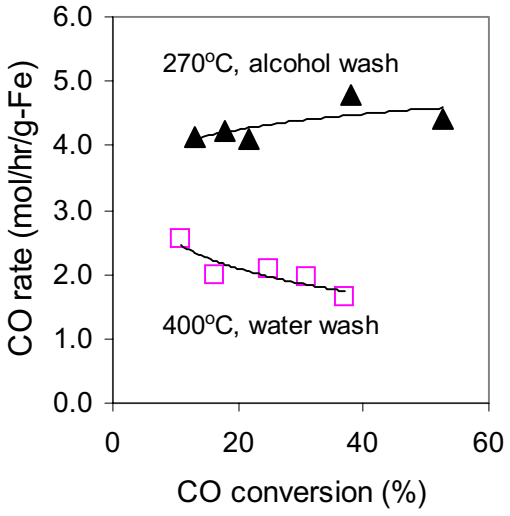

Figure 12. CO rate as a function of CO conversion on the Fe-Zn-Cu-K catalyst samples (Calcined at 400°C, water wash; and Calcined at 270°C, alcohol wash), 220°C, 31.6 atm, H_2/CO=2.

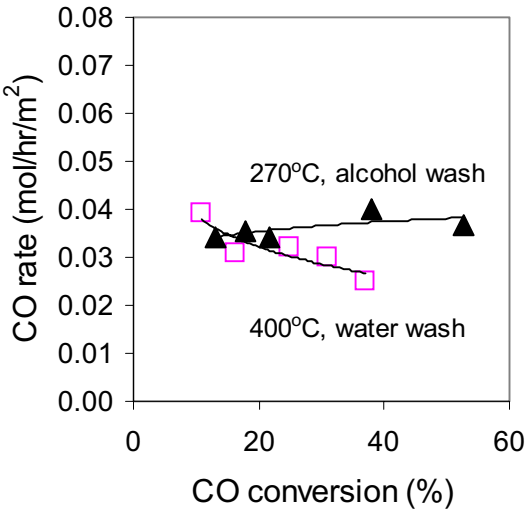

Figure 13. CO rate per surface area as a function of CO conversion on the Fe-Zn-Cu-K catalyst samples (Calcined at 400°C, water wash; and Calcined at 270°C, alcohol wash), 220°C, 31.6 atm, H_2/CO=2.

Table 4. Comparison of FTS parameters on the two Fe-Zn-Cu-K samples at 220°C, 31.6 atm, H_2/CO=2.

	FeZnCu1K2 (low SA)	FeZnCu2K4 (high SA)
CO conversion (%)	37	38
HC productivity (g/hr.g-Fe)	388	856
CO_2 selectivity (%)	21.8	22.4
HC selectivity (CO_2-free)		
CH_4 selectivity (%)	1.9	2.6
C_2-C_4 (%)	10.8	13.9
C_{5+} (%)	87.3	83.5
1 -C_6H_{12}/*1* -C_6H_{14}	2.2	2

From our results, it is clear that the effect of surface area on the catalysts is an improvement in the dispersion of the Fe_xC crystallites, which results in an increased activity for the FTS reaction. However, the chemical environment on the catalyst appears to be unchanged as explained by similar product selectivities.

4.2 Effect of H_2/CO ratio on the FTS rate and selectivity on a Fe-Zn-Cu-K catalyst

During the current reporting period, the behavior of a Fe-Zn-Cu-K catalyst (Zn/Fe=0.1, Cu/M=0.02, K/M=0.04) with high H_2/CO ratios was studied at 200°C, the temperature used for FTS reactions on Co-based catalysts. The aim of this study was to test if the Fe catalyst behaves similar to the Co/SiO_2 catalyst (studied previously) under similar surface H*/CO* ratios [20-23]. Since the hydrogen surface coverage is much higher on Co than on Fe, the experiments were conducted with a H_2/CO ratio that is much higher than 2. The catalyst was first pretreated in synthesis gas while the temperature was ramped from 25°C to 150°C at 10°C/min and from 150 to 270°C at 1°C/min. The temperature was held constant at 270°C for 1 hour and then the reactor was cooled to 200°C and the pressure was set at the desired values. Our preliminary approach involved the matching of the CH_4 selectivities on both catalysts at 200°C. This comparison was performed at low CO space times in order to exclude the significant contributions from autocatalytic water effects on Co catalysts. The CH_4 selectivities were similar when the experiments were conducted at a H_2/CO ratio of 20 on the Fe-Zn-Cu-K catalyst.

The CO conversion on the Co and Fe catalysts (H_2/CO=2 and 20) are shown in Figure 14 as a function of the reciprocal CO space velocity. The FTS run on the Fe catalyst at low H_2/CO ratio showed the lowest CO conversions. Upon increase in the H_2/CO ratio, the CO conversion increases at identical space velocities indicating a positive dependence of the FTS reaction rate on the hydrogen partial pressure. Similarly, the CO rate is shown in Figure 15 as a function of the CO conversion at both conditions. The Co/SiO_2 catalyst had a much higher CO conversion and rate than the Fe catalyst at this temperature.

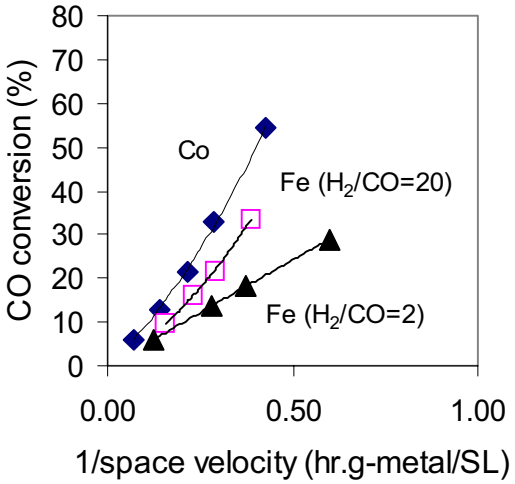

Figure 14. CO conversion as a function of reciprocal CO space velocity at 200°C on Co/SiO_2 (H_2/CO=2, 20 atm), Fe-Zn-Cu-K (H_2/CO=2, 20 atm) and Fe-Zn-Cu-K (H_2/CO=20, 32 atm).

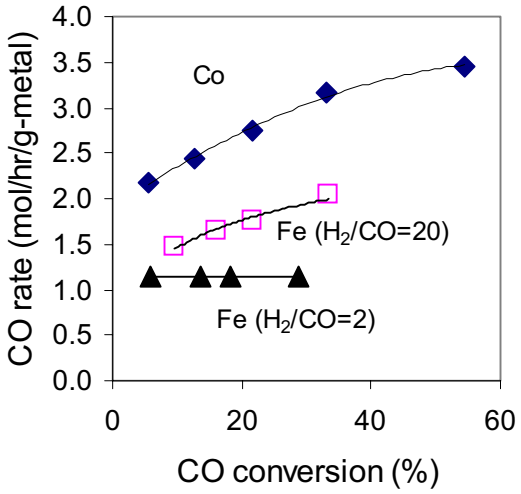

Figure 15. CO consumption rate as a function of CO conversion at 200°C on Co/SiO_2 (H_2/CO=2, 20 atm), Fe-Zn-Cu-K (H_2/CO=2, 20 atm) and Fe-Zn-Cu-K (H_2/CO=20, 32 atm).

The CO_2 selectivity in all three cases is shown as a function of CO conversion in Figure 16. While the Fe catalyst operated at a H_2/CO ratio of 2 showed higher CO_2 selectivities and exhibited a linear increase in its selectivity as a function of the CO conversion, a different behavior is observed when the same catalyst is operated at higher H_2/CO ratios (20). At these conditions, the CO surface coverage is much smaller than in the case of the former and hence the predominant mode of oxygen removal is as H_2O instead of CO_2. Since the slope of the CO_2 selectivity curve at the high H_2/CO ratio is almost zero, the secondary water gas shift reaction does not appear to take place at these conditions and the only route of CO_2 formation is *via* oxygen removal using CO.

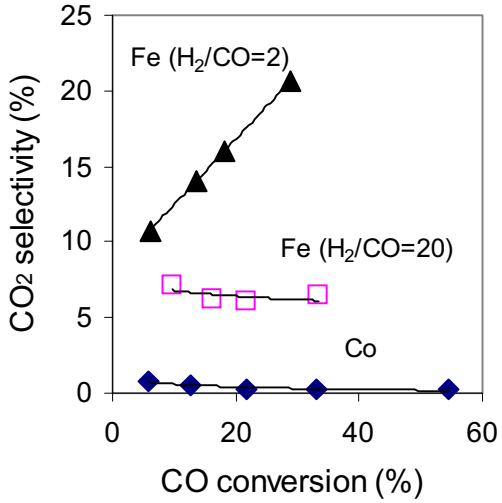

Figure 16. CO_2 selectivity as a function of CO conversion at 200°C on Co/SiO_2 (H_2/CO=2, 20 atm), Fe-Zn-Cu-K (H_2/CO=2, 20 atm) and Fe-Zn-Cu-K (H_2/CO=20, 32 atm).

The CH_4 selectivity curve of the Fe-Zn-Cu-K catalyst at $H_2/CO=20$ almost matches that of Co/SiO_2, and significantly higher than that of the Fe-Zn-Cu-K at $H_2/CO=2$ (Figure 17). The higher hydrogen surface concentration in the case of Fe-Zn-Cu-K leads to a significantly lower C_{5+} selectivity compared to the other two cases (Figure 18).

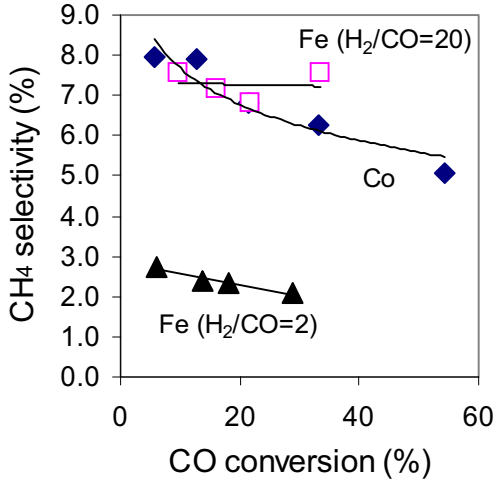

Figure 17. CH_4 selectivity as a function of CO conversion at 200°C on Co/SiO_2 ($H_2/CO=2$, 20 atm), Fe-Zn-Cu-K ($H_2/CO=2$, 20 atm) and Fe-Zn-Cu-K ($H_2/CO=20$, 32 atm).

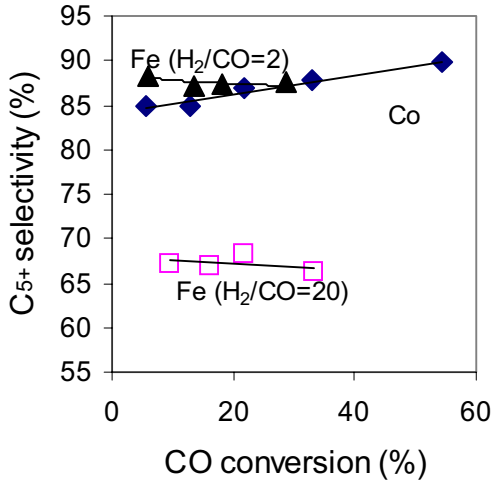

Figure 18. C_{5+} selectivity as a function of CO conversion at 200°C on Co/SiO_2 ($H_2/CO=2$, 20 atm), Fe-Zn-Cu-K ($H_2/CO=2$, 20 atm) and Fe-Zn-Cu-K ($H_2/CO=20$, 32 atm).

The α-olefin/*n*-paraffin ratio is shown as a function of the carbon number in Figure 19. At high surface hydrogen coverages, the Fe-Zn-Cu-K catalyst has a much lower olefin content than at the H_2/CO ratio of 2. For carbon numbers beyond C_2, the olefin/paraffin ratio is also lower than on the Co/SiO_2 catalyst. The *1*-hexene/*n*-hexane ratio is plotted as

a function of reciprocal space velocity in Figure 20. The decrease in this ratio on the Co/SiO_2 with space time has previously been attributed primarily to readsorption of olefins followed by subsequent chain growth and termination as higher carbon number chains [25,26]. The *1*-hexene/*n*-hexane ratio on the Fe catalyst, on the other hand, is independent of space time in both cases. This indicates the absence of any secondary hydrogenation or readsorption on these Fe catalysts.

A closer look at the C_5 selectivity distribution on the Fe-Zn-Cu-K catalyst at $H_2/CO=20$ shown in Figure 21, confirms the conclusions drawn above. While the total C_5 content is unchanged, the *1*-pentene and *n*-pentane contents are also relatively unchanged with space time pointing to the absence of secondary reactions. At such high surface hydrogen coverages on the Fe catalyst, chains get terminated at low carbon numbers with high probabilities, which explains the lower C_{5+} selectivity than at $H_2/CO=2$. While the methane selectivities in the case of the Fe catalyst ($H_2/CO=20$) and Co are similar, hydrocarbon selectivities from C_2 and beyond are lower for the Co catalyst because of a combination of the following two effects: a decreased intrinsic probability of termination of hydrocarbon chains at low carbon numbers and the readsorption of low and intermediate molecular weight olefins and their contribution to further chain growth [25,26].

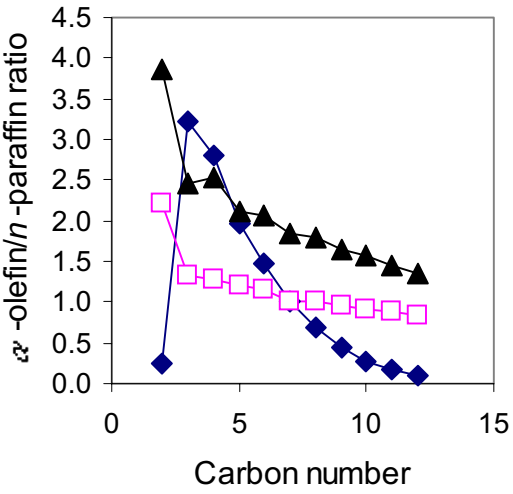

Figure 19. α–Olefin/*n*-paraffin ratio as a function of carbon number at 200°C on Co/SiO_2 (200°C, $H_2/CO=2$, 20 atm), Fe-Zn-Cu-K ($H_2/CO=2$, 20 atm) and Fe-Zn-Cu-K ($H_2/CO=20$, 32 atm).

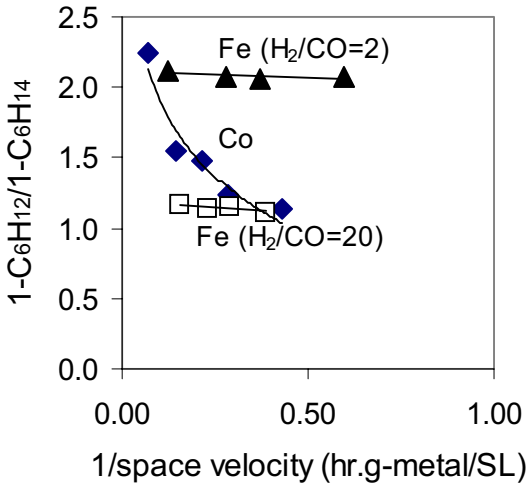

Figure 20. *1*–C_6H_{12}/*n*-C_6H_{14} ratio as a function of reciprocal space velocity at 200°C on Co/SiO_2 (200°C, $H_2/CO=2$, 20 atm), Fe-Zn-Cu-K ($H_2/CO=2$, 20 atm) and Fe-Zn-Cu-K ($H_2/CO=20$, 32 atm).

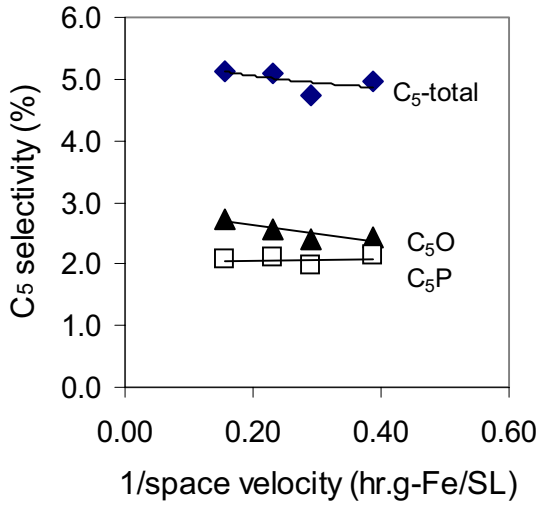

Figure 21. C_5 selectivity distribution as a function of CO conversion at 200°C on Fe-Zn-Cu-K (H_2/CO=20, 32 atm).

Further analysis of the wax samples collected during the above runs is expected to completed in the next quarter and this is expected to provide more information on the chain growth mechanism on the catalysts.

4.3. FTS reactions on Ru-promoted Fe-Zn-K catalysts: Effect of Ru loading

During the previous quarter, studies were continued with Fe-Zn-Ru-K catalysts in order to confirm the promotion effects of Ru for the FTS reaction [24]. The effect of Ru loading (0 to 1 at.%) on the activity and selectivity behavior of a Fe-Zn-K catalyst was studied.

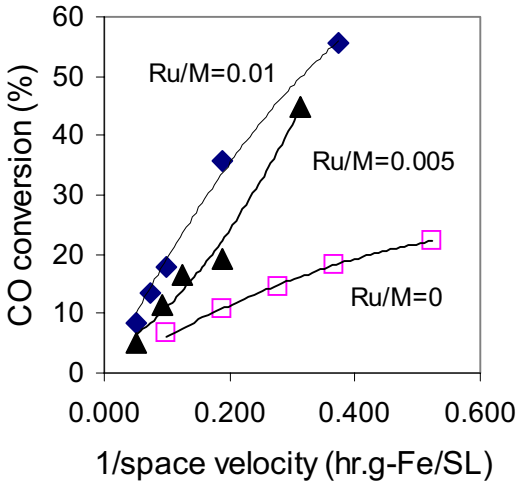

Figure 22. CO conversion as a function of reciprocal space velocity on the catalysts. Fe-Zn-Ru1-K (Zn/Fe=0.1, K/M=0.02, Ru/M=0.01), Fe-Zn-Ru0.5-K (Zn/Fe=0.1, K/M=0.02, Ru/M=0.005), Fe-Zn-K (Zn/Fe=0.1, K/M=0.02, Ru/M=0); 220°C, 31.6 atm, H_2/CO=2.

As shown in Figure 22, the CO conversion increases upon addition of Ru to Fe-Zn-K. Ru-addition was attempted initially to overcome one of the deficiencies of the Cu-promoted Fe-Zn-K catalysts, which is its high CO_2 selectivity. However, our results show that the replacement of Cu by Ru do not lead to a decrease in CO_2 selectivity during the FTS reaction. In fact, an increase in the Ru concentration in the 0-1 at.% range also increased CO_2 selectivities (Figure 23). Ru appears to increase CO_2 formation *via* its primary mode.

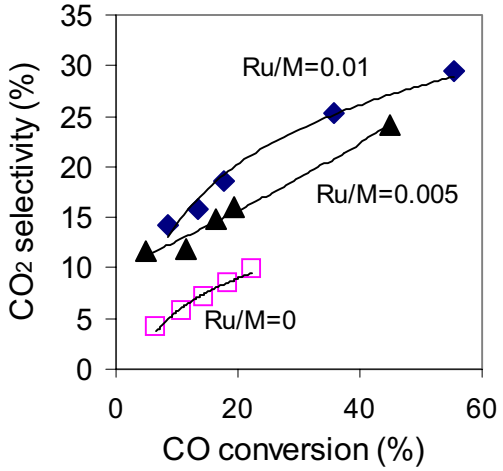

Figure 23. CO_2 selectivity as a function of CO conversion, Fe-Zn-Ru1-K (Zn/Fe=0.1, K/M=0.02, Ru/M=0.01), Fe-Zn-Ru0.5-K (Zn/Fe=0.1, K/M=0.02, Ru/M=0.005), Fe-Zn-K (Zn/Fe=0.1, K/M=0.02, Ru/M=0); 220°C, 31.6 atm, H_2/CO=2.

Table 5. FTS reaction parameters for Ru- promoted catalysts at 220°C, 31.6 atm, H_2/CO=2

	Fe-Zn-K	Fe-Zn-Ru-0.5-K	Fe-Zn-Ru1.0-K
CO conversion (%)	18.3	19.4	17.8
CO rate (mol/hr.g-at. Fe)	1.3	2.4	4.2
HC productivity (g/hr/kg.Fe)	290	514	860
CO_2 selectivity (%)	8.5	15.9	18.6
HC selectivities (CO_2 free)			
CH_4 (%)	1.8	2.2	2.6
C_2-C_4 (%)	10.7	11.4	11.9
C_{5+} (%)	87.5	86.4	85.5
1 -C_6H_{12}/*1* -C_6H_{14}	2.0	1.7	1.8

The addition of Ru also leads to a small decrease in the product molecular weight (lower C_{5+} selectivity) and to a small increase in the paraffin content due to the ability of Ru to improve hydrogen dissociation on the surface. However, since these selectivity effects are negligible compared to the extent of promotion of the FTS rates, the primary role of Ru is in improving the dispersion of Fe_xC sites on the catalyst surface. It is also possible that Ru prevents sintering of the catalyst during the pretreatment step.

Even though the addition of Ru leads to much higher hydrocarbon productivities than on Cu-promoted catalysts, the high cost of Ru makes the Ru contents used in this study impractical for commercial use [27-30]. However, Ru-promoted catalysts are attractive because they could be activated at much lower temperatures than the Cu-promoted ones.

II FISCHER-TROPSCH SYNTHESIS ON COBALT CATALYSTS

1. Study of the effect of H_2/CO ratios on a 21.9% Co/SiO_2 catalyst

During the previous quarter, the behavior of a Co/SiO_2 catalyst was studied at conditions involving lower H_2/CO ratios and higher temperatures typical of Fe-based FTS reactions. The aim of this study was to test if the Co catalyst behaves similar to Fe when the surface H*/CO* ratio approach each other. The experiments were carried out with a 21.9% Co/SiO_2 catalyst at 220°C and at a H_2/CO ratio of 1.0. Prior to the reaction, the catalyst sample was pretreated in H_2 (200 ml/g/min) from 25°C to 325°C at the rate of 10°C/min followed by reduction at 325°C for 1 h. The reactor was then cooled down to 160°C in H_2, the flow of synthesis gas (H_2/CO=2) was started, and the pressure was set to 20 atm and finally the temperature raised to 200°C. Upon verification of a data point at this condition, the CO pressure was raised to obtain a H_2/CO ratio of 1.0 (P_{H2}=19.6 atm, the same as that used for Fe-based catalysts at 220°C). Finally the temperature of the reactor was gradually increased to 220°C in order to prevent any initial exotherms or hot spots.

Fig. 24 shows CO conversion as a function of reciprocal space velocity for the Fe-Zn-Cu-K (high surface area) catalyst and a 21.9% Co/SiO_2 catalyst with H_2/CO=1 at 220°C. At this temperature, the Co catalyst has a higher CO conversion and rate than the Fe-Zn-Cu-K sample. Since it is likely that the CO rate has a negative dependence on the CO conversion, and the CO gas phase concentration is lower in the case of Co, this result indicates that the Co/SiO_2 has a significantly higher activity than the Fe-based sample. It is also interesting to note that the CO conversion rate increases with increase in time which points out to the existence of the autocatalytic water effect even under these conditions on Co [19-22].

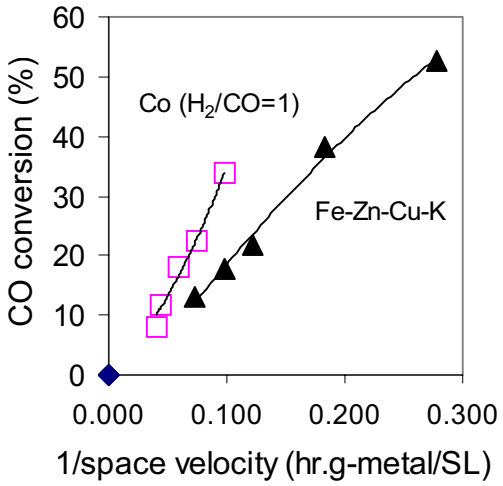

Figure 24. CO conversion as a function of reciprocal space velocity at 220°C on Co/SiO_2 (H_2/CO=1, 43.6 atm), and Fe-Zn-Cu-K (H_2/CO=2, 31.6 atm).

At this temperature, the Co/SiO_2 catalyst is likely to have a high selectivity to methane at $H_2/CO=2$. With a lower H_2/CO ratio, the CH_4 selectivity is significantly smaller (Figure 25) and decreases with increasing space time due to the fact that water plays a role in promoting chain growth as observed previously [19,25,26]. Similarly the C_{5+} selectivity increases with increasing space time on the Co/SiO_2 sample (Figure 26). While the CH_4 selectivity of the Co/SiO_2 sample ($H_2/CO=1$) is significantly smaller on Fe-Zn-Cu-K ($H_2/CO=2$), the C_{5+} selectivities are almost identical at low space times. This is because olefins (C_2 and beyond) undergo readsorption on the Co catalyst and terminate at higher carbon numbers with a high probability unlike in the case of the Fe catalyst on which such a mechanism does not take place.

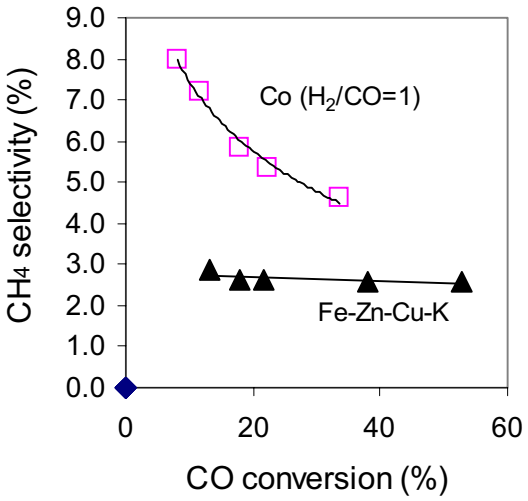

Figure 25. CH_4 selectivity as a function of CO conversion at 220°C on Co/SiO_2 ($H_2/CO=1$, 43.6 atm), and Fe-Zn-Cu-K ($H_2/CO=2$, 31.6 atm).

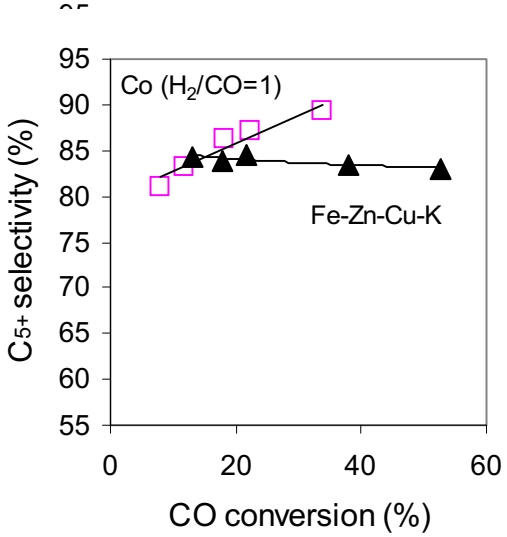

Figure 26. C_{5+} selectivity as a function of CO conversion at 220°C on Co/SiO_2 ($H_2/CO=1$, 43.6 atm), and Fe-Zn-Cu-K ($H_2/CO=2$, 31.6 atm).

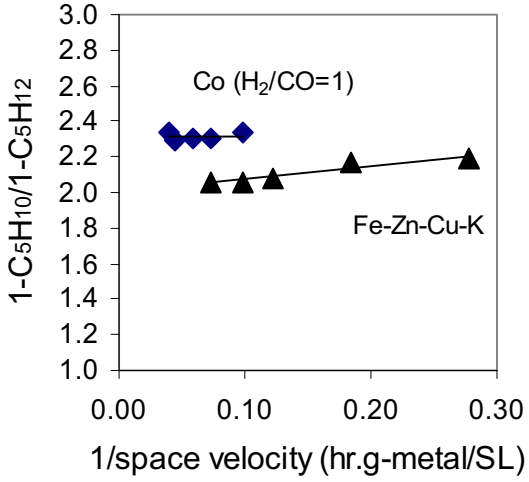

Figure 27. *1*-C_5H_{10}/*n*-C_5H_{12} selectivity as a function of reciprocal space velocity at 220°C on Co/SiO_2 ($H_2/CO=1$, 43.6 atm), and Fe-Zn-Cu-K ($H_2/CO=2$, 31.6 atm).

Since the surface CO*/H* ratio is enhanced by operation of the reaction at a H_2/CO ratio of 1 instead of 2, the Co surface appears to be less hydrogenating (Figure 27). While it has been observed in earlier quarters that the Co/SiO_2 catalyst promotes secondary hydrogenation reactions at 200°C and a H_2/CO ratio of 2, no secondary hydrogenation is observed as evidenced by the zero slope of the *1*-pentene/*n*-pentane curve. Flory plots for the Co catalyst at the two H_2/CO ratios at 200°C and 220°C are shown in Figure 28. A decrease in the H_2/CO ratio from 2 to 1 leads to unchanged Flory plots at a given reaction temperature, indicating that secondary chain growth by readsorption of olefins is unaffected by this increased CO coverage on the catalyst. However, at 220°C, the chain growth probability at higher carbon numbers appears to decrease which can be explained by the ease of desorption of α-olefins with increasing temperature and their subsequent non-participation in secondary chain growth reactions.

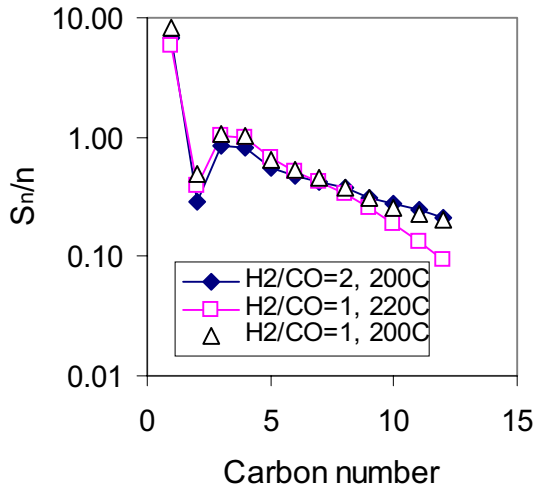

Figure 28. Flory plots for a 21.9% Co/SiO_2 catalyst at: 1) H_2/CO=2, 20 atm, 200°C, 2) H_2/CO=1, 43.6 atm, 220°C, and 3) H_2/CO=1, 43.6 atm, 200°C.

2. Effect of reaction pressure on the behavior of Co/SiO_2 for FTS reactions

During the previous quarter, FTS reaction was also conducted with a 21.9% Co/SiO_2 catalyst at different reaction pressure. This was done in anticipation of a series of for *in situ* FTIR spectroscopic experiments that will be carried out in the next quarter in order to study the autocatalytic water effects. Due to the pressure limitations of the transmission FTIR cell, fixed-bed reactor experiments were conducted at 200°C and 5 atm to study the FTS kinetics on the Co/SiO_2 catalyst under these conditions as well as to verify the existence of the autocatalytic water effect at these low pressures.

The Co site-time yields obtained on the 21.9% Co/SiO_2 catalyst at 5 atm and 20 atm are shown as function of the average water mole fraction in the reactor in Figure 29. The empty symbols represent data points corresponding to space velocity runs whereas the filled symbols represent water addition data. The site-time yields are similar at both

pressures and increase with increasing H_2O concentration as observed before confirming the existence of water effect even at low pressures [19-21,25]. Similarly the CH_4 and C_{5+} selectivities also are affected by water in both cases (Figures 30 and 31).

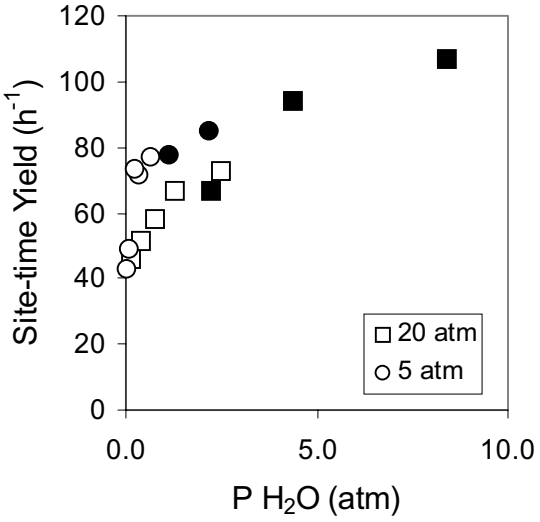

Figure 29. Co site-time yield as a function of average mole fraction of H_2O on a 21.9% Co/SiO_2 catalyst at 200°C; Empty symbols: Space velocity runs, Filled symbols: Water addition runs.

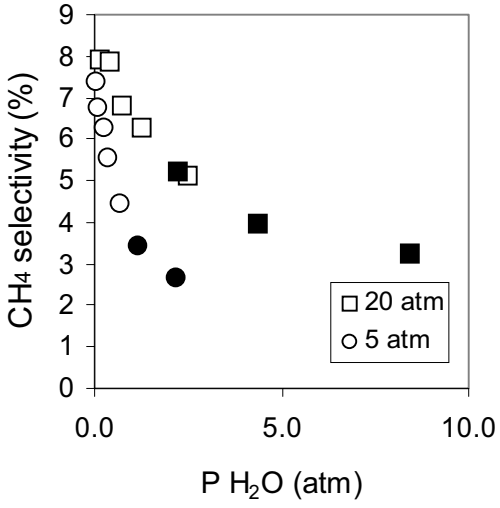

Figure 30. CH_4 selectivity as a function of average mole fraction of H_2O on a 21.9% Co/SiO_2 catalyst at 200°C; Empty symbols: Space velocity runs, Filled symbols: Water addition runs.

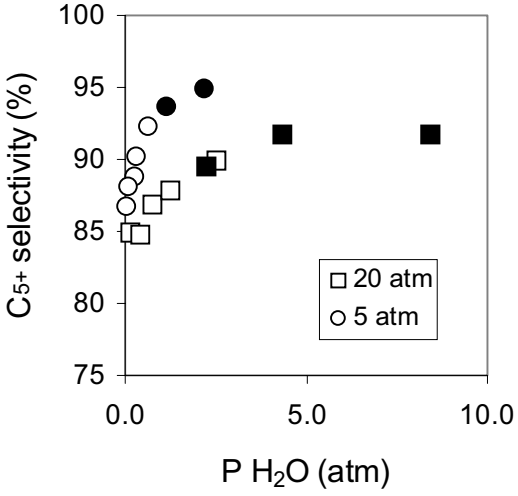

Figure 31. C_{5+} selectivity as a function of average mole fraction of H_2O on a 21.9% Co/SiO_2 catalyst at 200°C; Empty symbols: Space velocity runs, Filled symbols: Water addition runs.

Since our low-pressure FTS reaction studies have shown the existence of the water effect, this condition will be used for the *in situ* FTIR spectroscopic experiments with Co/SiO_2 both with and without the addition of water. The IR spectrometer has been relocated to a different unit and modifications are being done in order to carry out high-pressure experiments with the transmission IR cell. These studies are expected to be completed in the upcoming quarter.

II. APPENDIX
1. References

1. M. E. Dry, The Fisher-Tropsch Synthesis, in *Catalysis-Science and Technology*, Vol. 1, p. 160, J. R. Anderson and M. Boudart eds., Springer Verlag, New York, 1981.
2. F. Fischer and H. Tropsch, *Brennstoff-Chem.* 7 (1926) 97.
3. R. B. Anderson, in *Catalysis* Vol. 4, p. 29, P. H. Emmett eds., Van Nostrand-Reinhold, New York, 1956.
4. H. H. Storch, N. Golumbic and R. B. Anderson, *The Fischer-Tropsch and Related Syntheses*, Wiley, New York, 1951; R. B. Anderson, *The Fischer-Tropsch Synthesis*, Wiley, New York, 1984.
5. H. Kolbel and M. Ralek, *Catal. Rev.-Sci. Eng.* 21 (1980) 225.
6. J. W. Niemantsverdriet and A. M. van der Kraan, *J. Catal.* 72 (1981) 385.
7. J. A. Amelse, J. B. Butt and L. J. Schwartz, *J. Phys. Chem.* 82 (1978) 558.
8. G. B. Raupp and W. N. Delgass, *J. Catal.* 58 (1979) 348.
9. R. Dictor and A. T. Bell, *J. Catal.* 97 (1986) 121.
10. J. P. Reymond, P. Meriaudeau and S. J. Teichner, *J. Catal.* 75 (1982) 39.
11. C. S. Kuivila, P. C. Stair and J. B. Butt, *J. Catal.* 118 (1989) 299.
12. C. S. Huang, L. Xu and B. H. Davis, *Fuel Sci. Tech. Int.* 11 (1993) 639.
13. S. Soled, E. Iglesia and R. A. Fiato, *Catal. Lett.* 7 (1990) 271.
14. S. Soled, E. Iglesia, S. Miseo, B. A. DeRites and R. A. Fiato, *Topics in Catal.* 2 (1995) 193.
15. E. Iglesia, A research proposal submitted to the Division of Fossil Energy.
16. R. J. O'Brien, L. Xu. R. L. Spicer and B. H. Davis, *Energy and Fuels*, 10 (1996) 921.
17. D. B. Bukur, D. Mukesh, and S. A. Patel, *Ind. Eng. Chem. Res*., 29, 194 (1990).
18. 1st Quarterly report, 1999. U.S. Department of Energy under contract # DE-FC26-98FT40308.
19. 2nd Quarterly report, 1999. U.S. Department of Energy under contract # DE-FC26-98FT40308.
20. 3rd Quarterly report, 1999. U.S. Department of Energy under contract # DE-FC26-98FT40308.
21. 4th Quarterly report, 1999. U.S. Department of Energy under contract # DE-FC26-98FT40308.
22. 1st Quarterly report, 2000. U.S. Department of Energy under contract # DE-FC26-98FT40308.
23. 2nd Quarterly report, 2000. U.S. Department of Energy under contract # DE-FC26-98FT40308.
24. 3rd Quarterly report, 2000. U.S. Department of Energy under contract # DE-FC26-98FT40308.
25. E. Iglesia, *Appl. Catal. A*, 161 (1997) 59.
26. E. Iglesia, S.C. Reyes, R.J. Madon, and S.L. Soled, *Advances in Catal*., 39 (1993) 221.
27. D.O. Uner,, M. Pruski, and T.S. King, *Topics in Catal.*, 2 (1995) 59.
28. R.A. Dalla Betta, and M. Shelef, *J. Catal*., 48 (1977) 111.
29. C.S. Kellner, and A.T. Bell, *J.Catal*., 70 (1981) 418.
30. E. Iglesia, S.L. Soled, R.A. Fiato, and G.H. Via, *J. Catal.*, 143 (1993) 345.

Task 12. Reporting/Project Management

Four monthly and one quarterly reports have been completed.